3D-printing to innovate biopolymer materials for demanding applications: A review

Nannan Li [a,1], Dongling Qiao [b,1], Siming Zhao [a], Qinlu Lin [c], Binjia Zhang [a,*], Fengwei Xie [d,**]

[a] *Group for Cereals and Oils Processing, College of Food Science and Technology, Key Laboratory of Environment Correlative Dietology (Ministry of Education), Huazhong Agricultural University, Wuhan, 430070 China*

[b] *Glyn O. Phillips Hydrocolloid Research Centre at HBUT, School of Food and Biological Engineering, Hubei University of Technology, Wuhan 430068, China*

[c] *National Engineering Laboratory for Rice and By-product Deep Processing, College of Food Science and Engineering, Central South University of Forestry and Technology, Changsha 410004, China*

[d] *International Institute for Nanocomposites Manufacturing (IINM), WMG, University of Warwick, Coventry CV4 7AL, United Kingdom*

[*] Corresponding authors. Email address: zhangbj@mail.hzau.edu.cn (B. Zhang)

[**] Corresponding author. Email addresses: d.xie.2@warwick.ac.uk, fwhsieh@gmail.com (F. Xie).

[1] These authors contributed equally to this work.

Content

Abbreviations

3DP	3D printing
BSA	Bovine serum albumin
CFD	Computational fluid dynamics
CIJ	Continuous inkjet
CNC	Cellulose nanocrystal
CNF	Cellulose nanofibrils, or nanofibrillated cellulose
CNTs	Carbon nanotubes
DHT	Dry-heating treatment
DIW	Direct ink writing
DM	Degree of methoxylation (of pectin)
DOD	Drop on demand
E	Young's modulus
ECM	Extracellular matrix
FDM	Fused deposition modeling
G'	Storage modulus
G''	Loss modulus
GelMA	Gelatin methacryloyl
GMA	Glycidyl methacrylate
HA	Hyaluronic acid
HDL	High-density lipoprotein

IL	Ionic liquid
iPSC	Induced pluripotent stem cell
K	Flow consistency
LDL	Low-density lipoprotein
MPC	Milk protein concentrate
n	Power-law index
PEG	polyethylene glycol
PBS	Phosphate-buffered saline
SF	Silk fibroin
SLS	Selective laser sintering
SPI	Soy protein isolate
TA	Tannic acid
tan δ	Loss tangent
WPI	Whey protein isolate
η	Shear viscosity
$\dot{\gamma}$	Shear rate
γ	Strain
τ	Stress
τ_y	Yield stress

Abstract

Biopolymers are widely available, low-/nontoxic, biodegradable, biocompatible, chemically versatile, and inherently functional, making them highly potential for a broad range of applications such as biomedicine, food, textile, and cosmetics. 3D printing (3DP) is capable of fabricating some customized, complex material structures composed of single or multiple material constituents that cannot be achieved by conventional methodologies (e.g. internal structures design); thus, 3DP can greatly expand the application of biopolymer materials. This review presents a comprehensive survey of the latest literature in 3DP technology for materials from biopolymers such as polysaccharides and proteins. The most commonly used 3DP techniques (i.e. inkjet printing, extrusion-based printing, stereolithography, selective laser sintering, and binder jetting) in biomedical and food fields are discussed. Critical factors affecting the quality and accuracy of 3D-printed constructs, including rheological characteristics, printing parameters (e.g. printing rate, and nozzle diameter, movement rate and height), and post-printing processes (e.g. baking, drying, and crosslinking) are analyzed. The properties and the emerging applications of 3D-printed biopolymer materials in biomedical, food, and even wider applications (e.g. wastewater treatment and sensing) are summarized and evaluated. Finally, challenges and future perspectives are discussed. This review can provide insights into the development of new biopolymer-based inks and new biopolymer-based 3D-printed materials with enhanced properties and functionality.

***Keywords**:* Biopolymer 3D printing; Mechanical properties; Rheological properties; 3D Printability; Food application; Medical application

1. Introduction

Additive manufacturing (AM), commonly known as three-dimensional (3D) printing (3DP), refers to the fabrication of objects layer by layer through the deposition of a material using a printer head and nozzle onto a substrate based on a pre-design shape or geometry to create a 3D object [1, 2]. This technology is highly potential in a broad range of application areas such as construction [3], aerospace [1], food [4, 5], and biomedical fields [6-8].

3DP possess many potential advantages over traditionally used technologies. Using this technology and aided by computer-based model design, complex structures and customized designs composed of multiple material constituents that cannot be achieved by conventional methodologies (e.g. internal structures design) can be fabricated [9]. In biomedical areas, 3DP technologies enable the design and fabrication of various shapes with a porous structure, such as porous scaffold (e.g. meniscus and bone), membranous, organs (e.g. nose and ear), or tissues (e.g. vascular and skin) [10-13]. Besides, materials with a porous structure could assist the delivery of nutrients to cells, which promote cell proliferation and differentiation and maintain cell activity for the regeneration of organs or tissues. In food areas, 3DP allows the manufacture of nutritional, healthy, and portable snacks as well as traditional food with novel shapes [14-18]. 3DP offers the possibilities to apply geometrical design for specific needs [18, 19]. In even wider areas (e.g. wastewater treatment and sensing) [20-22], compared with conventional or subtractive methodologies, 3DP technology allows the reduction of material waste and improvement in manufacture cost-effectiveness [1, 23, 24].

However, the widespread adoption of 3DP technologies has been restricted by the lack of processable, environmentally friendly, and printer-friendly materials to match the performance and

fabrication requirements [25]. Natural biopolymers including polysaccharides (e.g. starch, cellulose, alginate, pectin, carrageenan, chitosan, hyaluronic acid, and xanthan gum) and proteins (e.g. collagen, silk fibroin, gelatin, keratin, casein, whey protein, and soy protein) are widely available, biodegradable, biocompatible, even edible, chemically versatile, and inherently functional (e.g. gelation behavior, antimicrobial activity, and pH-responsiveness). Therefore, there has been a research focus on developing various high-performance and renewable biopolymers materials by 3DP with improved printing efficiency and accuracy for widened applications [27].

Biopolymer 3DP has been an emerging field, which can be demonstrated from an increasing number of related articles published from 2013 to 2020 (**Fig. 1**). A few reviews [25, 28-31] have been published on 3DP of biopolymers. For example, Liu and Zhang [9] have reviewed food 3DP with a particular focus on the effect of formulation including additives. Their review emphasizes that the material 3D-printing behavior is highly correlated with their rheological properties. Goel, Meher, Gulati and Poluri [28] have reviewed different 3DP techniques for biopolymer materials that can be applied for organ replacements and tissue engineering. More recently, a review on the 3DP of biopolymers by Shahbazi and Jäger [32] has covered materials, processes, and applications in pharmaceutical, bioengineering and food areas. However, the effects of printing parameters, pre-printing process, and the characteristics of biopolymers on the structure and architecture of 3D-printed materials, as well as a full array of demanding applications of 3D-printed biopolymer materials, have not been systematically reviewed before, which forms the intention of this article.

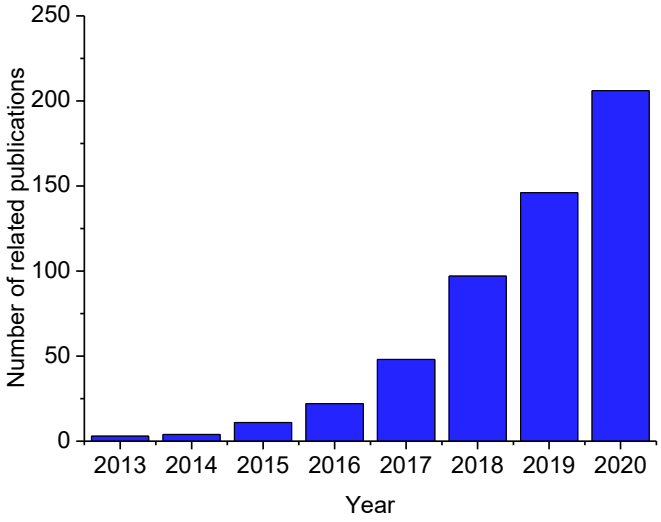

183

184 **Fig. 1** Statistical data of the research articles about the topic of biopolymers for 3D printing
185 techniques published during 2013-2019. The data was obtained from the ISI Web of Science
186 database on 28 February 2021. Search keywords used were “biopolymer”, “polysaccharide”,
187 “starch”, “cellulose”, “chitosan”, “chitin”, “lignin”, “hemicellulose”, “xanthan gum”, “κ-carrageenan”,
188 “hyaluronic acid”, “vegetable”, “fruit”, “alginate”, “pectin”, “protein”, “collagen”, “polyamino acids”,
189 “gelatin”, “whey protein”, “peptides”, “silk”, or “milk protein”, combined with “3D printing” or “additive
190 manufacturing”.

191

192 The quality and accuracy of the printed objects are determined by material properties (e.g.
193 mechanical strength, rheological properties, and compatibility), processing factors (e.g. printing rate,
194 nozzle diameter, nozzle movement rate, and nozzle height), and post-printing processes (e.g. baking,
195 drying, and crosslinking). A good understanding of these printing factors is important to achieve the
196 required printability of 3D-printed structures and printing precision and accuracy [9, 33]. The
197 research of 3D-printed biopolymer materials have been mainly focused on food and biomedical
198 application, but a wider application of these materials have also been reported such as wastewater
199 treatment and sensing areas [20, 21, 34].

This review surveys the latest literature in 3DP technology for biopolymers such as polysaccharides and proteins. The most commonly used 3DP techniques in the food and biomedical fields are discussed. Critical factors affecting the accuracy of 3D-printed constructs, including rheological characteristics, printing parameters, and post-printing processes are analyzed. The properties and applications of 3D-printed biopolymer materials in different applications are summarized (**Fig. 2**).

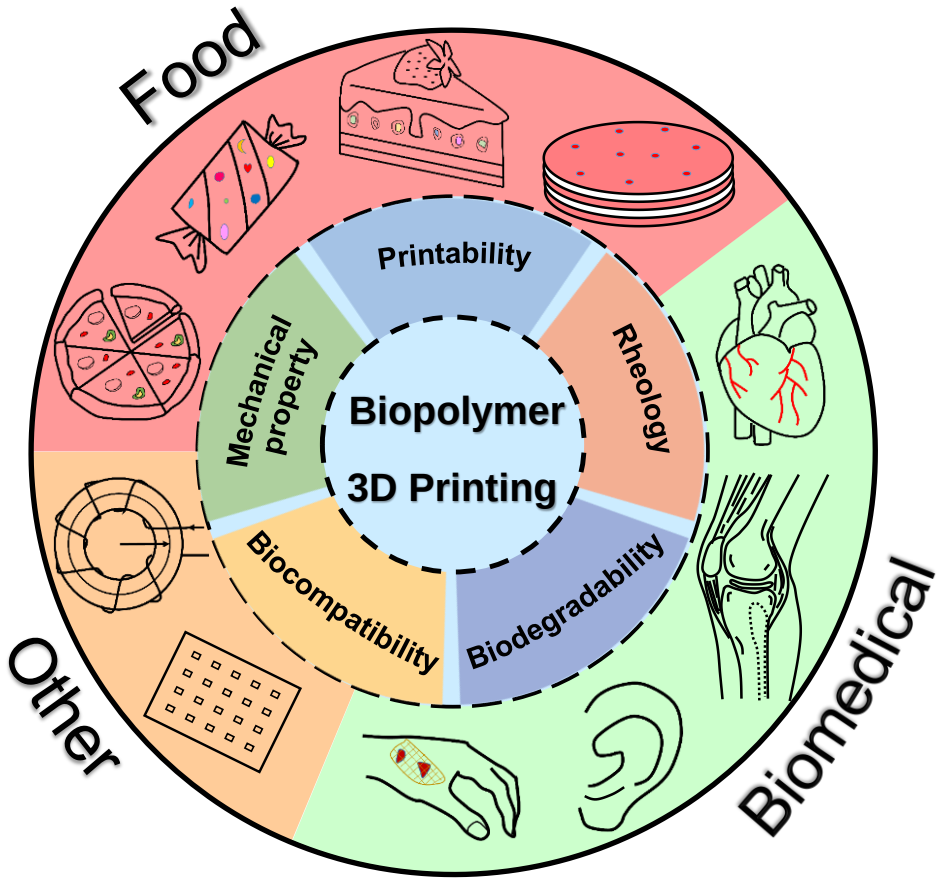

Fig. 2 Properties and applications of 3D-printed biopolymer materials.

2. Biopolymers for 3D-printed materials

Biopolymers are polymers that are directly extracted from plants [27, 29], animals [35], and microorganisms [36], mainly including polysaccharides and proteins (**Fig. 3**). These groups of biopolymers and their applications are summarized in **Table 1**. These biopolymers have received tremendous attention in materials development as they are widely available, low-/nontoxic, biodegradable, biocompatible, chemically versatile, and inherently functional. The biocompatibility of biomaterials influences the functional properties of 3D-printed tissues and organs. Cells need to adhere to the surface of implanted biomaterials to maintain their viability and proliferation, thereby promoting tissues regeneration [37]. Hence, the selection of biocompatible materials is crucial to the design of bioink formulations. In this section, the fundamental aspects of these different biopolymers are introduced, which can be linked to their processing and materials applications.

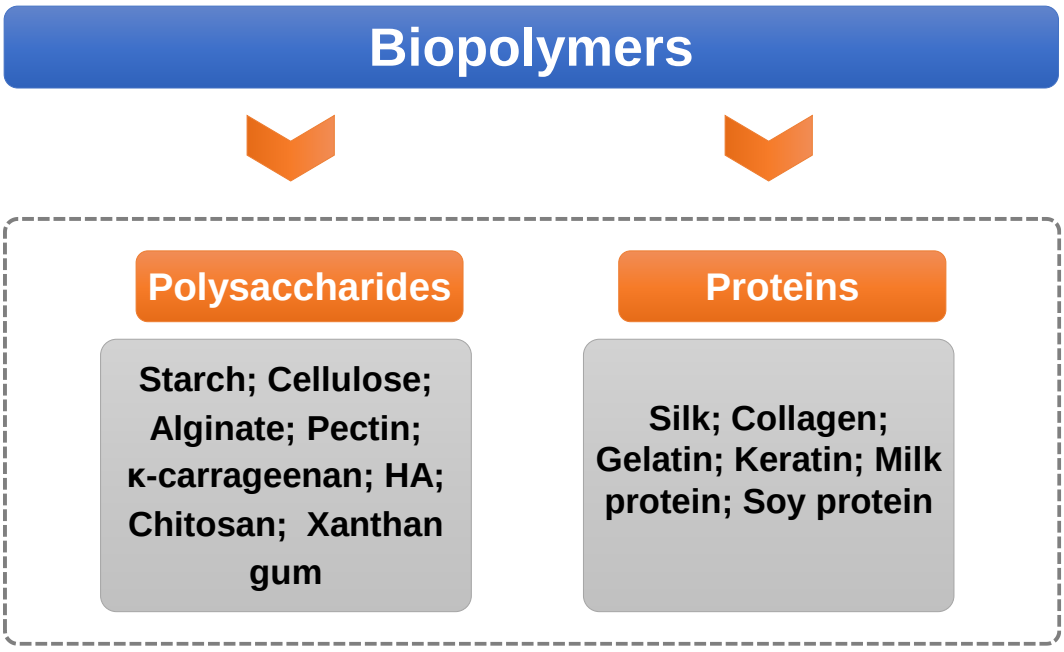

Fig. 3 Classification of 3D-printed biopolymer materials.

2.1. Polysaccharides

Polysaccharides are a class of biopolymers that are composed of monomer units connected via glycosidic linkages. A variety of polysaccharides such as starch, cellulose, alginate, chitosan, hyaluronic acid (HA), pectin, and carrageenan have been widely used owing to their widespread availability, low costs, and renewability [27]. They are naturally derived from various sources and have complex crystalline and amorphous structures caused by strong intra- and intermolecular hydrogen bonds within these polysaccharides.

2.1.1. Starch

Starch is isolated mainly from cereal, roots, and tubers of different origins such as maize, wheat, potato, cassava, and rice [38]. It is composed of two major constituent biomacromolecules, namely linear amylose with α(1,4)-linked D-glucose units and highly branched amylopectin with α(1,4)-linked D-glucose backbones and α(1,6)-linked branches [39-41]. These two biomacromolecules are organized to form starch granules with multi-scale structures [42-44]. The ratio of amylose/amylopectin strongly affects the physicochemical properties of starch such as gel formation and viscosity, which determine printability [45, 46].

Starch gelatinization is a process during which the ordered structure is changed into a disordered state by heating in water [47-49]. Starch gelatinization is accompanied by a series of physical changes such as granule swelling, the disruption of multi-scale order structures, and an increase in paste viscosity, allowing gel formation [47, 50]. The changes determine the functional properties of starch during processing [46]. In particular, compared with cereal starches, potato starch possesses

special gel characteristics (i.e. high peak viscosity and transparency), a slightly lower gelatinization temperature (48–67 °C), and a higher gelatinization enthalpy (10.1–11.4 J/g) [51]. Therefore, potato starch is usually used as a gelling agent and thickener in processing. Starch can be processed into films and hydrogels based on different processing methods (e.g. extrusion and film casting) [46, 52].

2.1.2. Cellulose

Cellulose is the most abundant polysaccharide on the Earth and its major sources are wood, cotton, algae, and bacteria [29, 53]. Cellulose is a linear biopolymer composed of glucose units by β(1,4)-glycosidic linkages [53] and cannot be melt-processed owing to their relatively high melt viscosity [54]. Also, cellulose is insoluble in water and common organic and inorganic solvents due to the preferential formation of intra- and intermolecular hydrogen bonds [55, 56]. Cellulose can only be dissolved in a few classes of solvent such as ionic liquids (ILs) [40, 57, 58] and *N*-methylmorpholine-*N*-oxide monohydrate (NMMO) [59, 60]. Therefore, cellulose is commonly modified to develop materials. Based on its abundant hydroxyl groups, cellulose can be modified via esterification, etherification, grafting, and crosslinking [61]. Cellulose can also be physically modified by radiation-induced treatments (e.g. electron beam and gamma radiation) to improve the accessibility of the solvent to promote the chemical modification, processing, or hydrolysis of cellulose [62]. After dissolution or modification, a series of cellulose-based materials can be fabricated, including hydrogels or aerogels [63-65], films [66], and composites [67]. Besides, several cellulose nanomaterials such as cellulose nanofibrils (CNFs) and cellulose nanocrystals (CNCs) have attracted great interest to develop bioink formulations due to their structural similarity mimicking the extracellular matrix (ECM) [27]. Moreover, the high mechanical properties of cellulose and cellulose

nanomaterials are a major advantage of maintaining product geometry [68, 69].

2.1.3. Alginate

Alginate is a linear polysaccharide existing as a component of the cell walls of brown seaweed or an extracellular polysaccharide of some bacteria. It consists of (1,4)-linked β-D-mannuronate (M-block) and α-L-guluronic acid (G-block) [70, 71]. Alginate can form gel via adding divalent cations (e.g. Ca^{2+}) [72, 73]. Sodium alginate is one of the most common water-soluble alginate and widely used in many areas due to its good gelling characteristic, high stability, thickening property, low cost and easy processing [74-76]. In particular in the biomedical area, alginate hydrogels have been prepared by various crosslinking methods (e.g. ionic crosslinking, covalent crosslinking, and thermal gelation) [70, 72].

2.1.4. Pectin

Pectin comes mainly from the wastes of vegetables and fruits (e.g. peel, core, and shell) and the wall of plant cells. It consists of α(1,4)-D-galacturonic acid units with different degrees of methylesterified carboxyl groups and rhamnogalacturonan [77, 78]. The applications of pectin as a gelling and thickening agent or stabilizer depends on the degree of methoxylation (DM), which can be categorized into high-methoxyl pectin (DM: > 50%) and low-methoxyl pectin (DM: < 50%) [79]. Low-methoxyl pectin gel is a food ink suitable for 3DP and generated through the formation of calcium ions crosslinks between free carboxyl groups [79].

2.1.5. Carrageenan

Carrageenan is a type of linear anionic heteropolysaccharide consisting of β(1,3)-sulfated-D-galactose and α(1,4)-3,6-anhydro-D-galactose (3-crosslinked-). They are obtained from marine red algae (*Rhodophyta*) [80, 81]. According to the degree of sulfation, carrageenan can be classified into three different types, namely, κ-carrageenan, ι-carrageenan, and λ-carrageenan [81]. In comparison with ι- and λ-carrageenan, κ-carrageenan possesses an excellent thermo-reversible gelling ability and self-sustaining capability and widely used in dairy products [81], active packaging [82], and drug delivery system [83].

2.1.6. Chitosan

Chitosan is an aminopolysaccharides obtained from the alkaline deacetylation of chitin, which is extracted mostly from the shrimp shells and other crustaceans in industry [84, 85]. Chitosan (in most cases, partially deacetylated) is composed of β(1,4)-2-acetamido-D-glucose and β(1,4)-2-amino-D-glucose units. It is insoluble in water but soluble in acidic aqueous solutions and has excellent gel-forming properties [86, 87]. Chitosan has been applied extensively in biomedical areas such as tissue engineering [88], drug delivery [89], and wound healing [90], not only because it has good biocompatibility, biodegradability and non-toxicity but because of its versatile biological activities such as antimicrobial activity and low immunogenicity [85, 89, 91]. Chitosan-based materials were fabricated into different forms such as gel [92], film [93], tablets [94], and capsules [95] by various methods (e.g. crosslinking, matrix coating, capsule shell, and solution casting) [85].

2.1.7. Hyaluronic acid (HA)

HA is a repetitive di-saccharide linked by β(1,4)-D-glucuronic acid and β(1,3)-*N*-acetyl-D-glucosamine [96]. HA is a non-sulfated glycosaminoglycan that is the main constituent of the ECM and is isolated from skin or joints [97]. HA has excellent biocompatibility, different elastic properties, and non-immunogenicity [98]. Therefore, HA has gained much attention in biomedical areas (e.g. bone regenerative therapy, wound healing, and drug delivery) [96, 99-101].

2.1.8. Xanthan gum

Xanthan gum is a high-molecular-mass extracellular polysaccharide produced by the microorganism *Xanthomonas campestris* [102, 103]. It is composed of a linear backbone of β(1,4)-linked D-glycosidic units with branched polymeric chains and has good water-solubility, excellent thermal stability, and biocompatibility [104, 105]. Xanthan gum solutions exhibit very high viscosity at low concentrations and have strong shear-thinning and rapid-recovery behaviors [104]. Therefore, it has been widely applied in the food [106], cosmetics [107], drug delivery [108], and construction industries [109].

2.2. Proteins

Proteins are natural polymers in which amino acid residues joined together through peptide bonds [110]. Proteins such as silk, collagen, gelatin, keratin, milk protein, and soy protein have been used in many fields because of their excellent biocompatibility, biodegradation, functional and nutritional properties [32, 111-113].

2.2.1. Collagen

Collagen is one of the most significant structural proteins, which is the major component of the ECM [28, 114]. Twenty-eight types of collagen have been identified, of which type I collagen is the most abundant (90%) in animals [114]. Collagen molecules are composed of three α-chains (two identical polypeptide chains α1 and one chain α2) intertwined to form a collagen triple helix [115, 116]. Collagen is mainly sourced from livestock, poultry, and fish, present in skins, bones, tendons, and cartilages [115-117], and plays an important role in tissue engineering. As an ECM protein, collagen has been widely considered as the most suitable biomedical material. However, due to the low viscosity and mechanical properties of printed collagen bioinks, the structure of the printed objects can hardly be maintained. Therefore, crosslinking is required to improve the mechanical properties of collagen. A serial of crosslinking methods such as physical (using e.g. high temperature while under vacuum, which is called dehydrothermal treatment) and chemical (using e.g. genipin and glutaraldehyde) modifications are usually used in the biomedical field [118-121]. Although physical crosslinking is a non-toxic method, it may not be enough to maintain collagen materials with high strength and uniformity. Therefore, it is common to combine physical and other crosslinking methods to improve the mechanical strength of collagen material [114].

2.2.2. Silk fibroin

Silk is a natural protein fiber produced by some arthropods such as silkworms and spiders [122]. As the main component of silk, silk fibroin (SF) consists of approximately two-thirds crystalline and one-third amorphous conformations in both one heavy chain of 390 kDa and one light chain of 25

342 kDa connected through a disulfide linkage [123, 124], resulting in low solubility in water or diluted
343 acid or common organic solvent [125]. Nonetheless, SF can be dissolved in ILs and concentrated
344 solutions of neutral salts such as LiBr and $CaCl_2$ [28, 123, 125, 126].

345 2.2.3. Gelatin

346 Gelatin is a fibrous protein derived polymer obtained from the partial hydrolysis of collagen.
347 The sources of gelatin are bovine (from bovine hides and cattle bones), porcine (from pig skins), or
348 fish (from fish skin) [127]. Gelatin has received much attention not only due to its unique properties
349 such as cold-setting, thermo-reversible with a melting point close to body temperature, but also it can
350 act as a gelling and thickening agent, which is easy to handle and use [128, 129]. Gelatin has a wide
351 range of viscosity depending on conditions (e.g. pH, temperature, source, and concentration) [127],
352 which allows it to be processed by 3DP [130].

353 2.2.4. Keratin

354 Keratin is a naturally derived polymer, classified into epithelial keratin and hair-cell keratin
355 [131]. It can be obtained from discarded wool, poultry feathers, and porcine hairs, and composed of a
356 central α-helical rod domain and variable terminal domains at its N- and C-termini [132]. Owing to
357 its characteristics such as excellent biocompatibility, biodegradability, and very low immune
358 reactions after implantation, keratin is widely used in bone, muscle, skin and nerve regeneration
359 [133].

2.2.5. Casein and whey protein

Casein (80%) and whey protein (20%) are the two main ingredients in milk protein [134, 135]. Casein is a family of related phosphoproteins with supramolecular structures (hydrodynamic diameter about 150–200 nm) ensuring its physical stability in milk. Casein produces a stable heterogeneous network structure when used in combination with hydrocolloids [136]. Moreover, acid and heat will cause gelation of casein micelles, forming a 3D network structure [137-139]. Whey protein is also a mixture of proteins. In contrast to casein, whey protein has a more-ordered structure. Gels can also form from whey protein due to the combination of non-covalent and covalent bonds between denatured proteins [140]. Besides, whey protein also possesses unique emulsification and thickening properties [141, 142].

2.2.6. Soy protein

Soy protein is a natural and excellent protein that mainly composed of albumins and globulins. It can be classified into three different forms, namely soy flour, soy protein concentrate (SPC), and soy protein isolate (SPI) [143]. SPI is a highly purified form of soy protein, with a minimum protein content of 90% and has excellent properties such as heat-induced thermoplasticity, biodegradability, and biocompatibility and, thus, has been widely used in various fields [143]. Soy protein can be formed in a variety of shapes and structures due to its thermoplasticity, which is suitable for 3DP [144].

3. Overview of 3D-printing technology for biopolymer materials

Various 3DP techniques have been discussed in detail elsewhere [145]. Whereas, this section

summarizes the most commonly used 3DP techniques specifically used for biopolymers, including inkjet printing, extrusion-based printing, stereolithography, selective laser sintering (SLS), and binder jetting (see **Table 2**). Printing material requirements and applications are also discussed in this section, while post-processing curing is discussed in section 4.3.2.

3.1. Inkjet 3D-printing

Inkjet 3DP process involves the deposition of ink droplets on a substrate followed by curing to realize 3D models. Inkjet 3DP has two working modes, namely continuous inkjet (CIJ) printing and drop-on-demand (DOD) inkjet printing [29, 146]. In CIJ systems, the liquid ink with low viscosity continuously passes through the nozzle and transforms into a droplet flow [147]. On the other hand, DOD printing is a non-contact technique as the printing is carried out using tiny ink droplets jetted with the aid of thermal actuators or piezoelectric (**Fig. 4**) [147]. Thermal DOD 3DP employs heat to generate vapor bubbles that are responsible for the forceful ejection of ink droplets. In piezoelectric DOD 3DP, electric stimuli are applied to a piezoelectric material to generate acoustic pulses to force the ejection of bioink droplets [145, 148]. Overall, this technique has gained much attention because of its ability to control the droplet uniformity, directionality, and size, as well as its higher printing speed and cost-effectiveness [149].

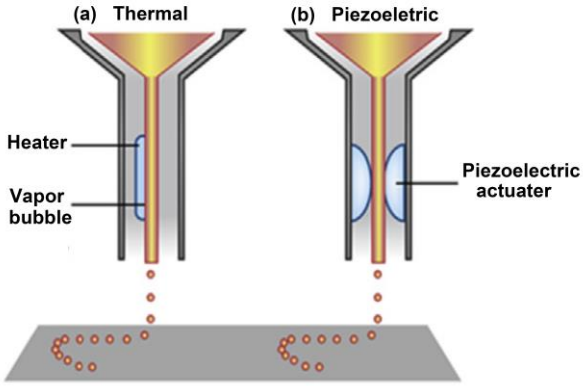

Fig. 4 Schematic diagram of a typical drop-on-demand (DOD) inkjet 3D printer. (a) Thermal actuator and (b) Piezoelectric actuation.

(a) and (b) are adapted from Ref. [150] with permission from Nature Publishing Group, Copyright 2014. The original was adapted from Ref. [151] with permission from Wiley-Blackwell, Copyright 2013.

3.2. Extrusion-based 3D-printing

Extrusion-based 3DP was first introduced by Crump [152]. While this technology was initially designed for prototyping plastic or metal, it is now widely used in the food and biomedical fields as well. Extrusion-based 3DP is suitable for dealing with a variety of fluids with a viscosity ranging from 30 $mPa{\cdot}s^{-1}$ to > $6{\times}10^{7}$ $mPa{\cdot}s^{-1}$ [150]. Based on the extrusion mechanism, extrusion techniques can be divided into pneumatic-based extrusion, piston-based extrusion, and screw-based extrusion [153], which all rely on the flow of a continuous ink to realize layer-by-layer deposition. Pneumatic-based extrusion can drive multiple heads while changing extrusion rates and is particularly suitable for low-viscosity materials [154]. Regarding piston-based extrusion, the extrusion rate can be adjusted easily by controlling the speed of motor movement [28]. Also, piston-based extrusion

414 allows high-viscosity inks to be extruded [28]. In screw-based extrusion systems, raw material is fed
415 into the cartridge and transported by a motor-driven auger screw, and the ink flows out through the
416 extrusion nozzle [154]. Irrespectively of type of extrusion of 3DP, the extrudate will be deposited
417 layer-by-layer on the print bed and then solidify, and the process repeats until the final 3D prototype
418 is obtained. Based on printing temperature, extrusion 3DP techniques can be divided into direct ink
419 writing (DIW) and fused deposition modeling (FDM) [155]. As shown in **Fig. 5,** during a DIW
420 process, a viscoelastic ink is squeezed out of the printing nozzle to form fibers at ambient
421 temperature, which can be deposited into a specific pattern as the nozzle moves [156, 157]. In
422 contrast, FDM is an extrusion-based technique in which a thermoplastic material is heated into a
423 semi-liquid or melt state and extruded from a movable nozzle onto a deposition stage [24, 157].
424 Compared with other 3DP techniques, extrusion-based 3DP is the most commonly used method as it
425 is simple and cost-effective and can manage a wide range of materials for manufacturing 3D objects.
426

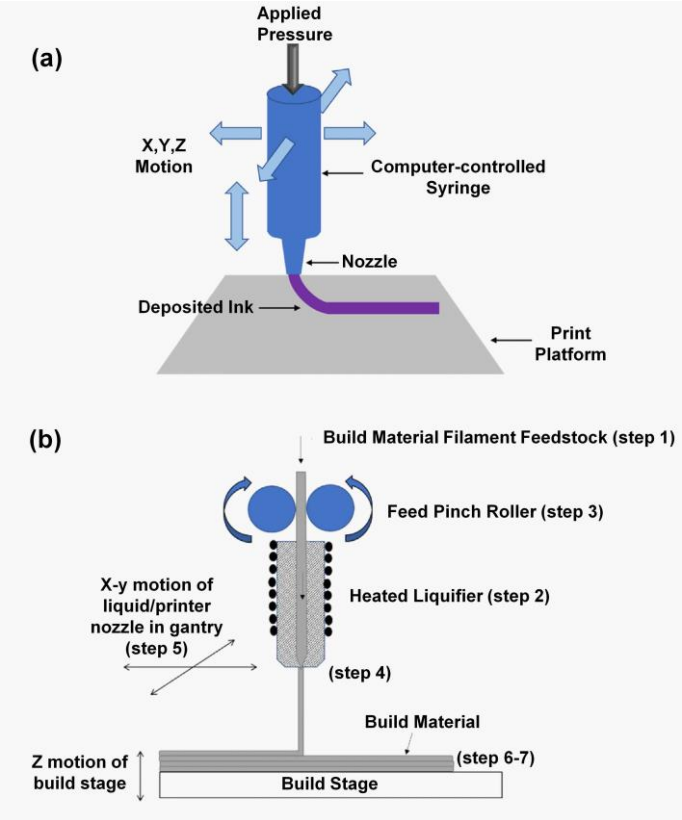

Fig. 5 Schematic illustration of extrusion-based 3DP process. (a) Direct-ink-writing (DIW) printer and (b) Fused-deposition-modeling (FDM) printer.

(a) is adapted from Ref. [156] with permission from Elsevier, Copyright 2019. (b) is adapted from Ref. [24] with permission from Elsevier, Copyright 2019. The original was adapted from Ref. [158] with permission from Emerald Publishing, Copyright 2014.

3.3. Laser-assisted 3D-printing

Laser-assisted 3DP techniques are based on light-dependent polymerization of polymers to fabricate 3D structures. Several light sources can be used for the polymerization of photo-curable polymers, such as UV, infrared, and visible light [28]. Stereolithography is one of the most commonly used laser-assisted printing techniques. It uses UV light to selectively cure the liquid resin via a layer-by-layer process (**Fig. 6a**) [159]. Compared with other 3DP techniques, the advantage of

stereolithography is that it can better control the dimensions and characteristics of the final printed 3D objects with high resolutions [160]. SLS, as shown in **Fig. 6b**, is also a laser-assisted printing technology that is a modified version of stereolithography. Unlike stereolithography using liquid resin, SLS employs an infrared/UV laser to melt a powder material at or above its melting point in order to selectively fuses the powder to form a layer of a desired shape [161].

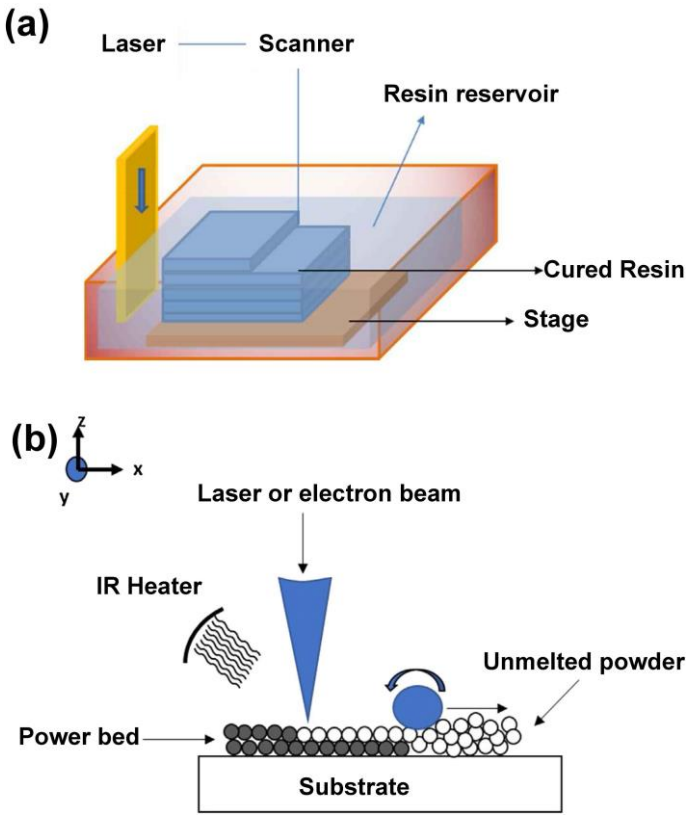

Fig. 6 Schematic illustration of the laser-assisted technique. (a) Stereolithography apparatus and (b) Selective-laser-sintering (SLS) apparatus.

(a) is adapted from Ref. [159] with permission from ACS Publications, Copyright 2017. (b) is adapted from Ref. [24] with permission from Elsevier, Copyright 2019. The original was adapted from Ref. [162] with permission from Elsevier, Copyright 2017.

3.4. Binder jetting

Binder jetting is a 3D inkjet printing technique first introduced by Sachs, Haggerty, Cima and Williams [163]. In this printing process, the powder is deposited layer by layer, and a binder material is filled between the layers (**Fig. 7**) [9]. The binder material should satisfy certain characteristics such as low viscosity, high binder content, and rapidly binding action in each layer so that the next layer of powder can be applied to it. The binding mechanism is caused by adhesive forces or chemical reactions between the powder and the binder. After printing, excess parts need to be removed and recycled for the next use. This technology can be used for fabricating complex 3D food structures and has the potential to produce food with varying flavors and textures [9, 163].

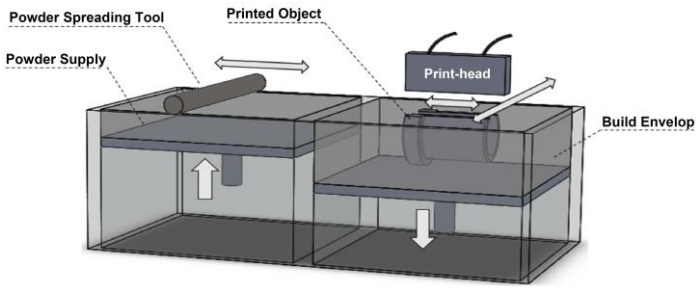

Fig. 7 Schematic illustration of a binder-jetting set-up.
Reproduced from Ref. [164] with permission from Elsevier, Copyright 2019.

4. Factors affecting 3D-printing precision of biopolymer materials

In this section, an overview of factors influencing 3DP processes for biopolymers materials is presented (**Fig. 8**). These factors are essential for creating ideal structures based on 3DP.

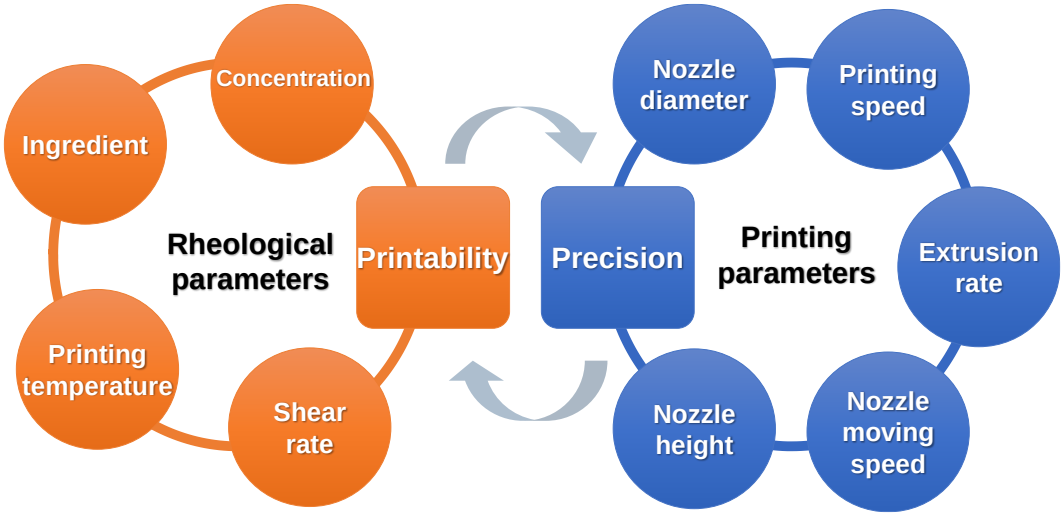

Fig. 8 Relationship between the rheological parameters in printability and printing parameters in precision.

4.1. Effect of rheological properties on printing behavior

Rheology is about the flow and deformation characteristics of materials under stress (τ). Rheological properties are crucial in controlling the resolution and shape fidelity of 3D-printed structures [165, 166]. Rheological measurements should be taken into account as a key part of material characterization to determine a series of printing conditions. **Table 3** summarizes the rheological properties and their applications of 3D-printed biopolymers.

4.1.1. Dynamic rheology

Polymers can be fluids or solids based on molecular mass and temperature and involve both viscosity and elasticity [167]. Storage modulus (G') and loss modulus (G'') represents the elastic solid-like behavior and the viscous response of a material, respectively [167]. They are important indexes to judge material viscoelastic behavior, which can be measured by oscillatory amplitude

sweep test [155]. In general, at low strain (amplitude), the small deformation is insufficient to disturb the internal structure (entangled and coiled state) of the polymer molecules as they have enough time to relax (elastic behavior, $G' > G''$). In this case, G' remains constant, as reflected by a linear viscoelastic region. As strain (γ) increases, the internal structure of molecules is destroyed resulting in liquid-like behaviors ($G' < G''$) [167]. In addition to G' and G'', loss tangent ($\tan \delta = G''/G'$) could better reflect whether a material is suitable for extrusion-based 3DP [168]. Inks with $\tan \delta > 1$ are predominantly viscous and can flow and be extruded; with $\tan \delta < 1$, the ink has an elastic solid-like structure [45, 169]. Markstedt, Mantas, Tournier, Martinez Avila, Hagg and Gatenholm [170] investigated the effect of different ratios of CNF/alginate (90:10, 80:20, 70:30, and 60:40, w/w) on rheological properties by frequency oscillation. Higher G' and G'' were observed with increasing CNF proportion in the bioink. Moreover, all bioinks showed $\tan \delta < 1$, indicating that the inks had solid-like structures [170].

Polymers particularly have viscoelasticity and their flow behaviors are highly affected by external conditions (e.g. concentration and temperature) and internal situations (e.g. molecular interaction). The viscoelasticity of extruded materials highly depends on ink concentration and printing temperature. For example, to improve the structural integrity of 3D-printed cell-laden bioinks, Berg, Hiller, Kissner, Qazi, Duda, Hocke, Hippenstiel, Elomaa, Weinhart, Fahrenson and Kurreck [171] mixed various contents of Matrigel (0, 5, 20, and 50%, w/v) with alginate (2%, w/v)/gelatin (3%, w/v) to form bioinks. G' increased significantly with the Matrigel concentration from 0% to 5% (w/v), and a further increase in the Matrigel concentration from 5% to 20% (w/v) resulted in a slight increase in G'. However, when the Matrigel concentration was increased to 50%

(w/v), G' decreased and even dropped below that of the sample with 5% (w/v) Matrigel [171]. Roehm and Madihally [172] investigated the effect of concentration and temperature on the rheological properties of 3D-printed chitosan/gelatin hydrogels. The results showed that, as the chitosan and gelatin concentration increased, G'' increased proportionally, especially at lower temperatures. Additionally, G' and G'' significantly increased with temperature increasing from 26 °C to 47 °C [172]. Liu, Chen, Zheng, Xie and Chen [33] showed that 3D-printed potato starch samples with 15–25% (w/w) concentration at 70 °C had preferable G', which can ensure the flowability of the ink during printing and the self-supporting strength after extrusion.

Very recently, computational fluid dynamics (CFD) was chosen as a method for describing the dynamic viscosity of printing material by the Bird-Carreau model. Guo, Zhang and Devahastin [173] studied the rheological properties of five kinds of coarse grains (black rice, Job's tears seeds, mung bean, brown rice, and buckwheat) via comparing CFD simulation and real printing experiments. This model shows a more accurate evaluation of the extrusion flow behavior of grain gels [173]. Thus, this method could allow a fast and accurate material evaluation for extrusion-based food 3DP [173].

By understanding the impact of rheological properties on printability, it is helpful to better guide the application of 3DP technology in biopolymers.

4.1.2. Steady rheology

Steady shear viscosity (η) is the most important rheological parameter in polymers for describing the flow. Polymer viscosity is sensitive to shear rate ($\dot{\gamma}$) as increasing the shear rate can promote disentanglement and orientation of polymer chains [167]. As a result, polymer inks generally have a shear-thinning behavior and exhibit reduced viscosity under higher shear rates [174]. The desired

viscosity should be both low enough to exhibit shear-thinning behavior for easy extrusion through the nozzle and high enough to form self-supporting layers for layer-by-layer deposition [175]. However, when the shear rate is low enough, the material does not exhibit shear-thinning behavior, which may cause the nozzle clogging; if the shear rate is excessively high, the ink viscosity is significantly reduced, resulting in insufficient mechanical strength to maintain the printed shape. Therefore, for high shape fidelity, the viscosity of the printing inks is an important consideration [176]. Besides, after extrusion, a short time for bioinks to return to the original state is also necessary for achieving ideal shape fidelity [174, 177]. Kim, Lee, Jung, Oh and Nam [178] observed that the viscosity of an alginate/κ-carrageenan/$CaSO_4$ hydrogel was increased with increasing κ-carrageenan concentration, with shear-thinning behavior. Besides, the recovery behavior of the alginate/carrageenan/$CaSO_4$ hydrogel at a low shear rate (0.1 s^{-1}) mimicked the stationary state with a recovery time of 60 s, while the recovery time at a high shear rate (100 s^{-1}) was just 10 s [178].

Based on the power-law relationship between $\dot{\gamma}$ and η, some researchers used the power-law index (n) and flow consistency (K) as the indicators of flow behavior to predict ink printability [34]. An ink exhibits shear thinning behavior with $n < 1$ and shear thickening with $n > 1$; when n approximates 1, the ink behaves like a Newtonian fluid [46, 176]. Liu, Bhandari, Prakash, Mantihal and Zhang [104] found that for a multicomponent gel system, n reduced significantly with the addition of xanthan gum and potato starch, especially at 35 °C and 45 °C, indicating more pronounced shear thinning behavior.

Yield stress (τ_y) is another very important variable affecting the rheological properties of inks. At low τ, the polymer materials are found to behave as elastic solids, while they tend to flow above a

549 critical value of τ, namely τ_y [176, 179]. According to Karyappa and Hashimoto [155], τ_y is
550 determined by η and shear stress (σ). With σ < a (the shear stress value at the intersection of the two
551 tangents of the curve, see **Fig. 9a**), the ink experiences elastic deformation but no flow occurs; with σ
552 ≥ a, the ink began to flow [155]. However, Liu, Bhandari, Prakash, Mantihal and Zhang [104]
553 indicated that τ_y is the crossover point of G' equal to G'' in stress sweep tests (see **Fig. 9b**). Suitable
554 τ_y is highly important for inks to squeeze out smoothly but stay with high shape fidelity. Pulatsu, Su,
555 Lin and Lin [180] found that the τ_y of cookie doughs was affected by recipe and higher τ_y was
556 favorable for maintaining the 3D shapes after printing. However, a higher milk content led to
557 reduced τ_y, resulting in samples being more liquid-like and could not hold the desired shape [180].
558 Liu, Chen, Zheng, Xie and Chen [33] demonstrated that increasing potato starch concentration from
559 10 wt% to 30 wt% significantly increased τ_y (from 44.41 Pa to 883.19 Pa), which could ensure
560 printing accuracy and strength. These results indicated that τ_y is strongly dependent on the content of
561 ingredients in the formulation [33].
562

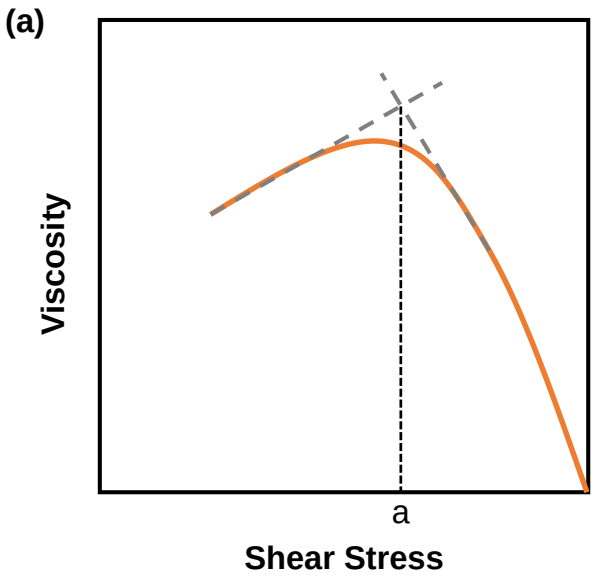

563

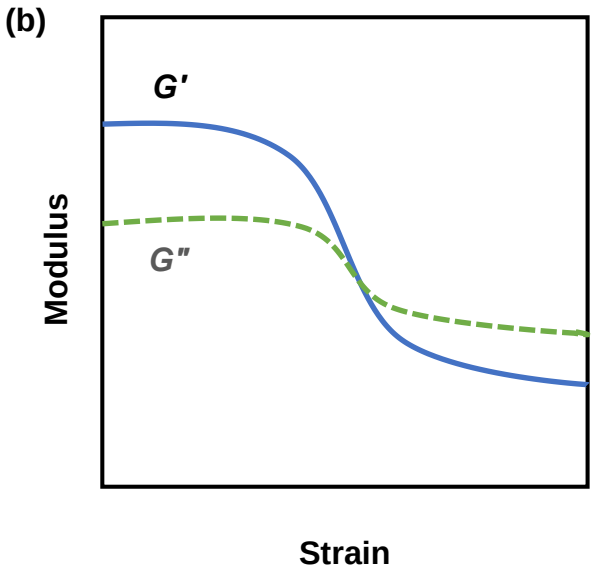

Fig. 9 Methods to determine yield stress: a) from a typical plot of viscosity as a function of shear stress using the intersection of two tangent lines; and b) the crossover point of elastic modulus (*G′*) equal to loss modulus (*G″*) in a strain sweep test.

For thermo-reversible behavior materials (such as κ-carrageenan), temperature also affects τ_y. Liu, Bhandari, Prakash, Mantihal and Zhang [104] found that the τ_y of an ink composed of κ-carrageenan (1 wt%)/xanthan (0.5 wt%)/potato starch (2 wt%) decreased from 553.1 Pa to 36.9 Pa with temperature increasing from 35 °C to 45 °C. However, for the κ-carrageenan (1 wt%)/xanthan (0.5 wt%) sample without starch, higher temperature led to the inks with liquid-like behavior, which could not form self-supporting layers [104].

4.2. Effect of printing parameters on printing behavior

There have been limited studies on the 3DP parameters for biopolymers and most of these studies were about food 3DP. The process of 3DP begins with the consideration of the printed shape, which is influenced by both printer- and material-related factors. Printer-related factors involve

579 nozzle diameter, extrusion rate, nozzle moving speed, and nozzle height. Material-related factors
580 generally include bioink formulation and printing temperature. These factors are discussed in detail
581 in the following subsections. By adjusting printing parameters (e.g. printing temperature, printing
582 time, and ink concentration and formation), the rheological characteristics of bioinks, good
583 printability, and shape fidelity can be regulated [181, 182]. **Table 4** summarizes printing parameters
584 for biopolymers with related applications. In general, a 0.41–2 mm nozzle diameter and a 2–70 mm/s
585 printing speed were found to be appropriate for 3DP of food constructs. For biomedical and tissue
586 engineering, 3D-printed structures can be achieved with a nozzle diameter of 0.15–0.6 mm and a
587 printing speed of 0.03–80 mm/s.

588 4.2.1. Nozzle diameter

589 Previous studies [183] demonstrated that nozzle diameter determined the accuracy and the
590 roughness of printed samples. Inks are required for extrusion through the narrow nozzle without the
591 occurrence of clogging [184]. A large nozzle diameter facilitates ink extrusion but may result in
592 relatively rough and poorly-structured printed models, while a small nozzle diameter means a longer
593 time to print [183, 185]. Therefore, an appropriate nozzle diameter is essential for 3DP. In general, a
594 0.41–2 mm nozzle diameter was found to be appropriate for the 3DP of food constructs. For 3D-
595 printed structures for biomedical and tissue engineering applications, a nozzle diameter of 0.15–0.6
596 mm could be suitable. Yang, Zhang, Bhandari and Liu [183] studied the influence of nozzle diameter
597 on the quality of 3D-printed constructs based on lemon juice gel (**Fig. 10a**). They found that a nozzle
598 diameter of 1.0 mm was better than other diameters (0.5, 1.5, and 2.0 mm), leading to a fast printing
599 process (about 200 s) to produce cylinder models with the highest resolution and accuracy [183].

Wang, Zhang, Bhandari and Yang [186] used fish surimi and NaCl to form a gel via extrusion 3D printing. The researchers optimized the printing parameters to prepare surimi gel with high accuracy and dimension. It was shown that the optimal nozzle diameter was 2.0 mm. The choice of suitable nozzle diameter is usually the first consideration for different formulations to be successfully printed [16].

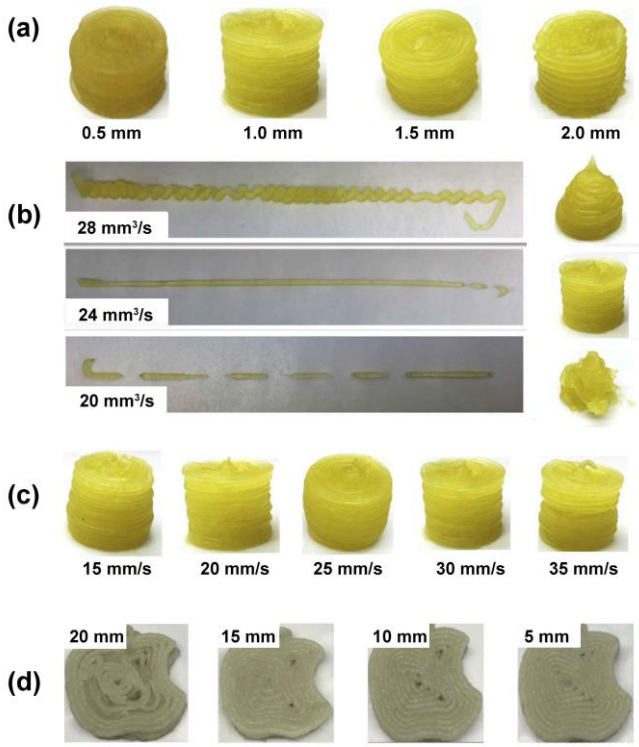

Fig. 10 3D-printed lemon juice gel and fish-surimi gel samples at varying printing parameters: (a) Nozzle diameter; (b) Extrusion rate; (c) Nozzle moving speed; (d) Nozzle height.
(a), (b), and (c) are adapted from Ref. [183] with permission from Elsevier, Copyright 2018. (d) is adapted from Ref. [186] with permission from Elsevier, Copyright 2018.

4.2.2. Extrusion rate

Extrusion rate influences printing accuracy as well. Yang, Zhang, Bhandari and Liu [183] further

investigated the relationship between extrusion rate and extrudate geometry for lemon-juice gels by line test and cylinder test at different extrusion rates from 20 mm^3/s to 28 mm^3/s (**Fig. 10b**). A high extrusion rate (28 mm^3/s) resulted in a greater overlap and a larger diameter of the printed filament and, thus, a higher amount of deposited material when 3D structures of significant height were being printed [183]. While a low extrusion rate (20 mm^3/s) induced decreased extrusion pressure, leading to extrudates to be droplets instead of continuous lines. The optimal extrusion rate was 24 mm^3/s, at which condition a smooth line and consistent lemon-juice gel could be obtained [183]. Wilson, Cross, Peak and Gaharwar [187] indicated that there was a positive relationship between cell survival rate and extrusion rate, and higher printing rates could reduce printing time that could improve cell survival, especially for manufacturing larger constructs.

4.2.3. Nozzle moving speed

Printing accuracy could also be largely affected by nozzle moving speed. Similarly, Yang, Zhang, Bhandari and Liu [183] also investigated the influence of nozzle moving speed on the quality of printed lemon juice gel (**Fig. 10c**). It was found that a too-low nozzle moving speed (15 mm/s) could result in deformation or collapse of the 3D-printed constructs under excessive deposition [183]. Besides, extruded-filament drag occurred when the nozzle moving speed was too high (35 mm/s), resulting in the breakage of the extruded slurry filament, which caused inaccuracies in the 3D-printed product [183]. Finally, the results revealed that 1 mm nozzle diameter, 24 mm^3/s extruded rate, and 30 mm/s nozzle movement speed were the optimal parameters to print 3D lemon-juice-gel samples [183]. Wang, Zhang, Bhandari and Yang [186] optimized the nozzle moving speed of surimi gel, indicating that the nozzle moving speed of 28 mm/s was most suitable with a higher resolution

and accuracy compared with other nozzle moving speeds (20, 24 and 32 mm/s). Moreover, they indicated that as other parameters remained unchanged, the critical height of the nozzle would be affected by nozzle moving speed [186].

4.2.4. Nozzle height

Nozzle height, the distance of the nozzle tip from the printed layer, could greatly influence the geometry of 3D-printed constructs [185]. The nozzle height (h_c) can be determined by the following equation [188]:

$$h_c = \frac{V_d}{v_n D_n} \quad (1)$$

where h_c is the optimal nozzle height (mm), V_d is volume extrusion rate (cm^3/s), v_n is nozzle moving speed (mm/s), and D_n is nozzle diameter (mm). For a given set of V_d and v_n, a nozzle height higher than h_c would result in a smaller filament diameter than that of the nozzle, and the space for the deposited slurry is too large to form the desired geometry of the extrudate. In contrast, a nozzle height lower than h_c would lead to a greater filament diameter than that of the nozzle and, as a result, the slurry forced out of the nozzle causes swelling of the extruded filament [188]. Thus, a suitable nozzle height is required for successful printing.

In a previous study [186], a series of nozzle heights for fish surimi gel was investigated. The results indicated the printed object could not be deposited due to the low nozzle heights, while the printed objects achieved the desired uniform shape with the highest fidelity when the nozzle height was 5 mm [186] (**Fig. 10d)**. For different materials, with h_c optimized, the desired shape and fidelity of printed objects could be maintained. Göhl, Markstedt, Mark, Håkansson, Gatenholm and Edelvik [189] investigated the effect of nozzle height for two inks namely 3 wt% CNFs/3 wt% alginate

(60:40, w/w) and CNF (4 wt%). The research revealed that a nozzle height of 0.5 mm was desired to achieve a better resolution for 4 wt% CNF [189]. However, for the other ink, the most favorable nozzle height was 0.3 mm or 0.4 mm, which allowed the retaining of the highest printing fidelity and resolution [189]. Wilson, Cross, Peak and Gaharwar [187] prepared a κ-carrageenan (2.5 wt%)/nanosilicate (5 wt%) bioink using a syringe-type 3D printer. They found that the fiber diameter was affected by nozzle height. At a nozzle height of 350 μm, the printed fiber diameter was 343 μm, which was close to the nozzle diameter (337 μm) and provided a high resolution [187]. However, when the nozzle height was 400 μm, the printed bioink could not be properly deposited on the substrate [187]. Thus, the optimized nozzle height could be the filament diameter, which is close to that of the nozzle diameter.

4.3. Pre- and post-printing treatments

4.3.1. Pre-printing treatment

Pre-treatment refers to processing the material before printing for maintaining the shape accuracy and stability of the final objects. Pre-treatment like microwave-assisted treatment [190], water-bath heating [191], pulsed electric fields [192], dry heating [193], and ultrasonication [194] can modify material properties and improve self-supporting performance. An example of microwave-assisted treatment is shown in **Fig. 11(a)**, in which case the effects of salt addition (20 ml, 3.5%, w/v) and microwave pre-treatment (power: 30, 50, and 70 W) on SPI-strawberry inks were investigated [195]. With the microwave power increased to 70 W, the final salted sample obtained the best self-supporting behavior and printing accuracy. Moreover, the addition of salt also promoted the shape

676 stability of the printed objects [195]. **Fig. 11(b)** shows a study of the effect of water-bath pre-
677 processing (temperature: 72, 76, 80, and 84 °C; time: 2, 4, 6, 8, and 10 min) on the printing behavior
678 of egg yolk-based food [196]. Among all the conditions, the egg yolk pastes heated at 76 °C for 8
679 min exhibited the most desirable shape after printing [196]. Jiang, Yao, Liang, Gao, Chen, Xia, Mi,
680 Jiao, Wang and Hu [194] used DIW to form lignin-based structural scaffolds. The lignin-based inks
681 were prepared by ultrasonication (in water) and crosslinking (using Pluronic F127) pre-treatment,
682 which softened the rigid structure of lignin and enabled the inks to be successfully printed with the
683 required stiff and self-supporting properties. Furthermore, the 3D-printed lignin-based structures
684 showed higher stability in water and under heat as well as UV-blocking performance compared to
685 printed cellulose structures [194].
686

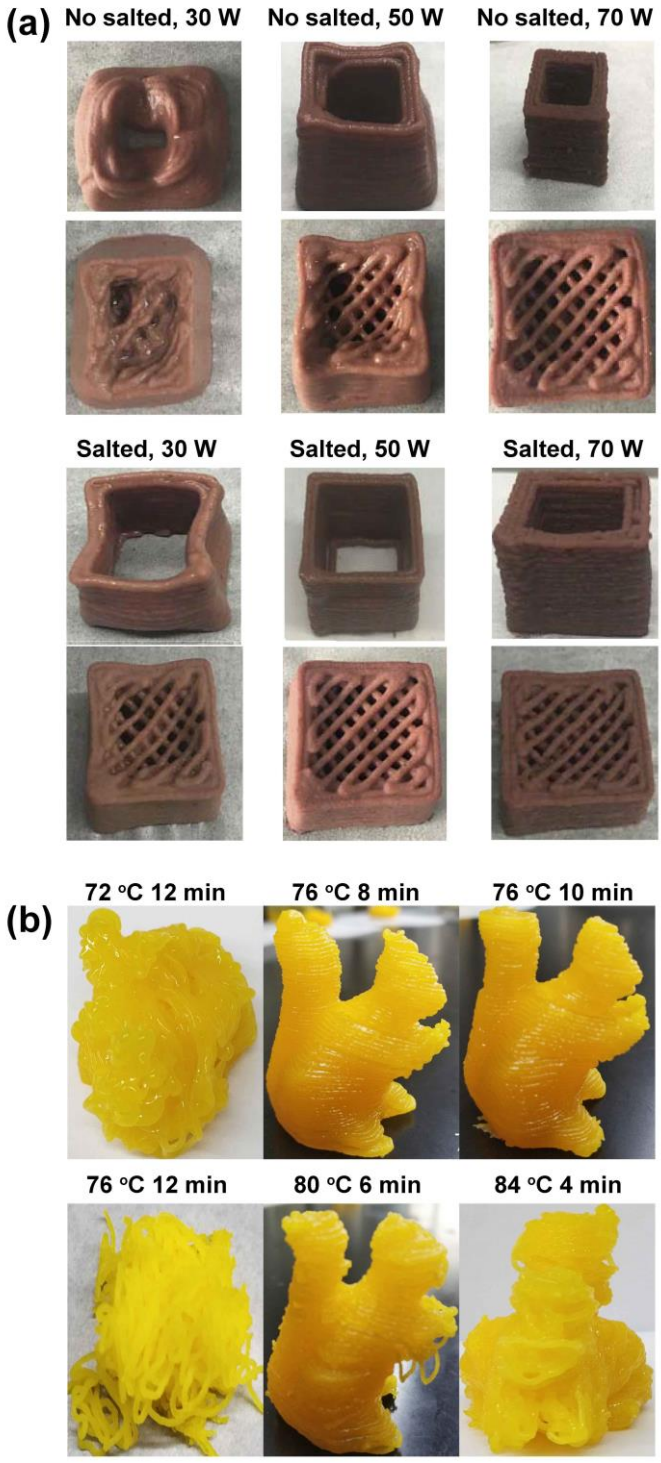

Fig. 11 Images of 3D-printed samples involved in different pre-treatments. (a) 3D-printed soy protein isolate (SPI)/strawberry by different microwave power without or with salt (3.5%, w/v). (b) 3D-printed egg yolk paste by different heat treatment.

(a) is adapted from Ref. [195] with permission from Elsevier, Copyright 2020. (b) is adapted from Ref. [196] with permission from Elsevier, Copyright 2020.

4.3.2. Post-printing treatment

After the 3DP process, post-printing treatment is usually required to retain the printed shape without collapse and to avoid changes in shape dimensions. Common post-printing treatment methods include baking, drying, and crosslinking.

4.3.2.1 Baking and drying

Baking could allow a series of chemical reactions to occur (e.g. protein denaturation and the Maillard reaction), which change the color, flavor, and texture of food [154]. Although baking may cause some changes in the product shape, the unique flavor produced in this process for baked food cannot be obtained by other processing methods; and the influence may be reduced by adjusting the ink formulation or processing parameters [15]. Pulatsu, Su, Lin and Lin [180] optimized the 3D-printed cookie dough recipe by a post-printing baking process. The result revealed that the best formulation was tapioca flour (100 g), sugar (37.5 g), milk (32.5 g), and shortening (62.5 g), which resulted in easier printing and high shape-retention capacity after baking [180].

Drying is also a commonly used post-printing treatment method, and the drying methods affect the shape stability of printed objects. Lille, Nurmela, Nordlund, Metsä-Kortelainen and Sozer [15] compared the effects of two different post-printing drying methods (i.e. oven drying and freeze-drying) on the shape stability and printability of 3D-printed mixtures of protein, starch, and fiber-rich materials, as shown in **Table 5**. Compared with the sample immediately after printing, further oven-drying at 100 °C led to partial shrinkage and color change, possibly due to heat-induced Maillard

713 reaction [15]. The freeze-dried samples were found to show greater printed-structure stability than
714 the oven-dried samples [15].
715 Håkansson, Henriksson, de la Peña Vázquez, Kuzmenko, Markstedt, Enoksson and Gatenholm
716 [63] investigated the effect of different drying processes (i.e. air-drying, air-drying with surfactants,
717 solvent exchange before drying, and freeze-drying) on 3D-printed structures based on CNFs, as
718 shown in **Fig. 12A**. While all four drying methods caused different degrees of shrinkage, freeze-
719 drying allowed the retaining of the desired complicated shapes and highly porous structure [63]. Li,
720 Dunn, Zhang, Deng and Qi [65] suggested that a DIW 3D-printed CNC aerogel subjected to freeze-
721 drying had minimal structural shrinkage or damage, suitable for application in tissue scaffold and
722 packaging. Therefore, freeze-drying could be a suitable drying method for 3D-printed cellulose-
723 based materials. Besides, Thibaut, Denneulin, Rolland du Roscoat, Beneventi, Orgeas and Chaussy
724 [197] investigated the effects of two different drying methods on cellulose-based paste after 3DP by
725 extrusion. Their results indicated that the printed objects treated by ethanol (95%) for 2 h had better
726 shape retention than that air-dried at 23 °C and 50% relative humidity for 48 h (see **Fig. 12B**) [197].
727 Moreover, Lam, Mo, Teoh and Hutmacher [198] indicated that for starch-based 3D-printed porous
728 scaffolds by a rapid prototyping technique, post-printing drying at 100 °C for 1 h could maintain the
729 integrity and increase the strength of the scaffolds.
730

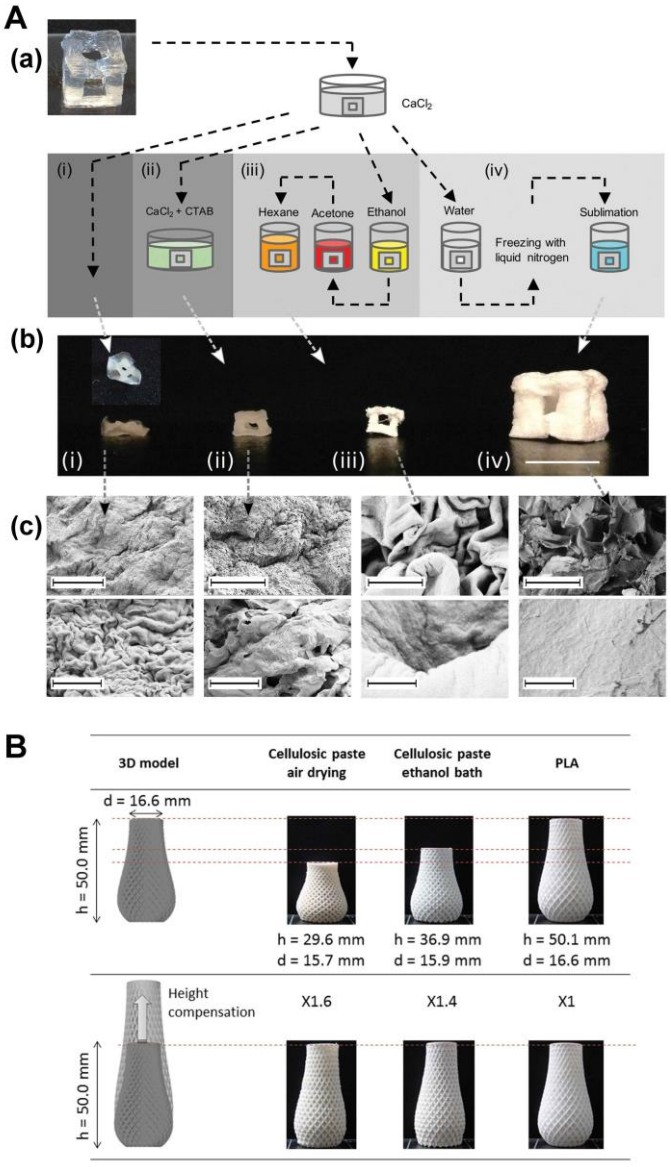

731

732 **Fig. 12** Drying method of 3D-printed structures. A) Solidification of 3D-printed cellulose nanofibril
733 (CNF)–based hydrogel. (a) CNF-based hydrogel after printing. (b) Images of dried 3D structures by
734 four different drying processes. (c) Scanning electron microscopy images of the 3D structure after
735 drying. B) 3DP of cellulosic paste–based spiral vase dried by air (23 °C for 48 h) or ethanol bath
736 (95% for 2 h).

737 (A) is reproduced from Ref. [63] with permission from Wiley-Blackwell, Copyright 2016. (B) is
738 reproduced from Ref. [197] with permission from Elsevier, Copyright 2019.

739

4.3.2.2 Crosslinking

Solidification enables the fabricated layers to form self-supporting platforms, which have sufficient strength to support the weight of its own and subsequent layers [199]. In particular with hydrogel-forming polymer, crosslinking is required to solidify the 3D-printed objects. Typical types of crosslinking include physical crosslinking, ionotropic crosslinking, enzymatic crosslinking, and photo-crosslinking (see **Table 6**). Moreover, crosslinking could occur before printing, during printing, and after printing. The pre-crosslinked bioink can provide sufficient stability to maintain its shape after printing, which facilitates the post-crosslinking step to fully cure the 3D-printed structure.

Physical crosslinking occurs by polymer chain entanglement or through chain interactions such as hydrogen bonding [200]. The cell-laden collagen scaffolds were crosslinked via forming hydrogen bonding with various tannic acid (TA) concentrations (0.1, 0.25, 0.5, 1, and 3 wt%) for 10 min and the results indicated that 0.5 wt% TA could significantly enhance the mechanical strength and biocompatibility of the 3D-printed porous cell-laden collagen structure [201]. Compaan, Song and Huang [202] developed an ink based on 5% (w/v) gelatin and 2% (w/v) alginate in phosphate-buffered saline (PBS), which was deposited in a 0.5% (w/v) gellan gum fluid gel to form a stabilized gelatin-based hydrogel 3D structure by cooling, during which physical crosslinking (aggregation of helical structures) would occur (**Fig. 13a**). Moreover, to avoid the use of toxic chemicals for crosslinking, a crosslinker-free bioink was developed using two different types of SF with self-gelling ability blended with gelatin [200]. A bioink network could be formed through entanglement between SF and gelatin (**Fig. 13e**), which possessed good print fidelity for application in cartilage tissue engineering such as the human ear [200].

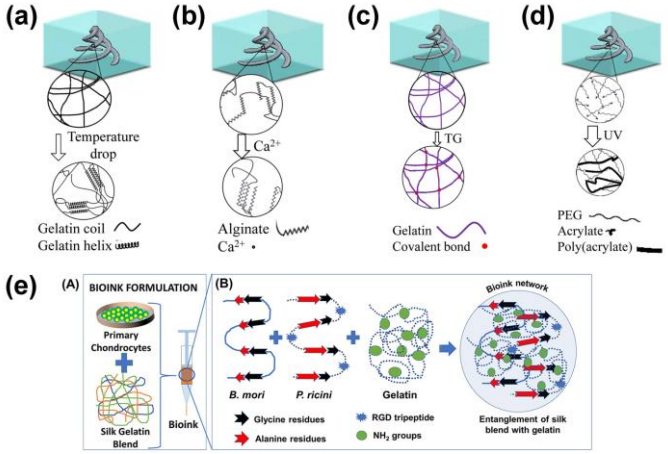

Fig. 13 Schematic diagram of different crosslinking methods: (a) Temperature-dependent physical crosslinking; (b) Calcium ionic crosslinking; (c) Enzymatic crosslinking; and (d) UV covalent crosslinking. (e) Schematic of silk fibroin (SF) and gelatin forming a gel ((A) Bioink formulation; (B) Entanglement and interaction of SF and gelatin).

(a), (b), (c) and (d) were reproduced from Ref. [202] with permission from ACS Publications, Copyright 2019. (e) is reproduced from Ref. [200] with permission from ACS Publications, Copyright 2019.

Although weak gels can be formed with physical interactions, these interactions are rarely strong enough for tissue engineering applications or layer-by-layer manufacturing. Therefore, the strength of hydrogels is usually enhanced by additional ionic interaction, electrostatic interactions, or chemical crosslinking [203].

Ionotropic crosslinking is an electrostatic interaction between polyanions and cations or between polycations and anions [203]. Ionotropic crosslinking can provide good self-healing ability, beneficial for many food and biomedical applications [203]. As shown in **Table 6**, $CaCl_2$ is a common crosslinking agent to maintain a 3D structure during printing. Appropriate concentrations of

$CaCl_2$ can induce crosslinking in a low-methoxyl pectin gel, which is a promising edible ink for the 3DP of food simulants. $CaCl_2$ solution was used to crosslink the low-methoxyl pectin gel based on two methods: a) 3D-printed pectin objects were incubated in a 300 mM $CaCl_2$ solution for 10 min [79]; and b) coaxial extrusion of a $CaCl_2$ solution (30–150 mM, outer flow) and pectin ink (15 and 35 g/L, inner flow) [204]. Compaan, Song and Huang [202] deposited the 3D-printed sodium alginate structure in a gellan gum fluid gel and then stabilized by ions crosslinking (Ca^{2+}) (see **Fig. 13b**).

Enzymes are usually used for pre-printing crosslinking to generate the intra- or intermolecular covalent bonds and improve the stability of protein-based materials [205, 206]. Typical enzyme crosslinkers are tyrosinase and transglutaminases for crosslinking SF and/or gelatin to form covalent linkages (**Fig. 13c**) [202, 207-209]. Chameettachal, Midha and Ghosh [207] demonstrated the applicability of tyrosinase as a crosslinking agent for SF/gelatin bioink for 3DP of cartilage constructs. The 3D-bioprinted constructs could extend cellular survivability *in vitro* and reduced hypertrophy, which makes tyrosinase crosslinked silk/gelatin hydrogels excellent candidates for tissue-engineering cartilage constructs [207]. Enzymatic crosslinking has a huge demand for hydrogel crosslinking for tissue engineering due to their mild reaction, high efficiency (7 to 20 min), and excellent biocompatible [210, 211]. However, enzymatic reactions require special substrates and expensive crosslinkers, which may limit their use in 3DP.

Taking advantage of rapid polymerization *in vivo* or *in vitro*, photo-induced (using UV or visible light) crosslinking strategies (**Fig. 13d**) have found many applications in the engineering of bone-equivalent tissue [212], cartilage [213], liver [119], and membranes [214]. The mechanism of photo-

crosslinking is that a polymer undergoes photolysis while being irradiated, that is, some bonds are broken, free radicals are generated, and activated molecules are bonded together, leading to a network structure [215]. When choosing a photoinitiator, its cytotoxicity, water solubility, and stability should be considered. Besides, the ink should have enough photo-responsivity [216].

The printed geometry can also be enhanced by other crosslinking agents such as TA [201], alginic acid [217], and *N*-hydroxysuccinimide/1-ethyl-3-(3-dimethyl aminopropyl) carbodiimide (NHS/EDC) [92]. Moreover, xylan was modified with different degree of substitution by tyramine groups to be crosslinkable, and then mixed with CNFs to form stable gels via crosslinking using horseradish peroxidase and H_2O_2 [218]. The resulting inks showed suitable mechanical strength and excellent printing properties [218].

5. Properties and emerging applications of 3D-printed biopolymer materials

Biopolymers have appealing properties such as biodegradability, biocompatibility, and non-cytotoxicity, making them potential for a broad range of applications such as food [79, 219], biomedicine [29], wastewater treatment [20], and electronics [21]. These different applications, which are linked to their properties and functionality, are discussed in this section, with a particular focus on food and medicinal areas.

5.1. Mechanical properties and structures of 3D-printed biopolymer materials

Mechanical properties are crucial in determining the sensory properties of food. **Table 7**

summarizes the textural properties of 3D-printed food, including compression strain (25–65%), hardness (1.407–1949.995 g or 0.02–36 N), springiness (0.222–0.98), cohesiveness (0.224–1.16), and gumminess (22.47–982.682).

The mechanical properties of printed objects could be largely determined by their structural characteristics [18, 220]. **Table 8** shows the pore size, porosity, infill level (the percentage of internal structure filling inside the printed object), and compression Young's modulus (*E*) of different printed objects for food applications. By varying these parameters, various patterns can be obtained. For example, Vancauwenberghe, Delele, Vanbiervliet, Aregawi, Verboven, Lammertyn and Nicolaï [221] designed four hexagonal honeycomb porous structures with different porosity and cell sizes and they found the *E* value of the honeycomb structure increased with increasing porosity but decreasing cell size. Liu, Zhang and Yang [45] fabricated cuboid-shape samples (32×32×16 mm) based on either strawberry juice gel and mashed potato with different infill levels. With infill level increasing from 40% to 100%, the printing time decreased from 614 s to 465 s and the *E* value and firmness increased significantly [45]. Liu, Zhang and Yang [45] also found that the hardness, cohesiveness, and gumminess of the printed material decreased with the height of each material layer (controlled via varying the number of layers). However, the variation of the internal shape structure (triangle, square, regular, hexagon, or round shape) at a 100% infill level did not alter the hardness and gumminess of the printed objects [45].

Table 9 provides the main mechanical characteristics parameters relevant to 3D-printed hard and soft tissues for biomedical applications. In biomedical areas, porous or customized scaffolds of various shapes are particularly important, because of the need to match the complex geometry of

defect sites. Besides, the mechanical properties of 3D-printed scaffolds should preferably match with the native scaffolds [222]. For example, for meniscus repair, Bandyopadhyay and Mandal [12] used an SF/gelatin-based bioink to fabricate scaffolds with different infill forms. Compared with the full-thickness tri-layered meniscus scaffold (147±4.8 kPa), the scaffolds with different filling shapes possessed different compression modulus: grid infill (188.5±25.4 kPa), concentric infill (152.4±31.1 kPa), and lamellar infill (130±6.5 kPa). All the scaffolds were still stable after 200 cycles of compression [12]. Thus, for SF/gelatin materials for tissue engineering, a suitable filling form should be selected according to the requirement of mechanical strength of 3DP objects.

Besides, 3D-printed scaffolds with suitable pore sizes have been considered as benchmarks in tissue engineering applications such as for skin, cartilage, and bone [223, 224]. **Table 10** lists the pore size, porosity, and mechanical properties of 3D-printed porous structures for biomedical applications. The pore diameter was 10–2125 μm and porosity 15.82–98%. Although these pores may reduce the mechanical properties of the scaffolds, they could benefit the nutrient supply to cells and the removal of metabolic waste out of the scaffolds in tissue regeneration. Moreover, macropores could promote cell migration while micropores could facilitate cell attachment and result in better mechanical properties [65, 225, 226].

5.2. Biopolymer 3D-printing for food applications

5.2.1. Starch-based food materials

Starch is widely used as a major component in food due to its gelatinization behavior [227]. For hot-extrusion 3DP, potato, rice and corn starches at a concentration of 15–25% were reported to

show shear-thinning behavior and self-supporting capability [228]. However, unmodified starches produce weak gels that could not maintain desired shapes. Consequently, modification of starch or addition of other gelling substances is necessary for obtaining strong gels based on starch (**Fig. 14A**). For example, Maniglia, Lima, Matta Junior, Le-Bail, Le-Bail and Augusto [52] modified cassava starch by pre-printing dry-heating treatment (DHT) to obtain 3D-printed hydrogels that displayed lower peak viscosity and better gel strength, higher resolution, and greater printability than the unmodified counterpart, with the hydrogel subject to DHT for 4 h showing the best results (**Fig. 14A(a)**).

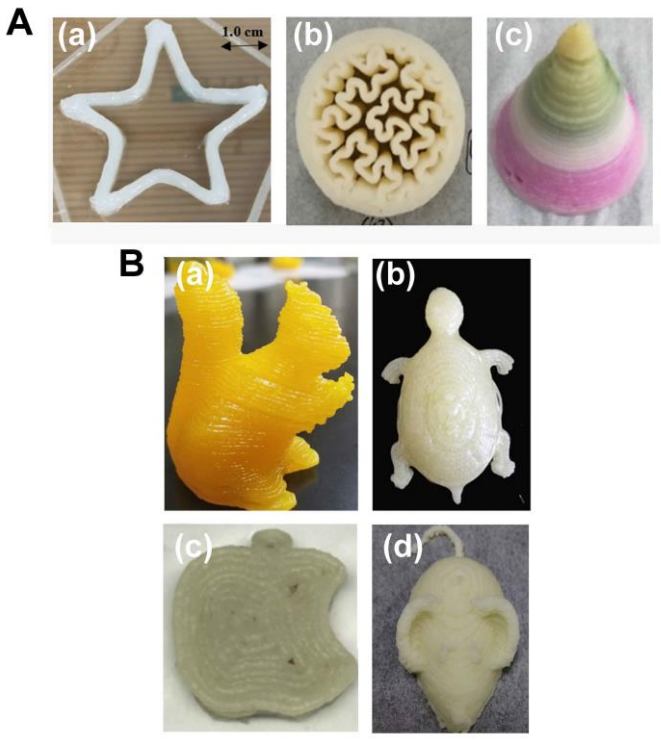

Fig. 14 A) 3D-printed starch-based constructs. (a) Cassava starch hydrogel produced with dry-heating treatment (DHT) for 4 h at 65 °C; (b) 3D-printed mashed potato construct with a "honeycomb" infill pattern (infill level: 40%); (c) 3D-printed mashed potato with color change 2.5 h after printing (the first layer was mashed potato with 15% potato flakes under acidic condition; the

second layer was mashed potato with 23% potato flakes under neutral condition; the third layer was mashed potato with 27% potato flakes under alkaline condition; and the last layer was purple sweet potato puree). B) 3D-printed protein-based constructs. (a) 3D-printed object from heat treatment (76 °C, 8 min) of egg yolk paste; (b) 3D-printed turtle model based on milk protein concentrate (MPC) gel (total protein contents: 450 g/L) after storage for 4 h; (c) 3D-printed surimi gels with 0.5 g/100 g NaCl; (d) 3D-printed mouse model based on MPC and whey protein isolate (WPI) (5:2 w/w). A): (a) is adapted from Ref. [52] with permission from Elsevier, Copyright 2020. (b) is adapted from Ref. [17] with permission from Elsevier, Copyright 2018. (c) is adapted from Ref. [229] with permission from Elsevier, Copyright 1300. B): (a) is adapted from Ref. [196] with permission from Elsevier, Copyright 2020. (b) is adapted from Ref. [230] with permission from Elsevier, Copyright 2019. (c) is adapted from Ref. [186] with permission from Elsevier, Copyright 2018. (d) is adapted from Ref. [111] with permission from Elsevier, Copyright 2018.

While adjusting biopolymer ink formulation generally could achieve desirable textural properties, Liu, Bhandari, Prakash and Zhang [17] reported that physical properties can also be tailored by internal construct design including changing the infill pattern (rectilinear, honeycomb, and Hilbert curve) and infill percentage (10, 40 and 70%) [17]. Specifically, using syringe-based DIW extrusion and 3:2 (w/w) κ-carrageenan/xanthan gum (1 wt% based on the weight of potato flake) mixed with potato flakes and boiling water (4:1, w/w) as the ink, the authors have successfully printed samples with a porous structure that matched the designated geometry (**Fig. 14A(b)**). This method could help to tailor-make samples with different internal shapes and texture requirements.

Recently, He, Zhang and Guo [229] reported multi-material dual-extrusion 3DP of purple potato puree/mashed potato (**Fig. 14A(c)**). As pH change and potato flakes could induce spontaneous discoloration of the dual-extrusion printed samples, they call the process “4D printing” (4DP). The

result indicated that the color change of the printed products relied on storage time and material distribution [229].

Besides, Severini, Azzollini, Albenzio and Derossi [14] observed that the addition of insects (*Tenebrio molitor*) into wheat flour dough improved the total essential amino acid and protein content of 3D-printed snacks. With insect enrichment increasing from 0 wt% to 20 wt%, the protein digestibility-corrected amino acid score (PDCAAS) and hardness of 3D-printed cereal-based snacks increased, beneficial for the manufacture of snacks with rich nutrition and crisp taste [14].

5.2.2. Protein-based food materials

For 3DP of food with high nutritional value, the printability of milk protein concentrate (MPC), edible insects, egg, and fish surimi have been studied (**Fig. 14B**) [14, 185, 186, 230, 231]. For example, according to Liu, Liu, Wei, Ma, Bhandari and Zhou [111], compared to pure milk protein, the presence of whey protein isolate (WPI) could improve the printability of protein food simulants and reduce the apparent viscosity and hardness of MPC paste while facilitating the printing process. Notably, MPC/WPI = 5/2 (w/w) was the most ideal ratio to prepare milk protein food simulants, which could be successfully extruded with better shape retention [111]. Thus, MPC and WPI could be promising protein materials for the development of personalized and digitalized nutritional food products.

Fish protein is also a good source of protein. Surimi is a high-protein, low-fat food ingredient, which is a promising food material. Wang, Zhang, Bhandari and Yang [186] used surimi and different levels of NaCl to make printable fish-surimi gels. Results showed that the addition of NaCl affected the printing accuracy of surimi gel. NaCl in surimi induced the dissolution and unfolding of

920 the myofibrillar protein, where interchain hydrogen bonding led to the formation of a stable and
921 elastic gel [232, 233]. The addition of NaCl at 1.5 g/100 g was helpful for the surimi gel to exhibit a
922 smoother surface and better match the designated 3D shape [186].
923 Besides milk and fish proteins discussed above, egg yolk, which consists of 68% low-density
924 lipoprotein (LDL) and 16% high-density lipoprotein (HDL) and has high nutritional value, was also
925 studied as a raw material for 3DP [196]. Specifically, a paste for printing was prepared by heating
926 egg yolk in a shaking water bath at 76 ℃ for up to 8 min. The 3D-printed object exhibits desired
927 printability (being easily extruded from the nozzle and maintaining refined shapes after printing) and
928 microstructure [196]. It was speculated that HDL played a particular role in the formation of a higher
929 viscoelastic egg yolk after heating [196].

930 ### 5.2.3. Dietary fiber-based food materials

931 Pectin-based hydrocolloids can be promising inks for 3DP of food because of its
932 biocompatibility, edibility, gelatability, and bio-functionalities [79, 234, 235]. For example,
933 Vancauwenberghe, Katalagarianakis, Wang, Meerts, Hertog, Verboven, Moldenaers, Hendrickx,
934 Lammertyn and Nicolaï [79] introduced 15–55 g/L pectin and 0–5 g/L bovine serum albumin (BSA)
935 (for forming pores) to fabricate pectin-based 3D-printed porous food simulants. The microstructure
936 and mechanical properties of the printed objects could be changed by varying pectin and $CaCl_2$
937 concentrations in the presence of BSA [79]. As shown in **Fig. 15A**, the cube and Gummy bear-
938 shaped objects were successfully produced. However, the process was still relatively slow due to
939 single-probe printing and required separate post-treatment with 300 mM $CaCl_2$ solution for 10 min
940 [79]. Based on the initial success in developing porous food, Vancauwenberghe, Verboven,

941 Lammertyn and Nicolaï [204] further investigated ways to speed up the manufacturing process and
942 avoid post-treatment for the 3DP of pectin-based porous objects. By coaxial extrusion, which
943 allowed gelation of the food-ink during printing, customizable pectin-based food was produced (**Fig.**
944 **15B**) [204]. The printed objects had *E* values similar to that resulting from simple extrusion 3DP, and
945 the object gelation could be accurately controlled. However, compared with simple extrusion 3DP,
946 coaxial extrusion led to printed objects with smaller volumes and lower interlayer adhesion, and it
947 required higher $CaCl_2$ concentration for binding the layers for enough mechanical properties [204,
948 236]. This work indicated that coaxial extrusion could be a promising alternative for bioinks
949 requiring post-processing, and the printing method largely determined printed-object properties
950 [204].
951

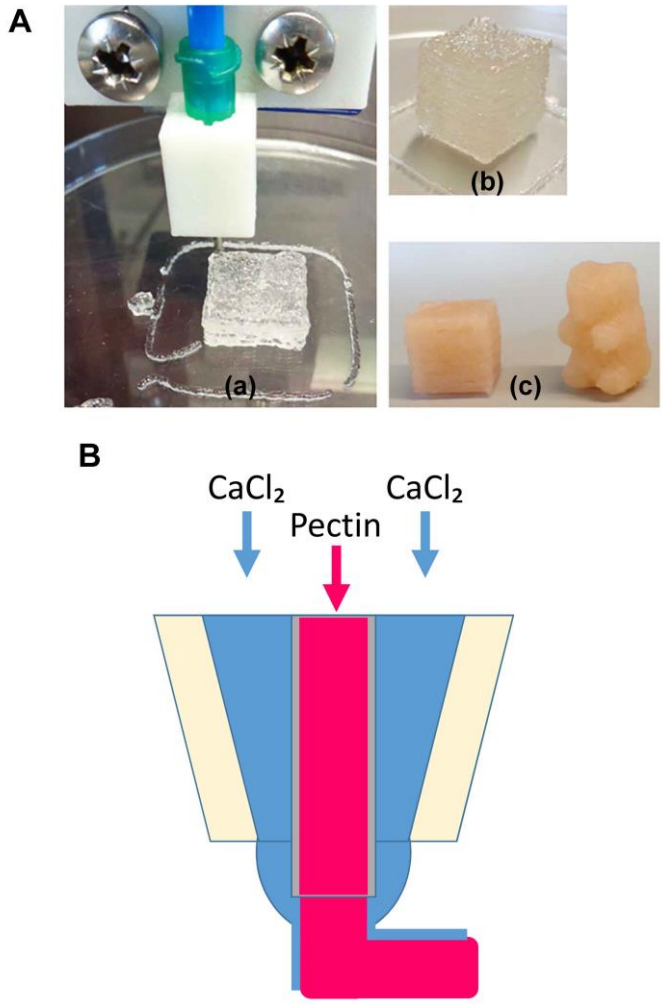

Fig. 15 A) 3D-printed pectin-based constructs. (a) 3D printing (3DP) of a cube 1.5×1.5×1.5 cm^3 prepared from 15 g/L low-methoxyl pectin +12.5 mM $CaCl_2$ + 50% (v/v) sugar syrup (total volume: 60 mL); (b) Picture of 3D-printed cube; (c) 3D-printed cube of 1.5×1.5×1.5 cm^3 and Gummy bear-shaped objects prepared from 55 g/L low-methoxyl pectin +12.5 mM $CaCl_2$ + 25% (v/v) sugar syrup + 5 g/L bovine serum albumin (BSA) + edible colorant (total volume: 60 mL). B) Schematic of coaxial extrusion.

(A) is adapted from Ref. [79] with permission from Elsevier, Copyright 2017. (B) is adapted from Ref. [204] with permission from Elsevier, Copyright 2018.

5.2.4. Plant-based food materials

Plant cell culture is a new technology for healthy plant-based food production [237]. This

964 technology could be introduced to 3DP for the manufacture of plant-based food with tissue structures
965 similar to those of real plants. This process involves embedding alive plant cells into matrix solution
966 (with culture medium) as bioink and extrusion at room temperature, followed by curing the 3D-
967 printed objects and culturing for a period [236, 238]. Vancauwenberghe, Baiye Mfortaw Mbong,
968 Vanstreels, Verboven, Lammertyn and Nicolai [236] fabricated 3D-printed plant tissue constructs
969 using lettuce leaf cells incorporating low-methoxyl pectin and BSA (**Fig. 16a**). The addition of pectin
970 improved the mechanical strength of the printed objects but caused a decrease in cell activity due to
971 the increased viscosity of the ink [236]. Moreover, compared with a pure pectin matrix, the
972 mechanical properties of the printed object was reduced due to the encapsulation of lettuce cells in
973 the pectin-based matrix [236]. Park, Kim and Park [238] used carrot cell dispersion and 4 wt%
974 alginate at varied ratios (1:2, 1:1, and 2:1, w/w) to print callus tissues for plant-based food
975 production (**Fig. 16c**). The gels with carrot cells/alginate ratios of 1:1 and 2:1 (w/w) showed high
976 viability and prolonged cell growth in a 35-day culture period. However, for these two 3D-printed
977 carrot-based gels (1:1 and 1:2, w/w), the mechanical strength decreased with cell growth until 28
978 days when it reached an equilibrium of 50% [238]. Therefore, these studies have demonstrated the
979 potential of the combination of 3DP and plant tissue regeneration for producing plant food simulants.
980 Besides, Lee, Won, Kim and Park [239] found that for a 3D-printed food-ink system of spinach
981 powder/xanthan gum/water (20:8:72, w/w/w), increasing the spinach powder particle diameter from
982 50 μm to 307 μm led to better printability and, thus, significant increases in porosity and mechanical
983 strength (**Fig. 16b**). This research could provide insights into the development of 3D-printed plant
984 tissue simulants with improved mechanical strength.

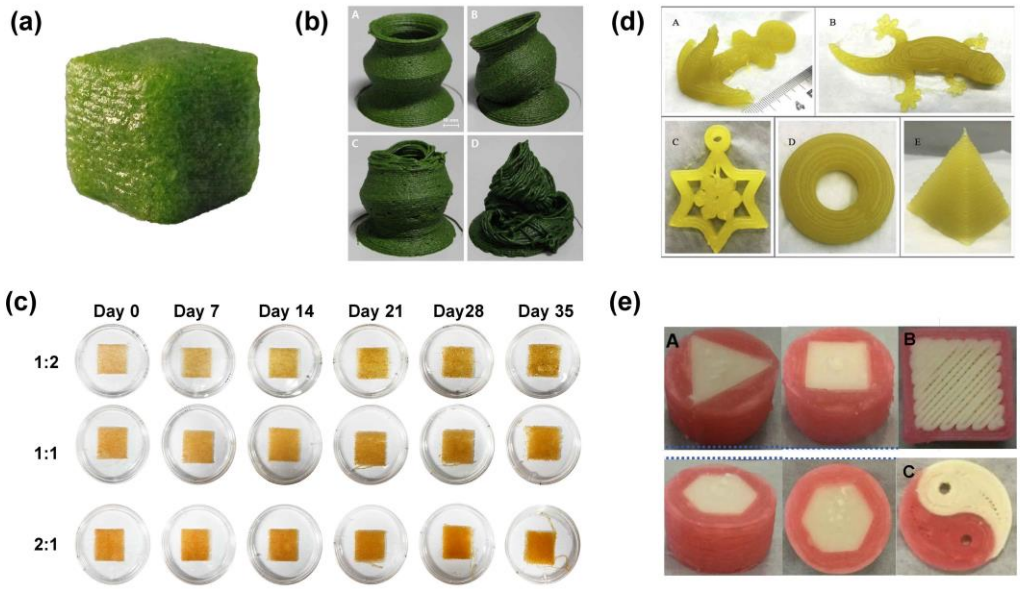

Fig. 16 3D-printed plant-based and fruit-based samples. (a) 3D-printed cube of 1.5×1.5×1.5 cm^3 with 15 g/L low-methoxyl pectin + 6.5 mM $CaCl_2$ + 2 g/L bovine serum albumin (BSA) + 50% lamb's lettuce cell suspension (pectin solution with cell / $CaCl_2$ solution = 1:1 (v/v), total volume 20 mL); (b) 3D-printed objects with various spinach powder particle sizes (A, 307 μm; B, 259 μm; C, 172 μm; D, 50 μm), samples made of spinach powder (20 g/100 g) + xanthan gum (8 g/100 g) + deionized water (72 g/100 g); (c) Cell growth of 3D-printed carrot-based samples with different cell concentrations during culturing for up to 35 days (carrot cell dispersion / alginate solution = 1:2, 1:1, and 2:1 (w/w)). (d) 3D-printed lemon juice gel products (15 g lemon juice/100 g starch); (e) 3D-printed objects of mashed potato/strawberry juice gel (17.5 g potato starch/100 g strawberry juice concentrate) (A, Samples with different inside shape structures; B, Infill percentage: 60%; C, Samples printed using a 2-nozzle 3D printer).

(a) is adapted from Ref. [236] with permission from Elsevier, Copyright 2019. (b) is adapted from Ref. [239] with permission from Elsevier, Copyright 2019. (c) is adapted from Ref. [238] with permission from Elsevier, Copyright 2020. (d) is adapted from Ref. [183] with permission from Elsevier, Copyright 2020. (e) is adapted from Ref. [45] with permission from Elsevier, Copyright 2018.

5.2.5. Fruit-based food materials

While fruit is generally consumed fresh, a series of deeply processed fruit products (e.g. dried fruits, fruit jam, and fruit yogurt) have also been developed. Direct 3DP of fruit-based food is challenging due to fruit characteristics such as high moisture and low viscosity [240]. Nonetheless, the printability of fruits could be improved by blending with starch [241]. Yang, Zhang, Bhandari and Liu [183] fabricated 3D-printed food objects of different shapes based on lemon juice mixed with different contents of potato starch (10, 12.5, 15, 17.5, and 20 g/100 g), which were steam-cooked for 20 min (**Fig. 16d**). They found that a lemon-juice gel with 15 g/100 g potato starch was suitable for DIW 3DP into the designed objects with the smoothest visual surface texture, best matching of the target geometry, minimal point defects, and no compressed deformation [183]. Besides, the effect of wheat starch content (15, 20, 25 and 30 wt%) on the printability of orange concentrate was investigated [240]. Among the four samples, wheat starch added at 30 wt% level led to the highest mechanical strength but poor extrudability [240]. Wheat starch added at 20 wt% level was found to result in suitable printability and the best mastication properties [240]. Thus, the 3DP of fruit concentrations could be a new process to develop novel food.

Liu, Zhang and Yang [45] investigated the printability of potato starch/strawberry juice concentrate by dual-extrusion 3DP (**Fig. 16e**). By varying the inside shape structure and infill percentage, 3D-printed objects with different textural properties could be obtained, which could become a new method to tailor textural characteristics of printed objects [45]. Besides, they also concluded that multi-material constructs with higher geometric complexity could be achievable through dual-extrusion 3DP [45].

5.2.6. Customization of snacks or traditional foods

With increasing interest in healthy food, there is a constant focus on customized snack products or traditional foods (**Fig. 17**). For example, to meet the daily energy requirements of children aged 3–10 years, Derossi, Caporizzi, Azzollini and Severini [5] developed a nutritional snack using 3DP technology, of which the formulation was composed of banana, white canned beans, dried non-fat milk, lemon juice, dried mushrooms, ascorbic acid, and pectin solution, containing 5–10% energy, calcium, iron and vitamin D. In this way, 3DP contributed to obtaining healthier food [5]. Besides, Lille, Nurmela, Nordlund, Metsä-Kortelainen and Sozer [15] fabricated healthy snacks with novel structures, consisting of 10 wt% cold swelling starch, 15 wt% skimmed milk powder, 60 wt% semi-skimmed milk powder, 30 wt% rye bran, 35 wt% oat protein concentrate, or 45 wt% faba bean protein concentrate. These snacks were rich in protein, starch, and fiber and low in fat or sugar, representing healthy food. Despite these limited efforts, the rheological and mechanical properties of various formulation ingredients for 3DP still need further research [15].

To investigate the effect of different components on the physical properties of baked dough, Yang, Zhang, Prakash and Liu [16] changed the proportion of ingredients as well as added water in traditional baked dough recipes. It was observed that the ratio of sucrose, butter, and flour exceeding a certain threshold would affect the printability of the printed material, making it impossible to form [16]. The optimized formulation of baked 3D-printed dough was icing sugar, butter, low gluten flour, egg, and water at a weight ratio of 6.6 : 6 : 48 : 10.4 : 29 [16]. These recipes helped to maintain the shape and quality of the baked 3D-printed dough, also providing a reference for practical production [16].

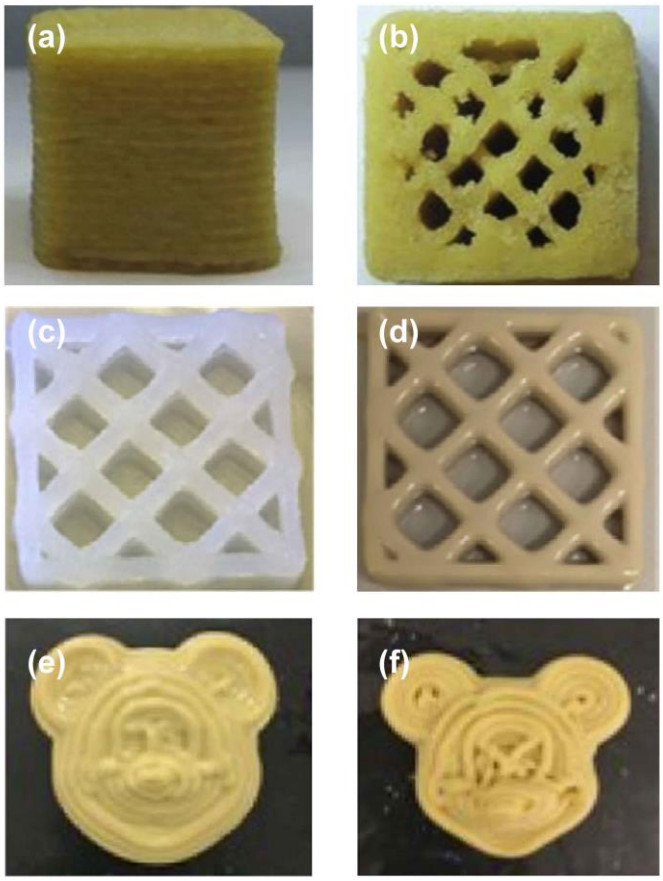

Fig. 17 3D-printed customized snacks or traditional food. (a) and (b) lateral and transversal views of the 3D-printed fruit-based snack (banana (73.5 wt%) + white canned beans (15 wt%) + dried non-fat milk (6 wt%) + lemon juice (3 wt%) + dried mushrooms (2 wt%) + ascorbic acid (0.5 wt%) + pectin solution (11 wt%)); (c) 3D-printed grid structure made of 1.5 wt% cellulose nanofibrils (CNFs) + 5 wt% starch; (d) 3D-printed grid structure made of 35 wt% oat protein concentrate (OPC); (e) baked 3D-printed dough with 3.3 g sucrose/100 g formulation; (f) baked 3D-printed dough with 9.0 g butter/100 g formulation.

(a) and (b) are adapted from Ref. [5] with permission from Elsevier, Copyright 2018. (c) and (d) are adapted from Ref. [15] with permission from Elsevier, Copyright 2018. (e) and (f) are adapted from Ref. [16] with permission from Elsevier, Copyright 2018.

5.3. Biopolymer 3D-printing for biomedical applications

Biopolymer 3DP has been devoted to customized applications in biomedical areas. This section covers the application of 3D-printed biopolymer materials in cartilage, bone and skin regeneration, wound healing, and vascular, neural and other tissue engineering applications.

5.3.1. Cartilage and bone tissue engineering

The damage to cartilage or bone is a common occurrence in the world. Unfortunately, the spontaneous repair capacity of cartilage is limited [242], especially for the elderly. Unlike cartilage, bones usually have the self-regenerative ability when injured, but they cannot regenerate and repair spontaneously in certain cases such as postsurgical defects or loss of tissues [243]. While various clinical treatments may possess long-term and complicated processes for cartilage and bone repair. 3DP technology has shown to be able to create complex structures to replace or repair damaged cartilage and bone tissues [244].

Cartilage and bone regeneration usually requires the restoration of favorable microenvironments (cells could stably adhere, growth, and differentiation) [245, 246] and mechanical properties by employing suitable scaffolds. Polycaprolactone (PCL) and polylactide (PLA) scaffolds have been widely used for cartilage and bone tissue engineering [247-249]. Nevertheless, their application are limited due to the undesirable cell adhesion, osteogenic differentiation, and mechanical properties [248, 250]. These characteristics can be improved through blending with biopolymers such as silk [248], alginate [251-255], and collagen [250, 256]. Using a screw extrusion 3DP process to fabricate 3D composite scaffolds [248], it was found that the addition of silk microparticles to PCL

1079 significantly enhanced the mechanical properties, improved cell metabolic activity and viability, and
1080 promoted cell proliferation [248].
1081 SF has been a promising biomaterial and gained much attention in the field of bone tissue and
1082 organ engineering [257, 258]. Under the different processing conditions, SF could be fabricated into
1083 different forms and structures such as film [123, 259], hydrogel [260], membrane [261], nanofiber
1084 [261, 262], and porous sponge [263]. While the poor mechanical strength of SF could restrict its use,
1085 additives such as collagen [264], gelatin [200, 265], silica [266], and hydroxypropyl methylcellulose
1086 [260] were shown to improve the mechanical strength of SF for cartilage and bone regeneration
1087 applications [267]. For example, it was reported that two kinds of SF were mixed with gelatin at
1088 37 °C to form SF/gelatin-based bioinks, which were used to produce 3D-printed cartilage tissue
1089 structures (meniscus and ear) with a syringe at 25 °C [12]. These 3D-printed scaffolds possessed
1090 excellent swelling, degradation, and mechanical properties, suitable for cartilage regeneration [12,
1091 200]. Moreover, tyrosinase-crosslinked SF-gelatin bioink possess the ability to regulate
1092 chondrogenesis and hypertrophy [207].
1093 However, most studies have focused on rheological properties, mechanical properties, and
1094 biocompatibility of SF hydrogel materials to address the requisites as biomedical materials [12, 200,
1095 224, 265]. Less attention has been paid to the dimensional stability of 3D-printed SF hydrogels.
1096 Recent research demonstrated that the addition of gelatin can effectively prevent the shrinkage of
1097 3D-printed SF hydrogels caused by the rapid formation of β-sheet structure [268].
1098 Alginate and gelatin are commonly used biopolymers for cartilage and bone repair. For the
1099 mixing of different biopolymers, 3D scaffolds are generally prepared by polymer cross-linking or

modification. For examples, to fabricated alginate/gelatin scaffolds for soft tissue regeneration, Chawla, Kaur, Joshi and Singh [269] used adequate infill (20% and 25%) and dual crosslinking (Ca^{2+} and UV light) to enhance the printability and mechanical properties of 3D-printed scaffolds. Schwarz, Kuth, Distler, Gögele, Stölzel, Detsch, Boccaccini and Schulze-Tanzil [270] prepared a 3D scaffold using oxidized alginate ($NaIO_4$ as an oxidant) and gelatin by enzymatic (microbial transglutaminase) and ionic (Ca^{2+}) crosslinking. The 3D-printed hydrogel exhibited good cell viability and long-term structures stability.

Compared with gelatin and alginate, decellularized extracellular matrix (dECM) is more representative of natural ECM [271]. Zhang, Liu, Luo, Zhai, Li, Zhang, Yuan, Dong, Zhang and Fan [272] prepared a crosslinker-free bioink by SF/dECM mixed with bone marrow mesenchymal stem cells (BMSCs). The resulting SF/dECM bioink were extruded into a meniscus structure with suitable mechanical strength and degradation rate, and the bioink was capable of promoting BMSCs proliferation and chondrogenic differentiation [272].

Collagen has been demonstrated to be the most common biomaterials for bone tissue engineering owing to good biocompatibility, high porosity, and benefits from mixing with other ingredients [273]. Moreover, Type I collagen is the major structural component in the ECM and plays an important role in cartilage bone tissue engineering [274, 275]. For instance, Kim, Lee and Kim [118] utilized collagen and genipin (as a crosslinking agent) to form a cell-laden 3D porous structure. The 3D collagen-based cell block showed higher cell viability, metabolic activities, and osteogenic differentiation compared with an alginate-based bioink [118].

Although collagen has become a promising biomaterial, its weak mechanical properties could

limit its applications. Crosslinking, composition, and pore structure have direct effects on the mechanical properties of collagen scaffolds. For example, some researchers used Type-I collagen/SF/de-cellularized ECM [264], fibrillated collagen/pluronic F-127 [276], and collagen/alginate [118, 275] to create 3D-printed porous scaffolds for bone tissue regeneration. Besides, Chen, Zhao, Zhang, Lu, Zhao, Fu, Sun, Zhang, Tu and Li [277] fabricated a 3D-printed scaffold based on crosslinking between heparin sulfate and collagen, which displayed excellent biocompatibility. Moreover, the mechanical properties of the 3D collagen/heparin sulfate composition scaffold were significantly improved compared with the collagen scaffold [277].

Nanocellulose is another natural polymer used as cartilage or bone tissue engineering materials, owing to its biodegradable, excellent mechanical properties, and biocompatibility [29, 197, 278, 279]. Generally, nanocellulose needs to be mixed with alginate [11, 170, 283-285] or HA [279, 284] or chemically modified (e.g. grafted by polyvinyl alcohol (PVA)) [286] to tailor bioink characteristics. Nguyen, Hägg, Forsman, Ekholm, Nimkingratana, Brantsing, Kalogeropoulos, Zaunz, Concaro, Brittberg, Lindahl, Gatenholm, Enejder and Simonsson [284] fabricated induced pluripotent stem cells (iPSCs) with different ratios of CNFs with alginate (CNF/alginate) or HA (CNF/HA). Compared to CNF/HA, the CNF/alginate (60/40, dry weight) bioink promoted hyaline-like cartilage tissue regeneration and cell proliferation, indicating that cells survived well after printing [284]. Therefore, the CNF/alginate bioink was suitable for 3D bioprinting of iPSCs to support cartilage production and, thus, repair damaged cartilage in joints [284]. Dutta, Hexiu, Patel, Ganguly and Lim [283] utilized CNCs to modify the mechanical stability and viscosity of an alginate/gelatin bioink. The CNCs/alginate/gelatin scaffolds (1%, w/v) exhibited enhanced

mechanical strength, cell proliferation, and bone formation [283]. The application of 3D-printed aerogel structures with biocompatibility and biodegradability in biomedical fields also represents a recent and rapid development trend [287]. Accordingly, there is an increasing interest in the production of cellulosic aerogels using microfibrillated cellulose (MFC) [288, 289], CNCs [290], or CNF [291-294]. For example, Li, Dunn, Zhang, Deng and Qi [65] used freeze-dried CNCs mixed with water by the DIW technique to produce CNC aerogel scaffolds (e.g. ear and nose) with aerogel and dual-pore (i.e. structural pores and random pores) structures. After freeze-drying, the 3D-printed structures showed negligible shrinkage or damage, and the porosity of the 20 wt% CNC gel could reach 90% [65]. Owing to their porous structures that could facilitate cell growth and proliferation, these scaffolds could enable more efficient cartilage tissue regeneration [65, 226].

5.3.2. Wound healing and skin regeneration

The development of ideal wound dressing and skin regeneration materials with excellent characteristics is currently a demand in wound therapy.

Chitosan is a suitable material for wound healing and resembles the glycosaminoglycans of ECM with guaiac and bacteriostatic functions [172, 296]. 3DP facilitated a precise control of the geometry of, and spatial distribution in, 3D chitosan structures; therefore, 3D-printed chitosan hydrogels were widely tested in skin repair and wound healing. For instance, Intini, Elviri, Cabral, Mros, Bergonzi, Bianchera, Flammini, Govoni, Barocelli, Bettini and McConnell [296] demonstrated that 3D-printed chitosan scaffolds had controlled and reproducible porous structure, accompanied by excellent biocompatibility and cell viability. Additionally, 3D-printed chitosan scaffolds were more beneficial to promote tissue regeneration and epidermis repair compared to traditional commercial

products [296] (**Fig. 18 a-g**). Hafezi, Scoutaris, Douroumis and Boateng [90] also fabricated a 3D-printed chitosan-based dressing crosslinked by genipin and plasticized by glycerol and poly(ethylene glycol) (PEG), which possessed the ability to adhere to a model surface and release model drugs, making it suitable for chronic wound healing applications. Similarly, Turner, Murray, McAdam, McConnell and Cabral [297] designed a novel blend bioink using peptide-functionalized succinylated chitosan/dextran aldehyde as a core laden with human umbilical vein endothelial cells and a gelatin methacryloyl (GelMA) shell laden with human bone-marrow-derived mesenchymal stems cells for the treatment of nonhealing or chronic wounds. The bioink was layer-by-layer deposited and UV-crosslinked to fabricate 3D constructs, which provided an appropriate microenvironment for cell growth, proliferation and differentiation, and showed about twofold skin wound healing rate *in vitro* that of the control [297].

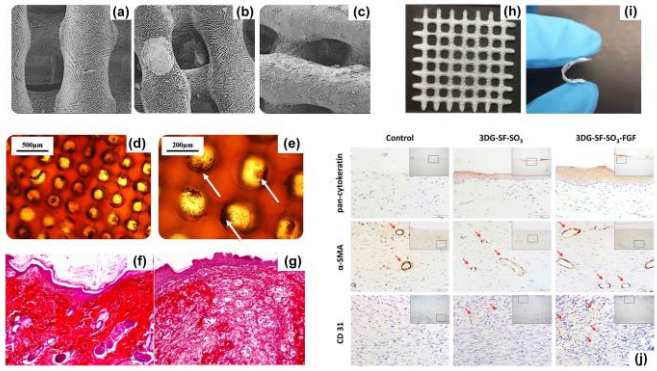

Fig. 18 Fibroblast and keratinocytes cells seeded together on a 3D-printed chitosan scaffold coated with a chitosan film at the base (the film coating was to improve the cell growth on the 3D-printed chitosan scaffold by keeping the cells inside). (a–c) Scanning electron microscope photographs of the 3D-printed chitosan scaffold without cells and with cells visualized after 20 days and 35 days, respectively; (d–e) Microphotographs under the transmitted light of an inverted microscope of cells 35 days after seeding on the 3D-printed chitosan scaffold at the base upon neutral red staining; (f–

g) Images of histological staining by hematoxylin and picrosirius red 14 days after wounds treated with the chitosan scaffold (f) or a commercial product (g); (h–i) Lyophilised 3D-printed chitosan/pectin hydrogel scaffold, which showed high flexibility; (j) Immunohistochemical staining of rat skin tissue sections to detect the expression of cytokeratin, spinal muscular atrophy (SMA), and CD31 after implantation 28 days after injury with scaffolds of a 3D-printed gelatin grid coated with sulfonated SF (3DG-SF-SO_3) and a 3D-printed gelatin grid coated by sulfonated SF with basic fibroblast growth factor (3DG-SF-SO_3-FGF). Scale bars = 50 μm.
(a–c), (d–e) and (f–g) are adapted from Ref. [296] with permission from Elsevier, Copyright 2018. (h–i) are adapted from Ref. [298] with permission from Elsevier, Copyright 2019. (j) is adapted from Ref. [299] with permission from Nature Publishing Group, Copyright 2017.

Pectin also exhibits valuable properties for wound dressing [300, 301]. A study by Long, Etxeberria, Nand, Bunt, Ray and Seyfoddin [298] indicated that 3D-printed chitosan/pectin hydrogels exhibited self-adhesion (bioadhesion strength between 86.5 g and 126.9 g), which is similar to marketed wound dressing products. Meanwhile, good mechanical integrity and flexibility could improve comfort in contact with the wound [298] (**Fig. 18h–i**). They demonstrated for the first time that the feasibility of 3D-printed chitosan/pectin hydrogel as a potential wound dressing candidate for lidocaine hydrochloride delivery [298]. The printed 3D scaffold enabled the controlled the release of lidocaine hydrochloride drug with cumulative release reaching 88–94% [298].

Alginate has excellent mucoadhesion properties. It can be blended with PEG [302], methylcellulose [303], and nanocellulose [304] to be applied for wound dressings. Ilhan, Cesur, Guler, Topal, Albayrak, Guncu, Cam, Taskin, Sasmazel, Aksu, Oktar and Gunduz [302] prepared a novel bioink using *Satureja cuneifolia* plant extract mixed with different concentrations of sodium alginate and PEG. The 3D-printed porous scaffold not only showed desired porosity and an excellent

antibacterial effect (against gram-positive bacteria), but also simulated cell proliferation, with the highest density on the 3rd day. Therefore, this composite scaffold is suitable for diabetic wound dressing application [302].

For skin regeneration, the blood vessel formation ability of 3D-printed scaffolds is critical for them to a play positive effect. Recently, Chu, He, Wang, Liu, Li, Wu, Chen and Tu [305] developed a proangiogenic 3D scaffold with peptide nanofiber hydrogel and UV-cured gelatin that was applicable for the regenerative repair of skin. The 3D-printed scaffold exhibited controlled porosity and pore size, which facilitated cellular migration, cell proliferation, and the growth of blood vessels [305]. Especially, the scaffolds containing 20% peptide hydrogel revealed the fastest blood vessel and dermal regeneration [305]. Besides, 3D-printed gelatin/SF composite scaffolds combined with fibroblast growth factor 2 (FGF-2) were shown to promote the epidermis and blood vessel formation in skin defects (**Fig. 18j**), which facilitated skin regeneration [299].

5.3.3. Vascular tissue engineering

Cardiovascular disease is a serious disease for the elderly, which usually shows complex pathogenesis related to the decline of vascular performance. For solving the issue of vascularization, there is an urgent need to create *in vitro* vascular tissue models [306]. 3DP methods such as extrusion and inkjet printing have been used to print vascular tissues based on collagen and sodium alginate [307-311]. For example, Xu, Chai, Huang and Markwald [312] prepared 3D zigzag-shaped cellular tubes and vessel-like structures using sodium alginate (2%, w/v) and cell suspension at a ratio of 1:1 (v/v) as bioink by inkjet printing technology. Lee, Lanzi, Haygan, Yoo, Vincent and Dai [309] fabricated a 3D-perfused functional vascular network structure consisting of two millimeter-scale

fluidic channels within a 3D collagen gel and a mixture of fibrin cells (endothelial cells and fibroblast) located between the channels. The vascular system enabled successful diffusion of 10 kDa dextran molecules into tissues through vessels [309]. Gao, He, Fu, Liu and Ma [313] described a method based on coaxial extrusion to fabricate blood vessel-like micro-channels using sodium alginate crosslinked in $CaCl_2$ solution (**Fig. 19B**). This is similar to the research of Gao, Liu, Lin, Qiu, Liu, Liu, Wang, Xiang, Chen, Fu and He [307], who used collagen and sodium alginate to form a bioink, which was used, by coaxial extrusion, to fabricate a 3D hydrogel structure for multi-scale circulation flow for vascular tissue engineering. The printed vascular network structure based on a solution of 4% (w/v) alginate hydrogel exhibited adequate mechanical strength (0.184±0.008 MPa) and cells survival over 90% after 7 days [307].

Liu, Zhang, Hu, Shen, Rana and Ramalingam [308] created composite bioinks based on sodium alginate and albumen to fabricate scaffolds via pneumatic-based single-probe extrusion 3DP. As shown in **Fig. 19A**, endothelial cells could adhere to the composite scaffold and maintain high activity. Furthermore, the scaffold could stimulate the sprouting of blood vessels and the formation of a new vascular network [308]. These results demonstrated that the 3D-printed albumen/sodium alginate bioink possessed vasculogenesis potential [308].

While 3D-printed large-sized blood vessels (>6 mm) have been used clinically, there are still some challenges in the replacement of small-sized vessel (<6 mm) [314]. Therefore, researchers have been trying to develop novel inks for small-sized blood vessels applications. For instance, Li, Qin, Peng, Chen, Nie, Liu and Song [315] fabricated 3D vessel constructs using gelatin, sodium alginate, and carbon nanotubes (CNTs) by $CaCl_2$ crosslinking, and the internal diameters of the bionic blood

vessel and the average thickness of the wall were 3 mm and 0.5 mm, respectively. The addition of CNTs effectively enhanced the mechanical properties of scaffolds but had little effect on cytotoxicity [315]. To mimic the native blood vessels, Zhou, Nowicki, Sun, Hann, Cui, Esworthy, Lee, Plesniak and Zhang [316] prepared a two-layer blood vessel by coaxial extrusion 3DP. The vessel wall was composed of a blend of GelMA/PEG-diacrylate/alginate/lyase laden with vascular smooth muscle cells, and Pluronic F127 was utilized as a temporary inner supporting layer and then removed to form a hollow-core tube-like vessel. Vascular endothelial cells in a 0.5% (w/v) gelatin solution (1×10^6 cells/mL) were injected into the lumen to form an inner layer of the vessel-like matrix. Small-diameter vessel replacements (1 mm of lumen diameter and 0.3 mm of wall thickness) prepared in this way showed steadily cell proliferation and good angiogenesis expression [316].

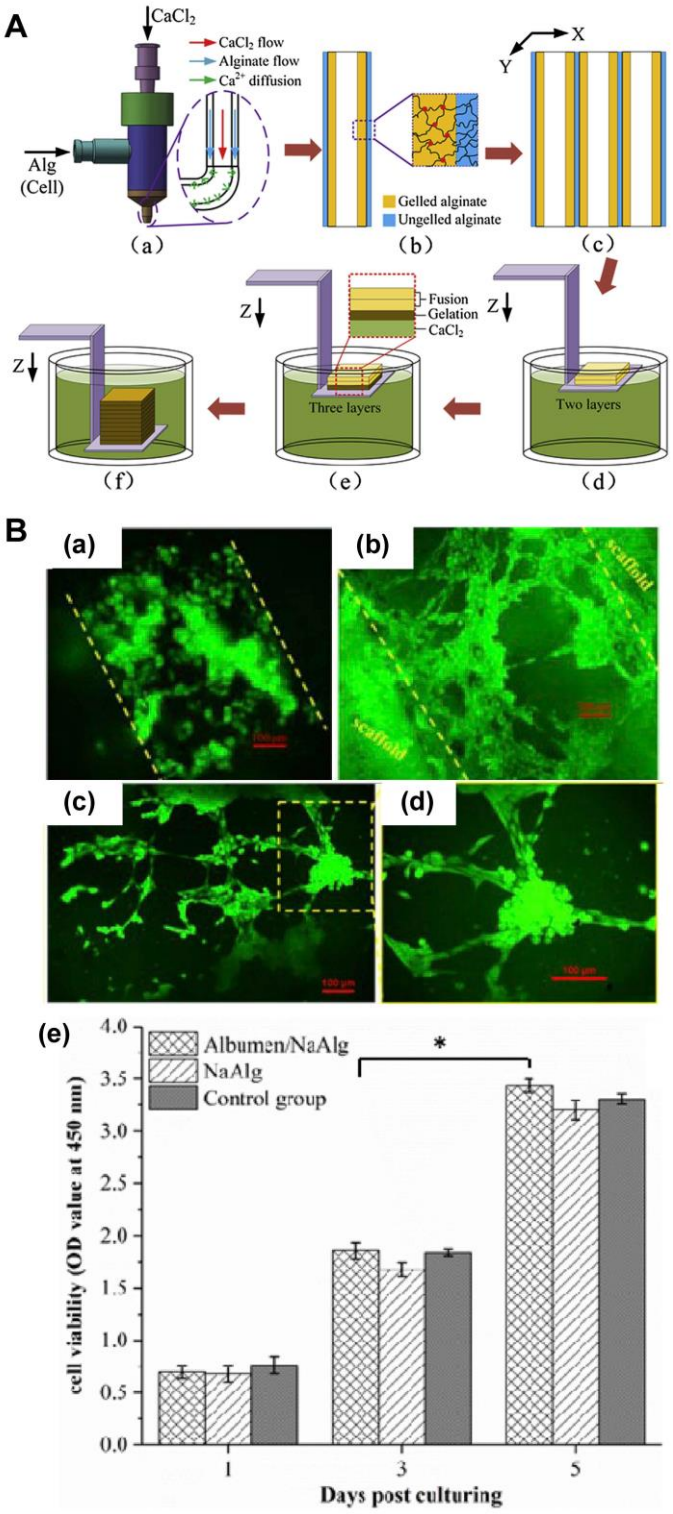

Fig. 19 A) Fabrication process for alginate 3D microchannel structure; and B) Fluorescent microscopy images of human umbilical vein endothelial cells (HUVECs) cultured on the 3D-printed albumen/sodium alginate scaffold for 4 days. (a) HUVECs on the surface of the 3D-printed albumen/sodium alginate scaffold; (b) Endothelial cells sprouting between filaments of the 3D-

printed albumen/sodium alginate scaffold; (c) Vascular network formation within the 3D-printed albumen/sodium alginate scaffold; (d) Magnified microscopic image of (c); (e) HUVECs viability after culturing 1, 3, and 5 days.

A) is adapted from Ref. [313] with permission from Nature Publishing Group, Copyright 2018. B) is adapted from Ref. [308] with permission from Elsevier, Copyright 2020.

5.3.4. Neural tissue engineering

Peripheral nerve injury causes the loss of motor and sensory capabilities [317, 318]. Unfortunately, the capacity of the nervous system for self-healing is inherently limited [319]. While autologous nerve grafting and end-to-end suturing are the most common treatment methods, they still have several limitations and unsatisfactory repair effects [317]. Biopolymer 3D nerve scaffolds based on gelatin [320], sodium alginate [321], CNFs [322], and collagen [323] have been developed for neural tissue repair. For examples, Wu, Li, Xie, Shan and Cai [321] fabricated a hydrogel-based scaffold with gelatin and alginate containing rat Schwann cells via 3DP, which possess higher levels of nerve growth factor release and mRNA expression of related factors (brain-derived neurotrophic factor, nerve growth factor, glial-derived neurotrophic factor, and platelet-derived growth factor) than 2D culture. Moreover, the 3D-printed scaffold provided a suitable microenvironment for cells growth and the survival rate of Schwann cells was 93.20% on day 7 [321]. Ye, Li, Yu, Xie, Wang, Zheng, Zhang, Xiu, Yang, Zhang, He and Gao [320] utilized GelMA hydrogels to prepare nerve guidance conduits for peripheral nerve repair. In their work, digital light processing was used as the printing method considering its high resolution and printing speed. The researchers optimized the printing parameters to fabricate a complex 3D bionic structure [320]. Result demonstrated the possibility of

using pure GelMA to prepare nerve guidance conduits, which support the survival, proliferation, and migration of neural cells [320]. Kuzmenko, Karabulut, Pernevik, Enoksson and Gatenholm [322] fabricated a conductive bioink based on CNFs (80 wt%) combined with CNTs (20 wt%), showing an electrical conductivity of 3.8×10^{-1} S·cm^{-1}. The conductivity facilitated neural tissue development and cell attachment on the scaffold surface [322]. Jiang, Liu, Chen, Dai, Niu, Dai, Chen and Zhang [323] utilized 3DP to form scaffolds with small volume and abundant pores. To overcome the poor mechanical properties and thermal stability of natural collagen, heparin sulfate was added into the system [323]. Results showed that the 3D-printed collagen/heparin sulfate scaffold not only boosted the regeneration of nerve fibers and vessels but also facilitated motor function recovery of hemiplegic limbs [323]. Additionally, the good physical properties, cytocompatibility, and suitable degradation rate of collagen/heparin sulfate scaffolds can also contribute to its application in traumatic brain injury [323].

5.3.5. Other tissue engineering applications

3D-printed biopolymer materials have been applied to even wider tissue engineering applications. For instance, Henriksson, Gatenholm and Hägg [324] used living cells in a bioink of nanocellulose and HA to construct cell-laden structures. Compared with standard 2D culture systems, the 3D-printed scaffold displayed high cell activity (95%), increased lipid accumulation and the adipogenic gene expression of adipocytes. Therefore, nanocellulose and HA might be promising 3D-printable materials for adipose tissue engineering [324]. Sk, Das, Panwar and Tan [325] prepared a novel bioink using gelatin, glycidyl methacrylate (GMA), and human hepatocytes to form a photo-crosslinkable 3D-printed hydrogel scaffold, which improved liver cell differentiation, viability and

proliferation. A 10-fold increment in the number of liver cells was found after 14 days of culture. Moreover, there were a higher cell number and better proliferation in the gelatin/GMA hydrogel construct than in the GelMA scaffold (control). This indicated that this photo-crosslinkable gelatin/GMA hydrogel material is suitable for liver tissue application [325].

Keratin is a natural renewable material resource derived from human hair. The novel keratin-based materials mainly used in the field of tissue engineering and regenerative medicine [133]. It was reported that 95:5 (w/w) α-keratin/γ-keratin was dissolved in PBS to fabricate 3D-printed keratin constructs with UV crosslinking, which displayed an appropriate swelling degree (16.80–18.48), mechanical properties (5.49–15.45 kPa), and cell metabolic activity (90.9–96.3%) [133].

Starch has also been used to fabricate tissue scaffolds by 3DP. A study by Lam, Mo, Teoh and Hutmacher [198] demonstrated that 50 wt% cornstarch, 30 wt% dextran, and 20 wt% gelatin dissolved in distilled water could be used to create porous cylindrical scaffolds by 3DP. Subsequently, the printed scaffolds were soaked in water for 10 min and dried at 100 °C, which showed suitable mechanical properties (stiffness of 0.059–0.102 MPa), useful in tissue engineering [198].

5.4. Biopolymer 3D-printing for other emerging applications

In addition to applications in food and biomedical fields, 3DP technology could also enable biopolymers to be used in even wider applications such as for wastewater treatment and sensing (**Table 11**) [63].

The bacteriostatic effects of chitosan and the photocatalytic activity of TiO_2 can effectively degrade antibiotic pollutants in wastewater [85, 326, 327]. Bergamonti, Bergonzi, Graiff, Lottici,

Bettini and Elviri [20], for the first time, fabricated 3D-printed chitosan grid scaffolds using chitosan (6%, w/v) as a matrix and TiO_2 (1%, w/v) as a filler for wastewater treatment. The 3D-printed chitosan scaffolds can be used as a reusable substrate for the photocatalytic degradation of amoxicillin in wastewater because it allows designed geometries to meet actual shape and size requirements, thus causing a very high area/volume ratio, which is a key parameter for amoxicillin photocatalysis [20]. Hydrogel-based biopolymers are favorable choices for wastewater purification as they can be used to remove many pollutants. Shahbazi, Jäger, Ahmadi and Lacroix [328] reported that an alginate/nanoclay ink formed a crosslinked network upon electron beam irradiation (5–60 kGy) before 3DP was favorable for maintaining 3D-printed structure, and no post-crosslinking was required. The 3D-printed hydrogels exhibited a fast adsorption speed and high adsorption capacity for effectively removal of various heavy metal ions (e.g. Pb^{2+}, Fe^{3+}, Cr^{3+}, Co^{2+}, and Ni^{2+}) pollutants from wastewater [328].

Some biomedical equipment components (e.g. pacemakers and cochlear ear implants) are silicon-based electronics, which are incompatible with host tissues [21, 67]. Therefore, developing new biodegradable and biocompatible alternatives has become an inevitable trend. Using a hand-held 3D extrusion printer, a novel conductive device (edible electrodes) was prepared using bioresorbable and biodegradable food-grade materials based on gelatin and gellan gum, along with genipin as a covalent crosslinker and NaCl [21]. The conductivity of the device was demonstrated, which could be suitable for application as flexible conductor elements in electronic circuits [21]. These edible conductive devices provide a potential for novel drug delivery systems and gastrointestinal monitoring devices [21, 34]. Besides, skin-like wearable sensors have been recently explored [329-

331] to monitor the physiological activities of human bodies. Wei, Xie, Zhang, Zou, Ping, Wang, Xie, Shen, Lei and Fu [330] designed a hydrogel-based wearable strain sensor based on CNTs, sodium alginate, and Ca^{2+}-crosslinked polyacrylic acid (PAA). The 3D-printable hydrogel with self-healing ability, stretchability, and electronic and ionic conductivities [330]. Furthermore, the sensor had high sensitivity (gauge factor of 6.29) and stable responsiveness to external stimuli (finger and knee bending, and breathing after exercise) [330]. Similar research was made by incorporating CNCs into a chelate of Al^{3+} with PAA and deep eutectic solvents, leading to a printed strain sensor with high sensitivity (gauge factor up to 3.3) and stable responsiveness to the human body by the change in electrical resistance [331]. Moreover, wearable sensors may also be used as UV-responsive devices for monitoring UV radiation. For example, Finny, Jiang and Andreescu [329] used alginate, gelatin, TiO_2 and colored dyes (malachite green, methyl orange, and methylene blue) to fabricate 3D sensors. The hydrogel-based sensors showed excellent reproducibility in quantifying UV exposure by the change in color [329].

6. Conclusions

As an emerging technology, 3DP is expected to change the traditional ways of manufacturing. Along with that, biopolymer 3DP has also experienced significant development although the main applications are still limited to be mainly in food and biomedical areas.

Various 3DP techniques, such as inkjet printing, extrusion-based printing, laser-assisted printing, and binder jetting have been widely used to fabricate objects of different geometries or shapes [9, 332]. Among these different 3DP techniques, extrusion-based 3DP is the most commonly used. A series of printer- and material-related factors determine the accuracy of 3DP. For example, material-

related factors include bioink formulation and printing temperature, influencing the viscoelasticity of inks especially melts. Appropriate rheological properties are important to ensure the flowability of the ink during printing and the self-supporting strength after extrusion. Printer-related factors involve nozzle diameter, extrusion rate, nozzle moving speed, and nozzle height. By adjusting these printing parameters, the quality and precision of printed objects can be regulated. In general, the nozzle diameter can be the first consideration for different formulations to be successfully printed. Besides, post-printing treatments (e.g. baking, drying, and crosslinking) also determine the quality of printed samples.

Some biopolymers have been successfully used in 3DP with much room for further exploration. Biopolymers such as starch, pectin, κ-carrageenan, xanthan gum, milk protein, and soy protein have been mostly employed in 3DP food because of their advantages like gel-forming ability, edibility, and high nutritional values. Besides, some biopolymers such as cellulose, alginate, chitosan, HA, SF, collagen, gelatin, and keratin have been employed particularly in the biomedical field due to their excellent biocompatibility, biodegradation, and functional properties. In general, these biopolymers are dissolved in water or solvents to prepare the inks. However, ink formulations are quite limited and new bioinks need to be developed that can meet a wider range of material property requirements (i.e. rheological, mechanical, and physicochemical properties). Therefore, incorporation of additional materials to biopolymer matrices or mixing several biopolymers for reinforcement effects provides solutions.

7. Challenge and future perspectives

Despite the remarkable progress made in the 3DP of biopolymers, this area of research still faces

some important challenges that need to be addressed urgently.

Biopolymers have proven to be interesting raw materials for 3DP applications due to their advantages such as environment-friendliness, sustainability, and non-toxicity [25, 40]. However, there are still several shortcomings of some biopolymers, such as poor processability and solubility in water or common organic solvents. Therefore, it is necessary to develop new solvents for biopolymer processing and 3DP. In particular in food and biomedical applications, solvents must be safe, green, and harmless. In this regard, biobased ILs are worth to be investigated.

Currently, food 3DP is mainly applied to the production of customized food, snacks, and desserts [333] but not our daily food. Also, there is still a long way to go from lab to kitchen regarding biopolymer 3DP. There are several main challenges related to the 3DP of biopolymers for food applications:

1) The 3DP of starch-based food is mainly limited to the use of mashed potato [17, 45, 183, 229, 334] or modified cassava starch [52, 335] because they have better gelatinization and rheological properties [45] and can be designed to present various geometry shapes [17]. In contrast, it is more challenging to meet structure and property requirements using other starches. Modification methods could be explored to broaden starch resources for 3DP.
2) Food 3DP is mainly limited to produce simple structures or shapes (mostly, cylindrical or square). More research is needed to achieve more complex food structures.
3) Most of the printing probes are single or double, leading to low printing efficiency. 3DP techniques for multi-dimensional and multi-material printing are still highly demanded.

Besides, there is still a lack of research for personalized nutrition or flavor in 3D-printed food.

In biomedical areas, tissue biomimicry is a key challenge. While multiple biopolymers and live cells can be printed into complex tissue structures (e.g. kidney, heart, lung, and liver tissues), more complex systems such as vessels, neurons, nerves, and lymphatics cannot be easily fabricated yet by 3DP. The ultimate goal in this area should be to develop biocompatible tissues or organs that can function normally in the organism. Therefore, more attention needs to be paid to tissue compatibility, interactivity with living cells, and cell proliferation rate and viability.

To improve the mechanical strength and stiffness of printed objects, the hydrogels usually need to be crosslinked after printing. However, in addition to the most commonly used salt $CaCl_2$, some crosslinkers (e.g. glutaraldehyde) are potentially cytotoxic and few other suitable crosslinkers are available. Therefore, it is worth to develop new "green" crosslinking agents (e.g. carboxylic acids [336] and citric acid [337]) and new technologies [32, 338] for biopolymer 3DP, which can offer versatile properties to the printed materials (e.g. printability, biocompatibility, biodegradation, and mechanical strength).

To fabricate complex 3D constructs with the required functionality, 4DP is likely to become a promising potential technology. The concept of 4DP is ascribed to the extension of 3DP with the addition of the time dimension and can provide 3DP with cost-effectiveness for the fabrication of smart devices or complex human organs or tissues with blood vessels and nerves. Besides, 4DP allows food to have some unique changes in e.g. structure, flavor, nutrition, and color after 3DP [339, 340].

The concept of 5D printing (5DP) has emerged. 5DP was first implemented by the Mitsubishi Electric Research Laboratories (MERL) by Yerazunis, who invented a 5D printer to printing 3D objects using thermoplastic materials such as acrylonitrile butadiene styrene [341, 342]. 5DP depends on a moving plateau that allows for the print head to make different angles from five dimensions and create a part with curved layers. Compared with 3DP or 4DP, 5DP applies to efficient manufacturing of complex curved structures with excellent strength [343]. Research has been started on 4DP and 5DP in the biomedical fields, but much more efforts are worth to devote to the application of this emerging technology for the manufacture of advanced biopolymer-based materials.

Acknowledgements

The authors acknowledge the funding support from the National Natural Science Foundation of China (grant No. 31701637) and the China Association for Science and Technology (grant No. 2018QNRC001).

Tables

Table 1 Summary of various biopolymers and their applications.

Biopolymer	Chemical structure	3D printing technique	Application	Ref.
Polysaccharide				
Starch	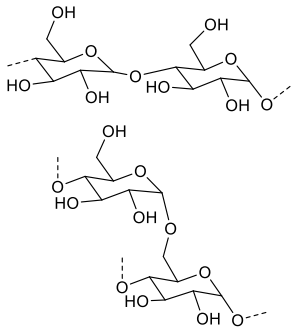 D-glucose	Extrusion	Food; Chemistry; Material (plastic); Fermentation; Paper; Pharmaceutical	[38, 45, 344]
Cellulose	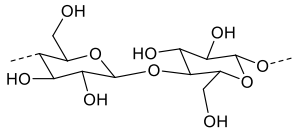 D-glucose	DIW; Inkjet printing; FDM	Construction; Pulp and papermaking; Textile	[53, 65, 345-347]
Alginate	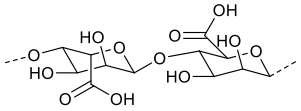 β-D-mannuronic acid and α-L-guluronic acid	Extrusion	Wound healing; Tissue engineering	[28, 70, 348]

Pectin	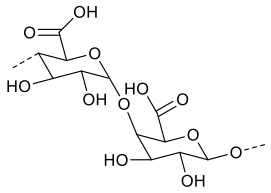 D-Galacturonic acid	Extrusion; Inkjet printing	Food; Pharmaceutical	[28, 79, 349, 350]
κ-Carrageenan	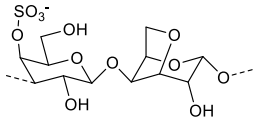 D-anhydroglucopyranose	UV stereolithography; DIW	Food; Pharmaceutical; Cosmetic; Textile	[351-354]
Chitosan	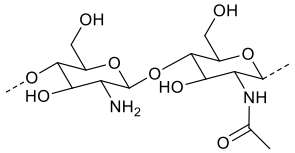 D-glucosamine	Extrusion; Stereolithography	Cosmetic; Pharmaceutical; Food; Biotechnological; Environmental	[86, 355, 356]
Hyaluronic acid	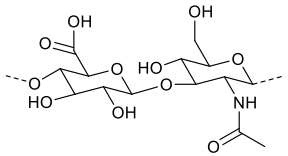 D-glucuronic acid and N-acetyl	Extrusion	Biomedicine; Tissue regeneration; Cosmetic; Nutricosmetic	[96, 100]

Xanthan gum	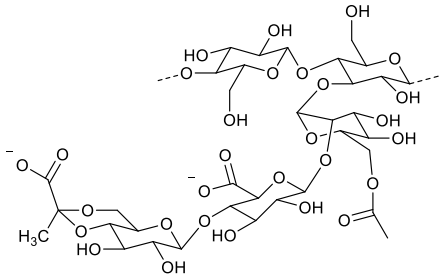 D-glucose, D-mannose and D-glucuronic acid	Binder jetting; Extrusion	Food	[103-105, 357]
Protein				
Silk	GAGAGS	Micro-extrusion; Stereolithography; Hybrid inkjet printing/electrospinning	Biomedical; Textile	[28, 124, 256, 266, 358, 359]
Collagen	Gly-X-Y	Extrusion; Inkjet printing	Cosmetic; Medical cosmetology; Photographic; Biomedical; Food; Leather	[28, 114, 181, 360]
Gelatin	Ala-Gly-Pro-Arg-Gly-Glu-4Hyp-Gly-Pro	Extrusion; Stereolithography	Cosmetic; Biomedical	[28, 117, 181, 361, 362]
Keratin	A(Cys-Cys-X-Pro-X); B(Cys-Cys-X-SerThr-SerThr)	UV lithography	Biomedical; Cosmetic; Food; Textile	[131-133, 363]
Milk protein	Casein (α_{s1}, α_{s2}, β, and κ); Whey protein (lactalbumins, lactoglobulins)	Extrusion	Food	[230, 364]

Soy protein	Albumins; Globulins	Extrusion	Food; Biomedical	[144, 365]

Abbreviations: DIW, Direct ink writing; FDM, Fused deposition modeling.

Table 2 Different 3D printing techniques used for biopolymers.

Printing technique	Material for 3D printing	Processing Factor	Solidification method	Application	Ref.
Inkjet printing	Hydrogel; low-viscosity material (cotton fabrics, pectin-nanocellulose, alginate)	Heat gradient or electric stimuli	$CaCl_2$ solution; Steam	Food; Tissue engineering	[349, 363, 366]
Extrusion	Thermoplastic; hydrogel; viscous biopolymer (cellulose nanocrystal; κ-carrageenan; maize protein; starch; alginate/gelatin)	Heating and extruding	Freeze-drying; Physical crosslinking (freeze-thawing)	Tissue engineering; Drug delivery; Packaging; Biomedical; Pharmaceutical; Food	[65, 155, 185, 351, 367]
Stereolithography	Photo-polymerizable liquid resins (alginate; cellulose nanocrystals; silk fibroin)	Laser; visible light or UV	$CaCl_2$ solution; UV	Tissue and organ engineering	[257, 368-370]
Selective laser sintering (SLS)	Thermoplastic; powdered material (maltodextrin; protein)	Laser	Baking; Laser	Food with complex structures	[371, 372]
Binder jetting	Powdered materials (cellulose composite powders)	Liquid binding agent	Recrystallization	Food	[357, 373]

Abbreviations: SLS, Selective laser sintering.

1452 **Table 3** Summary of the rheological properties and applications of 3D-printed biopolymer materials.

Formulation (bioink)	Printing method and printed object shape	G' (Pa)	G'' (Pa)	η (Pa·s)	Application	Ref.
Sample 1: 100 g of mashed potato mixed with 1 g of KG/XG (3:2, w/w) in boiling water; Sample 2: 17.5 g of potato starch added to 100 g of strawberry juice, followed by steam-cooking for 20 min	Dual-extrusion (triangle; square; regular hexagon and round shape)	8,000–30,000	–	–	Food	[45]
Lemon juice mixed with potato starch (content: 10, 12.5, 15, 17.5, and 20 g/100 g), followed by steam-cooking for 20 min	Extrusion (cylinder)	4,924.2	760.8	1,000–8,079.3	Food	[183]
Banana (73.5 wt%) / white canned beans (15 wt%) / dried non-fat milk (6 wt%) / lemon juice (3 wt%) / dried mushrooms (2 wt%) / ascorbic acid (0.5 wt%), in pectin solution (11%, w/w)	Extrusion (cube 18×18×18 mm)	–	–	350.4–25,600	Food	[5]
Tomato paste	Extrusion	15–9,000	15–900	–	Food	[374]
XG (0.5%, w/v) dissolved in glycerin/water (1:1, w/w) solution, accounting for 65 wt% of the ink; the other 35 wt% of the ink was MPC/WPI (6:1, 5:2, and 4:3, w/w), which was added to the above prepared solution.	Extrusion (Chinese character; cylinder)	30–80,000	200–30,000	40–200,000	Food	[111]

XG (0.5 g) / SPI (30 g) added to NaCl solution (1, 2, and 3 g of NaCl in 100 mL of distilled water), adjusted to pH 7 using NaOH (0.1 mol/L), microwave-treated (100 W, 5 min) to form gel.	Extrusion (Celtic triangle; cube; smile heart; fruit slice; rabbit)	1,573–2,095	337–456	11–16	Food	[375]
SMP (15 wt%) dissolved in deionized water, then added with starch (10 wt%)	Extrusion (25 mm × 25 mm squares filled with diamond-like structures)	280	43.5–10,600	–	Food	[15]
Water (29 g), sucrose (6.6 g), butter (6.0 g), flour (48 g) and egg (10.4 g) per 100 g formulation	Extrusion (mickey mouse and a square frame)	0–700	0–120	0.08–50	Food	[16]
Potato flakes (80 wt% based on water) mixed with 1 wt% KG/XG (3:2, w/w) in boiling water, potato flakes/water = 4:1 (w/w)	Extrusion (rectilinear; honeycomb and Hilbert curve)	20,000–30,000	≤5,000	1,018–42,608	Food	[17]
Mashed potato: potato flakes (15, 19, 23, and 27 wt% based on water) mixed with 2 wt% SA in boiling water, added with 1 wt% citric acid and 1 wt% sodium bicarbonate; Purple sweet potato puree: 30 g of purple sweet potato powder mixed with 2 g of SA in 100 g of boiling water	Dual extrusion (cylindrical model)	1,500–40,000	900–5,000	600–80,000	Food	[229]
30 mg/g KG stirred (1500 rpm, 30min) in water at room	Extrusion (discs and star-	100–10,000	100–10,000	–	Food and pharmaco-	[352]

temperature	shaped)				nutrition	
LM pectin (15, 35, and 55 g/L) dissolved in 45 mL of sugar syrup/water mixture (0, 25, and 50%, v/v), added with 15 mL of $CaCl_2$ solution (12.5, 15, and 17.5 mM); BSA (0, 2.5, and 5 g/L) was added before printing.	Extrusion (honeycomb infill pattern; cube of 1.5×1.5×1.5 cm^3)	100–2,000	35–500	–	Food	[79]
KG (1–2%, w/w) / XG (0.25–0.5%, w/w) / potato starch (0–2%, w/w) dissolved in water, added with 0.1% (w/w) food colorant	Extrusion (hollow cylinder)	51.2–9,017	39.4–1,026	0.1–110	Food	[104]
Egg yolk sealed in plastic bags (without air), heated (at 72, 76, 80, and 84 ℃) for up to 12 min	Extrusion (a squirrel; 10% with a rectilinear fill pattern)	0.5–5,000	4–3,000	–	Food	[196]
Sample 1: 3 wt% CNFs mixed with 3 wt% alginate in water; Sample 2: 4 wt% CNFs in water	Extrusion (grid)	2,000–20,000	300–1,000	1.048–4.38×10^4	Human tissue constructs	[189]
8.35% (w/v) of CNFs diluted in 200 mL of Milli-Q water, further mixed with aqueous SWCNTs dispersion (1%, w/v); The resulting mixture had CNFs/CNTs dry weight ratio of 80/20.	Extrusion (parallel lines)	5–4,000	40–1,000	0.5–100,000	Neural tissue engineering	[322]
CNFs (1.5–2.25 wt%) / alginate (0.25–1 wt%) / water	Extrusion (small grid;	2,000–50,000	400–5,000	0.2–100,000	Cartilage tissue	[170]

(97.5 wt%)	large grid; a solid disc; human ear; sheep; meniscus)				engineering	
6 wt% SA and 3 wt% gelatin dissolved in water at 50 °C, mixed with 6 wt% CNCs to reach a CNCs/SA/gelatin ratio of 70:20:10 (w/w/w)	Extrusion (block porous hydrogel scaffold)	1.98×10^4	3.02×10^3	$10–10^5$	Biomedical	[226]
Nanocellulose water dispersion (1.9 wt% dry content) mixed with either alginate (3%, w/v) or alginate sulfate (6%, w/v) solution at 4.2:1 (v/v)	Extrusion (ear)	3,000–15,000	–	0.01–10,000	Cartilage tissue engineering	[285]
Method 1: GelMA powder mixed with CNFs gel (1%, w/v) at 50 °C, resulting in 0.2 and 0.5% (w/v) final GelMA concentrations Method 2: 1 mL of GelMA solution (10%, w/v) added to 9 mL of CNFs gel (1%, w/v)	Extrusion (cubic grid scaffolds)	0–320	–	$1–2\times10^3$	Wound healing	[376]
0, 1, 2, and 3 wt% GGMMA powder added to CNFs gel (1 wt%), heated at 50 °C	Extrusion (spruce tree model)	80–60,000	–	0.2–2,000	Biomedical	[205]
CNFs diluted in Dulbecco's PBS to achieve 0.25 wt% concentration, heated to 70 °C, added with gelatin (5 wt%) / alginate (4 wt%) powder	Extrusion (cubic grid)	10,000–50,000	–	56–1,143	Bone tissue engineering	[377]

30 mg/g KG stirred (1500 rpm, 30min) in water at room temperature	Extrusion (discs and star-shaped)	600–20,000	100–2,000	–	Food and pharmaco-nutrition	[352]
Silk dissolved in LiBr (9 M) to achieve 1.5% (w/v) SF solution, mixed with 7% (w/v) gelatin at 37 ℃	Extrusion (3D model of the lateral meniscus)	1×10^{-4}–1×10^{4}	10–1,000	–	Biomedical	[12]
SF powder dissolved in water to achieve a 2.5–10% (w/v) solution, mixed with PEG400 (80%, w/w) at 1:1 (v/v), heated at 37 °C for gelation	Extrusion (disk-shaped with pore; grid-shaped; ear-shaped	1,000–200,000	40–1,000	0.2–400,000	Biomedical	[378]
Silk dissolved in LiBr (9 M) to achieve 15 wt% SF solution, mixed with gelatin (1:2, w/w) and glycerol (5:1, w/w), added with BCNFs dispersion; three samples with BCNFs/Total = 0.35, 0.7, and 1.40 wt% in the bioink prepared	Extrusion (cubic grid)	100–10,000	20–100,000	0.2–10,000	Tissue engineering	[379]
Silk dissolved in LiBr (9 M) to achieve 0.5–2% (w/v) SF solution, mixed with gelatin 1–9% (w/v)	Extrusion (grid-like structure and human ear)	10–2,000	4–100	–	Cartilage tissue engineering	[200]
6% (w/v) silk dissolved in 9.3 M LiBr, mixed with glycerol (700 mg/mL) and gelatin (400 mg/mL)	Extrusion (cheek implants; cylindrical constructs with concentric pattern)	2.04–4.94×10^{4}	1.01–1.87×10^{5}	0.1–400	Tissue integration	[265]
Silk dissolved in LiBr (9 M) to achieve 5% (w/v)	Extrusion (grid-like	10^{2}–10^{4}	10^{2}–10^{3}	10^{-1}–10^{4}	Cartilage tissue	[207]

solution, mixed with 15 wt% gelatin	structure)				engineering	
Alginate (2%, w/v) / gelatin (3%, w/v) / Matrigel (0, 5, 20, and 50%, w/v) / 2.5% $CaSO_4$ / A549 cells (7×10^6 cells/mL)	Extrusion (nose; letter T, U; cubic grid)	250–1,250	23–80	0.1–0.5	Biomedical	[171]
KG (0.5, 1.0, or 1.5%, w/v) mixed with SA solution (2%, w/v), added with $CaSO_4$ solution (0.5, 1.0, 1.5, 2.0, or 3.0%, w/v)	Extrusion	220–900	–	$1–10^4$	Tissue engineering and regenerative medicine	[178]
Alginate (3%, w/v) / gelation (10%, w/v)	Extrusion (Y-shaped)	50–300	6–16	300–2,000	Regenerative medicine	[380]
15 g of gelatin dissolved in 100 mL of DMEM/F12, added with 2.0 g of alginate	Extrusion (bilayered membranous construct)	10–20,000	30–1,000	$1–5\times10^4$	Skin tissue engineering	[10]
1% (w/v) SA and 3% (w/v) gelatin in water heated at 70 °C	Extrusion (porosity; grid pattern)	300–350	50–100	0.2–1.2	Biomedical	[381]
TiO_2 nanoparticles (0.1%, w/v) and β-TCP (1.0%, w/v) added to $CaCl_2$ solution (0.20%, w/v), then slowly added with alginate (2%, w/v) / gelatin (0.5%, w/v)	Extrusion (voronoi; hexagon; grid)	0.1–150	5–50	1–2,000	Tissue engineering scaffolds	[382]
Alginate (30 mg/mL) mixed with alginate-sulfate (5, 10, or 30 mg/mL), dissolved in DMEM	Extrusion (cell; porosity; grid pattern)	1,000–2,000	–	50–8,000	Tissue engineering	[383]
20% (w/v) gelatin powder and 4% (w/v) sodium alginate	Extrusion (cell; grid	1.95–595	12.6–31,400	–	Stem cells	[181]

powder dissolved in 0.5% (w/v) NaCl solution	structures)					
10% (w/v) dex-HEMA dissolved in HEPES buffer (100 mM, pH 7.4) or chondrocyte culture medium, added with HA (2, 4, and 6%, w/v)	Extrusion (hydrogel with grid)	1–20,000	100–2,000	1–8,000	Tissue engineering	[384]
KG and polyacrylamide dissolved in water to form double-network hydrogel (18 wt%)	UV stereolithography (a hollow triangular prism and a hollow cube)	1–11,000	5–1,000	0.7–2,000	Robotics and human motion detection	[353]
LM-pectin added to nanocellulose gel, stirred at room temperature until complete dissolution; CNFs/LM-pectin ratio = 3:1, 1:1, and 1:3 (w/w), the total solid weight per volume was 1.59%, 2.38%, and 4.76%, respectively	Extrusion (grid hydrogel scaffold)	800–5,000	8×10^2–2×10^4	0.2–400	–	[349]

Abbreviations: BCNF, Bacterial cellulose nanofiber; BSA, Bovine serum albumin; β-TCP, β-Tricalcium phosphate; CNC, Cellulose nanocrystal; CNF, Cellulose nanofibril; CNT, Carbon nanotube; Dex-HEMA, Hydroxyethyl-methacrylate-derivatized dextran; DIW, Direct ink writing; DMEM, Dulbecco's modified Eagle medium; η, Viscosity; GelMA, Gelatin methacryloyl; G', Elastic modulus; G'', Loss modulus; GGMMA, Galactoglucomannan methacrylate; HEPES, 4-(2-hydroxyethyl)-1-piperazineethanesulfonic acid; KG, κ-Carrageenan gum; LM, Low methoxyl; MPC, Milk protein concentration; PBS, Phosphate-buffered saline; PEG400, Polyethylene glycol; SA, Sodium alginate; SDS, Sodium dodecyl sulfate; SMP, Skimmed milk powder; SPI, Soybean protein isolate; SWCNT, Single-walled carbon nanotube; WPI, Whey protein isolate; XG, Xanthan gum.

1459 **Table 4** Summary of 3D printing parameters and applications.

Formulation (bioink)	Printing method	Nozzle diameters (mm)	Printing speed ($mm \cdot s^{-1}$)	Application	Ref.
Sample 1: 100 g of mashed potato mixed with 1 g of KG/XG (3:2, w/w) in boiling water; Sample 2: 17.5 g of potato starch added to 100 g of strawberry juice, followed by steam-cooking for 20 min	Dual extrusion (triangle; square; regular hexagon and round shape)	–	25	Food	[45]
Lemon juice mixed with potato starch (10, 12.5, 15, 17.5, and 20 g/100 g), followed by steam-cooking for 20 min	Extrusion (cylinder)	0.5–2	15–35	Food	[183]
Banana (73.5 wt%) / white canned beans (15 wt%) / dried non-fat milk (6 wt%) / lemon juice (3 wt%) / dried mushrooms (2 wt%) / ascorbic acid (0.5 wt%) / pectin solution (11 wt%)	Extrusion (cube 18×18×18 mm)	–	30, 50, 70	Food	[5]
Tomato paste	Extrusion	0.8, 1.2	18, 25	Food	[374]
XG (0.5%, w/v) dissolved in glycerin/water (1:1, w/w) solution, accounting for 65 wt% of the ink; the other 35 wt% ink was MPC/WPI (6:1, 5:2, and 4:3, w/w), which was added to the above-prepared solution	Extrusion (Chinese character; cylinder)	–	35, 50	Food	[111]

SPI (30 g) / XG (0.5 g) added to NaCl solution (0, 1, 2, and 3 g of NaCl in 100 mL of distilled water)	Extrusion (Celtic triangle; cube; smile heart; fruit slice; rabbit)		15	Food	[375]
SMP (15 wt%) dissolved in water, added with starch (10 wt%)	Extrusion (25 mm × 25 mm squares filled with diamond-like structures)	0.41	2	Food	[15]
Egg powder dissolved in water, added with rice flour; Egg powder / rice flour ratio = 1:1 and 1:2 (w/w)	Extrusion (model “Kitty Nury”)	0.84, 1.22	6.7–20	Food	[185]
Water (29 g), sucrose (6.6 g), butter (6.0 g), flour (48 g), and egg (10.4 g) per 100 g of formulation	Extrusion (Mickey Mouse and square frame)	0.8, 1.5, 2.0	25	Food	[16]
1 wt% (based on potato flakes) KG/XG (3:2, w/w) and potato flakes mixed in boiling water; Potato flakes / boiling water ratio = 4:1 (w/w)	Extrusion (rectilinear, honeycomb and Hilbert curve)	0.8	25	Food	[17]
Sample 1: 15, 19, 23, and 27 wt% potato flakes mixed with 2 wt% SA powder in boiling water, added with 1 wt% citric acid and 1 wt% sodium bicarbonate; Sample 2: 30 g of purple sweet potato powder mixed with 2 g of SA, added with 100 g of boiling water	Dual Extrusion (cylindrical model)	1.2	15	Food	[229]
30 mg/g KG stirred (1500 rpm, 30 min) in water at room temperature	Extrusion (discs and star-shaped)	–	10–60	Food	[352]

LM pectin (15, 35, and 55 g/L) dissolved in 45 mL of sugar syrup/water mixture (0, 25, and 50%, v/v), added with 15 mL of $CaCl_2$ solution (12.5,15, and 17.5 mM); BSA (0, 2.5, and 5 g/L) was added before printing	Extrusion (honeycomb infill pattern, cube of 1.5×1.5×1.5 cm^3 were printed; porous food)	0.838		Food	[79]
KG (1–2%, w/w) / XG (0.25–0.5%, w/w) / potato starch (0–2%, w/w) dissolved in water, added with 0.1% (w/w) food colorant	Extrusion (lattice scaffold model; hollow cylinder)	0.8	22	Food	[104]
Egg yolk sealed in plastic bags (without air), heated (at 72, 76, 80, and 84 ℃) for to 12 min	Extrusion (squirrel; 10% with a rectilinear fill pattern)	0.84	40	Food	[196]
Sample 1: 3 wt% CNFs mixed with 3 wt% alginate in water; Sample 2: 4 wt% CNFs in water	Extrusion (grid)	0.42	10	Human tissue constructs	[189]
8.35% (w/v) of CNFs diluted in 200 mL of Milli-Q water, further mixed with aqueous SWCNTs dispersion (1 wt%); The resulting mixture had CNFs/CNTs dry weight ratio of 80/2.	Extrusion (parallel lines)	0.3	10	Neural tissue engineering	[322]
CNFs (1.5–2.25 wt%) / alginate (0.25–1 wt%) / water (97.5 wt%)	Extrusion (small grid; large grid; a solid disc; human ear; sheep meniscus)	0.3	10–20	Cartilage tissue engineering	[170]

6 wt% SA and 3 wt% gelatin dissolved in water at 50 °C, mixed with 6 wt% CNCs to reach a CNCs/SA/gelatin ratio of 70:20:10 (w/w/w)	Extrusion (block porous hydrogel scaffold)	0.41	10–80	Tissue repair and regeneration	[226]
Nanocellulose water dispersion (1.9 wt% dry content) mixed with either alginate (3%, w/v) or alginate sulfate (6%, w/v) solution at 4.2:1 (v/v)	Extrusion (ear)	0.15, 0.3	–	Cartilage tissue engineering	[285]
2 wt% CNFs / 98 wt% water	Extrusion (10×10×10 mm^3 grid cubes, with 3×3×3 mm^3 pillars)	0.3	5	Packaging; Textiles; Biomedical devices; Furniture with conductive parts	[63]
Method 1: GelMA powder mixed with CNFs gel (1%, w/v) at 50 °C, resulting in 0.2 and 0.5% (w/v) final GelMA concentrations; Method 2: 1 mL of GelMA solution (10%, w/v) added to 9 mL of CNFs gel (1%, w/v)	Extrusion (cubic grid scaffolds)	0.45–0.6	16.67–33.3	Wound healing	[376]
0, 1, 2, and 3 wt% GGMMAs powder added to CNFs gel (1 wt%), heated at 50 °C	Extrusion (spruce tree model)	–	5	Biomedical	[205]
CNFs gel diluted in Dulbecco's PBS to achieve 0.25 wt% concentration, heated to 70 °C, added with gelatin	Extrusion (cubic grid)	–	15–65	Bone tissue engineering	[377]

(5 wt%) / alginate (4 wt%) powder					
Silk dissolved in LiBr (9 M) to achieve 15 wt% SF solution, mixed with gelatin (1:2, w/w) and glycerol (5:1, w/w), added with BCNFs dispersion; three samples with MBCNFs/Total = 0.35, 0.7, and 1.40 wt% in the bioink prepared	Extrusion (cubic grid)	0.41, 0.6	–	Tissue engineering	[379]
Silk dissolved in LiBr (9 M) to achieve 0.5–2% (w/v) SF solution, mixed with gelatin 1–9% (w/v)	Extrusion (grid-like structure and human ear)	0.25	6–8	Cartilage tissue engineering	[200]
Mixture of cells (1×10^6 mL^{-1}) and collagen solutions (3, 5, and 7 wt%) as collagen bioink	Extrusion (cell-laden collagen-mesh structure)	–	10	Biomedical	[118]
KG (0.5, 1.0, and 1.5%, w/v) mixed with SA solution (2%, w/v), added with $CaSO_4$ solution (0.5, 1.0, 1.5, 2.0, and 3.0%, w/v)	Extrusion	–	1–16	Tissue engineering and regenerative medicine	[178]
1% SA (w/v) and 3% (w/v) gelatin heated at 70 °C	Extrusion (porosity; grid pattern)	–	14	Therapeutic stem cell	[381]
TiO_2 nanoparticles (0.1%, w/v) and β-TCP (1.0%, w/v) added to $CaCl_2$ solution (0.20%, w/v), then slowly added with alginate (2%, w/v) / gelatin (0.5%, w/v)	Extrusion (Voronoi; hexagon; grid)	–	4.5	Tissue engineering scaffolds	[382]
Alginate (30 mg/mL) mixed with alginate-sulfate (5, 10, and 30 mg/mL), dissolved in DMEM	Extrusion (cell; porosity; grid pattern)	0.3	–	Bone tissue engineering	[383]

20% (w/v) gelatin powder and 4% (w/v) sodium alginate powder dissolved in 0.5% (w/v) NaCl solution	Extrusion (cell; grid structure)	–	0.03	Stem cells	[181]

Abbreviation: BCNF, Bacterial cellulose nanofiber; BSA, Bovine serum albumin; β-TCP, β-Tricalcium phosphate; CNC, Cellulose nanocrystal; CNF, Cellulose nanofibril; CNT, Carbon nanotube; DIW, Direct ink writing; DMEM, Dulbecco's modified Eagle's medium; GelMA, Gelatin methacryloyl; GGMMA, Galactoglucomannan methacrylate; KG, κ-Carrageenan; LM, Low methoxyl; PBS, Phosphate-buffered saline; SA, Sodium alginate; SF, Silk fibroin; SMP, Skimmed milk powder; SPI, Soybean protein isolate; SWCNT, Single-walled carbon nanotube; XG, Xanthan gum.

Table 5 Comparison of different 3D-printed structures [15]. Copyright 2018. Reproduced with permission from Elsevier.

Sample	1.5 wt% CNFs + 5 wt% Starch	15 wt% Starch	30 wt% Rye bran	35 wt% OPC	45 wt% FBPC	0.8 wt% CNF + 50 wt% SSMP	60 wt% SSMP
During printing		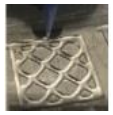				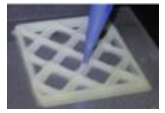	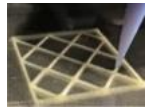
After printing	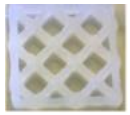						
After oven-drying							
After freeze-drying					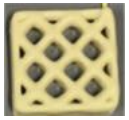		

Abbreviations: CNF, Cellulose nanofibril; FBPC, Faba bean protein concentrate; OPC, Oat protein concentrate; SSMP, Semi-skimmed milk powder.

1468 **Table 6** Overview of crosslinking methods for biopolymer 3D printing and their applications.

Formulation (bioink)	Properties	Crosslinking method	Application	Ref.
LM pectin (15, 35, and 55 g/L) dissolved in 45 mL of sugar syrup/water mixture (0, 25, and 50%, v/v), added with 15 mL of $CaCl_2$ solution (12.5,15, and 17.5 mM); BSA (0, 2.5, and 5 g/L) before printing	*E*: 15–700 kPa	Post-printing: 12.51–7.5 mM $CaCl_2$	Food	[79]
LM pectin (15–35g/L) dissolved in water with stirring at 23 °C	*E*: 1.55–118.58 MPa	Post-printing: 11–15 mM $CaCl_2$	Food	[221]
Nanocellulose/HA (70:30, w/w)	*E*: 0.169 MPa; Cell viability: 95%	Post-printing: 0.001% (v/v) H_2O_2 for 5 min	Adipose tissue	[324]
Chitosan (2%, w/v) / HA (20 $mg \cdot ml^{-1}$)	*E*: 14.97 kPa; Cell viability: >90%	Post-printing: thermal crosslinking at 37 °C	Bone tissue engineering	[385]
Nanocellulose/alginate (33:66, 15:85, and 10:90, w/w) dissolved in water	Moisture uptake: 150%	Post-printing: 90 mM $CaCl_2$	Wound dressings	[280]
TiO_2 nanoparticles (0.1%, w/v) and β-TCP (1.0%, w/v) added to $CaCl_2$ solution (0.20%, w/v), then slowly added with alginate (2%, w/v) / gelatin (0.5%, w/v)	*E*: 20 MPa	Pre-printing: 0.2% (w/v) $CaCl_2$	Tissue engineering	[382]
LM-pectin added to nanocellulose gel, stirred at room temperature until complete dissolution; CNFs/LM-pectin ratio = 3:1, 1:1, and 1:3 (w/w), the total solid weight per volume was 1.59%, 2.38%,	Swelling degree: 1860%	Post-printing: 3% (w/v) $CaCl_2$ for 10 min	Tissue engineering	[349]

and 4.76%, respectively				
6 wt% SA and 3 wt% gelatin dissolved in water at 50 °C, mixed with 6 wt% CNCs to reach CNCs/SA/gelatin ratio of 70:20:10 (w/w/w)	Pore sizes: 80–2125 μm; *E*: 1.54 MPa	Post-printing: 3 wt% $CaCl_2$ solution for 24 h and again 3 wt% glutaraldehyde for 24 h	Tissue repair and regeneration	[226]
2 wt% CNFs / 98 wt% water	*E*: 114±14 MPa; Stiffness: 4.3±0.3 GPa	Post-printing: 0.2 M $CaCl_2$ bath	Biomedicine	[63]
15 g of gelatin dissolved in 100 mL of DMEM/F12, added with 2.0 g of alginate	*E*: 280 kPa; Cell viability: >95%	Post-printing: 2 wt% $CaCl_2$ at 4 °C	Skin tissue engineering	[10]
Collagen (5 wt%) / cell (5×10^6 cell/ml)	*E*: 23.34 kPa	Post-printing: 1 wt% tannic acid	Tissue regeneration	[201]
0.06 g/mL gelatin dissolved in NaCl solution, further dissolved with 0.05 g/mL alginate	*E*: 1.44 MPa; Cell viability: 83.2%	Post-printing: 300 mM $CaCl_2$	Aortic valve conduits	[386]
Silk dissolved in LiBr (9.3 M) to final 3% (w/v) concentration, mixed with collagen (4 wt%) / dECM	Compressive modulus: 0.3 MPa	Post-printing: 100 mM EDC at 22 °C for 1 h	Bone tissue regeneration	[264]
15 wt% gelatin added to a 5% (w/v) autoclaved SF solution	Cell viability: 90%	Pre-printing: 700 U tyrosinase	Cartilage tissue engineering	[207]
Gelatin (10%, w/v) / alginate (2%, w/v) in PBS	Stiffness: 5–12 kPa	Pre-printing: 2% (w/v) TG covalently crosslinked	Biomedical	[202]
Keratin (4, 5, and 6%, w/v) dissolved in PBS (4%, w/v)	Compressive modulus: 15.45kPa;	Post-printing: UV	Tissue	[133]

	Swelling capacities: 20%		engineering and regenerative medicine	
0, 1, 2, and 3 wt% GGMMAs powder added to CNFs gel (1 wt%), heated at 50 °C	Compressive stiffness: 2.5−22.5 kPa	Post-printing: UV	Tissue engineering	[205]
10% (w/v) dex-HEMA dissolved in HEPES buffer (100 mM, pH 7.4) or chondrocyte culture medium, added with HA (2, 4, and 6%, w/v)	*E*: ~26 kPa	Post-printing: UV	Tissue engineering	[384]
HA (0.5%, w/v) / gelatin (3.0%, w/v) dissolved in PBS (pH 7.4)	*E*: ~2.2 kPa	Post-printing: visible light	Tissue engineering and regenerative medicine	[387]
Alginate (1, 2, 3, and 4%, w/v) / f-GelMA (4, 5, and 6%, w/v) in water	Compressive modulus: 130 kPa; Swelling capacities: 38%	Two-step crosslinking: during printing crosslinked Ca^{2+}, post-crosslinked: UV	Biomedicine	[388]
GelMA (30%, w/v) and chitosan (3%, w/v) dissolved in acetyl acid (1%, v/v), respectively, then mixed at different ratios to achieve final concentration of GelMA/chitosan was 10/0.5, 10/1, 10/2, 5/1, 15/1, and 20/1(w/v)	*E*: 59.43 kPa	Post-printing: UV	Tissue engineering	[389]

Collagen (0.72%, w/v) and chitosan (2%, w/v) blended at different ratios to final concentration of collagen/chitosan was 0.36/0.50, 0.54/0.50, 0.24/1.0, 0.36/1.0, 0.18/1.5, and 0.45/1.5% (w/v)	*E*: ~1.95 MPa	Post-printing: NHS/ EDC (15 mM/6 mM)	Tissue engineering	[92]

Abbreviations: BSA, Bovine serum albumin; β-TCP, β-Tricalcium phosphate; CNC, Cellulose nanocrystal; CNF, Cellulose nanofibril; dECM, De-cellularized extracellular matrix; Dex-HEMA, Hydroxyethyl-methacrylate-derivatized dextran; DMEM, Dulbecco's modified Eagle medium; EDC, 1-ethyl-3-(3-dimethylaminopropyl) carbodiimide; *E*, Young's modulus; GelMA, gelatin methacryloyl; GGMMA, Galactoglucomannan methacrylate; HA, Hyaluronic acid; HEPES, 4-(2-hydroxyethyl)-1-piperazineethanesulfonic acid; LM, Low methoxylated; NHS, *N*-hydroxysuccinimide; PBS, Phosphate-buffered saline; SA, Sodium alginate; SF, Silk fibroin; TG, Transglutaminases.

1475 **Table 7** Textural properties of 3D-printed food.

Formulation (bioink)	Printing method	Compression strain/%	Hardness	Cohesiveness	Gumminess	Springiness	Ref.
Sample 1: 100 g of mashed potato mixed with 1 g of KG/XG (3:2, w/w) in boiling water; Sample 2: 17.5 g of potato starch added to 100 g of strawberry juice, followed by steam-cooking for 20 min	Dual-extrusion	45–65	232.39–517.22 g	0.224–0.266	56.39–120.22	0.222–0.262	[45]
Lemon juice mixed with potato starch (10, 12.5, 15, 17.5, and 20 g/100 g), followed by steam-cooking for 20 min	Extrusion	–	151.31–406.14 g	0.65–0.94	98.80–379.74	0.85–0.94	[183]
Egg powder dissolved in water, added with rice flour; Egg powder/rice flour ratio = 1:1 and 1:2 (w/w)	Extrusion	–	0.02–0.13 N	0.25–0.61	–	0.37–0.98	[185]
Water (29 g), sucrose (6.6 g), butter (6.0 g), flour (48 g), and egg (10.4 g) per 100 g of formulation	Extrusion	–	1.407–22.83 g	–	–	–	[16]
1 wt% (based on mashed flakes) KG/XG	Extrusion	45	101.21–451 g	–	22.47–163.40	–	[17]

(3:2, w/w) and mashed flakes mixed in boiling water; Potato flakes / boiling water ratio = 4:1 (w/w)							
Sample1: potato flakes (15, 19, 23, and 27 wt%) mixed with 2 wt% SA powder in boiling water, added with 1 wt% citric acid and 1 wt% sodium bicarbonate; Sample 2: 30 g of purple sweet potato powder was mixed with 2 g of SA, and added with 100 g of boiling water	Dual extrusion	40	322.186–1949.995 g	–	65.634–982.682	–	[229]
MPC added to sodium caseinate dispersion (20%, w/v) to prepare milk protein composite gels at 350, 400, 450, and 500 g/L	Extrusion	50	155–999 g	0.71–1.16	107–476	0.71–0.98	[230]
XG (0.5%, w/v) dissolved in glycerin/water (1:1, w/w) solution, accounting for 65 wt% of the ink; the other 35 wt% ink was MPC/WPI (6:1, 5:2, and 4:3, w/w), which was added to the above-prepared solution	Extrusion	50	72.38–269.11 g	–	–	–	[111]

XG (0.5 g) / SPI (30 g) added to a NaCl solution (1, 2, and 3 g in 100 mL of distilled water), then adjusted to pH 7 using NaOH (0.1 mol/L), and microwave-treated (100 W, 5 min) to form gel	Extrusion	–	103–107 g	0.29–0.33	30–35	0.3–0.35	[375]

Abbreviations: KG, κ-Carrageenan; MPC, Milk protein concentrate; SA, Sodium alginate; SPI, Soybean protein isolate; WPI, Whey protein isolate; XG, Xanthan gum.

1478 **Table 8** Pore size, porosity, and infill level on mechanical properties of 3D-printed porous food.

Formulation (bioink)	Printing method	Pore size	Porosity	*E*	Morphology	Ref.
LM pectin (15, 35, and 55 g/L) dissolved in 45 mL of sugar syrup/water mixture (0, 25, and 50%, v/v), added with 15 mL of $CaCl_2$ solution (12.5,15, and 17.5 mM); BSA (0, 2.5, and 5 g/L) before printing	Extrusion (honeycomb infill pattern, cube of 1.5×1.5×1.5 cm^3)	72–309 µm	–	15–700 kPa	 A	[79]
Mixing of a pectin solution (15 and 35 g/L) with a cell (50% v/v)/$CaCl_2$ suspension (6.5 and 10 mM)	Extrusion	–	0.02–26.42%	30–200 kPa	 B	[236]
LM pectin (15–35 g/L) and 2 drops of red food colorant were dissolved in distilled water, and $CaCl_2$ (10–15 mM) solution was added	Coaxial extrusion (honeycomb pattern with 85% infill density)	–	0.82–5.02%	22.85–143.31 kPa	 C	[204]
LM pectin 15–35 g/L and 2 drops of red food colorant were dissolved in distilled water, and $CaCl_2$ (11–15 mM) solution was added	Extrusion (hexagonal honeycomb pattern)	2.4–7.8 mm	43.11–71.64%	1.55–118.58 kPa	 D	[221]
1 wt% KG/XG at a ratio of 3:2 (w/w) mixed in boiling water; 1 wt% (based on potato flakes) KG/XG (3:2,	Extrusion (infill levels:10, 40 and 70%, infill patterns: rectilinear, honeycomb and	–	6.05–59.60%	0.97–11344.43 Pa	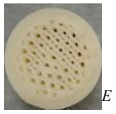 E	[17]

w/w) and potato flakes mixed in boiling water; Potato flakes/boiling water ratio = 4:1 (w/w)	Hilbert curve)

Abbreviations: BSA, Bovine serum albumin; KG, κ-Carrageenan gum; LM, Low methoxyl; XG, Xanthan gum.

[A] Reproduced from Ref. [79] with permission from Elsevier, Copyright 2017; [B] Reproduced from Ref. [236] with permission from Elsevier, Copyright 2019; [C] Reproduced from Ref. [204] with permission from Elsevier, Copyright 2018; [D] Reproduced from Ref. [221] with permission from Elsevier, Copyright 2018; [E] Reproduced from Ref. [17] with permission from Elsevier, Copyright 2018.

1484 **Table 9** Mechanical properties of 3D-printed biopolymer materials and their applications in biomedical fields.

Formulation (bioink)	Printing method	Compression strength	*E*	Application	Ref.
Silk dissolved in LiBr (9 M) to achieve 1.5 wt% SF solution, mixed with 7% (w/v) gelatin at 37 °C	Extrusion	–	130–188.5 kPa	Biomedical	[12]
Silk dissolved in LiBr (9 M) to achieve SF solution (0.5–2%, w/v), mixed with gelatin (1–9%, w/v)	Extrusion	–	30–114 kPa	Cartilage Tissue Engineering	[200]
1 g of collagen I and 50 mg of heparin sulfate dissolved in 50 mL of acetic acid solution (0.05 M)	Extrusion	162.5–308.9 kPa	2.43–3.36 MPa	Biomedical	[277]
Sample 1: SA dissolved in culture medium and agarose dissolved in water; then, the agarose solution (15 mg/mL) and the SA solution (0.1 g/mL) mixed at 1:4 ratio (v/v) at 65 °C; Sample 2: Collagen solution (15 mg/mL) mixed with SA solution (0.1 g/mL) at ratio of 1:4 (v/v)	Extrusion	30–70 kPa	–	Cartilage tissue engineering	[275]
Nanocellulose/HA (70:30, w/w)	Extrusion	0.055–0.169 MPa	–	Biomedical	[324]
CNFs (2.0–3.3 wt%) / XT (5.11–10.6 wt%) / water (86.8–92.3 wt%)	Extrusion	24–67 kPa	200–450 kPa	Tissue engineering or Wound dressings	[218]
0, 1, 2, and 3 wt% GGMMAs powder added to CNFs gel (1 wt%), heated at 50 °C	Extrusion	–	5–22 kPa	Biomedical	[205]

Carboxymethyl cellulose (5–20 wt%) / cellulose fiber (15–45 wt%) mixed with distilled water	Extrusion	–	2.7–5.4 GPa	Biomaterials	[197]
2 wt% CNFs / 98 wt% water	Extrusion	0.031–4.3 GPa	–	Biomedicine	[63]
Sample1: Gelatin (6%, w/v) dissolved in PBS at 60 °C, further dissolved with alginate (1, 3, 5, 7, and 9%, w/v); Sample2: Gelatin (2, 4, 6, 8, and 10%, w/v) dissolved in PBS at 60 °C, further dissolved with alginate (2%, w/v)	Extrusion	29.8–48.0 kPa	–	Biomedicine	[390]
15 g of gelatin dissolved in 100 mL of DMEM/F12, and added with 2.0 g of alginate	Extrusion	359–554.5 kPa	192.3–280 kPa	Skin tissue engineering	[10]
0.06 g/mL gelatin dissolved in NaCl solution, further dissolved with 0.05 g/mL alginate	Extrusion	–	0.96–1.44 MPa	Biomedical	[386]
Alginate (3%, w/v) / gelation (10%, w/v) in water	Extrusion	–	35–65 kPa	Vascular tissue substitution	[380]
Chitosan solution (6%, w/v) / acetic acid (2%, v/v)	Extrusion	–	105 kPa	Skin tissue engineering	[296]
Sample 1: 1–2.5 wt% KG dissolved into DPBS solution at 80 °C; Sample 2: 6−9 wt% gelatin dissolved into DPBS solution at 50 °C	Extrusion	–	11.04–17.97 kPa	Biomedical	[391]

Abbreviations: CNFs, Cellulose nanofibril; DMEM, Dulbecco's modified Eagle medium; DPBS, Dulbecco's phosphate-buffered saline; GGMMA, Galactoglucomannan methacrylate; HA, Hyaluronic acid; KG, κ-Carrageenan; PBS, Phosphate-buffered saline; SA, Sodium alginate; SF, Silk fibroin; XT, Conjugation of xylan with tyramine.

Table 10 Pore size, porosity, and mechanical properties of 3D-printed biopolymer-based porous materials and their application in biomedical fields.

Formulation (bioink)	Printing method	Pore size	Porosity	Compressive modulus	*E*	Application	Morphology	Ref.
11.8, 15, 20, and 30 wt% CNCs mixed with water	DIW	20–800 μm	75–92.1%	–	7–8.94 MPa	Tissue scaffold templates; drug delivery	 A	[65]
6 wt% SA and 3 wt% gelatin dissolved in water at 50 °C, mixed with 6 wt% CNCs to reach a CNCs/SA/gelatin ratio of 70:20:10 (w/w/w)	Extrusion	80–2125 μm	15.82–95.11%	–	1.54 MPa	Tissue regeneration	 B	[226]
6.9% (w/v) SF solution (dissolved in LiBr) mixed with 6.9% (w/v) gelatin solution (dissolved in water) at ratios of 0:3, 1:2, and 2:1 (w/w)	Extrusion	350 μm	–	–	4–17 kPa	Repair cartilage injury	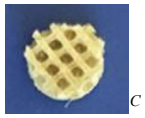 C	[224]
4, 5, and 6% (w/v) keratin dissolved in PBS (4%, w/v)	Lithography	~10–30 μm	–	3.11–15.45 kPa	–	Tissue engineering; Regenerative medicine	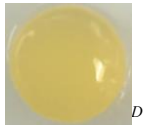 D	[133]

Mixture of cells (1×10^6 mL^{-1}) and collagen solutions (3, 5, and 7 wt%) as collagen bioink	Extrusion	452 µm	–	1.5 MPa	–	Biomedical	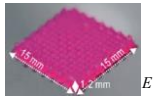 *E*	[118]
4 wt% collagen / 38 wt% Pluronic F-127 dissolved in PBS at 1:1 (v/v) ratio	Extrusion	150–250 µm	98%	–	160–250 kPa	Regenerating bone tissue	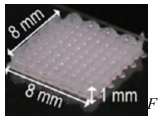 *F*	[276]
Silk dissolved in LiBr (9.3 M) to final 3% (w/v) concentration, mixed with collagen (4 wt%) / dECM	Extrusion	446.6–614.1 µm	–	0.03–0.3 MPa	–	Bone tissue regeneration	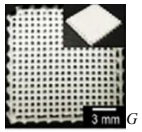 *G*	[264]
4–16% (w/v) gelatin / 2% (w/v) elastin / 0.5% (w/v) sodium hyaluronate in water	Extrusion	286–374 µm	–	–	–	Ocular surface damage	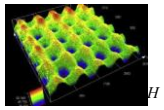 *H*	[392]
1% SA (w/v) and 3% (w/v) gelatin heated at 70 °C	Extrusion	247–265 µm	–	20.4–21.9 kPa	–	Therapeutic stem cell	 *I*	[381]
50 wt% cornstarch / 30 wt% dextran / 20 wt% gelatin dissolved in water	Extrusion	–	33.5–59%	0.18–1.77 MPa	–	Porous scaffold	 *J*	[198]

Abbreviations: CNC, Cellulose nanocrystal; dECM, De-cellularized extracellular matrix; DIW: Direct ink writing; PBS: Phosphate-buffered saline; SA: Sodium alginate; SF: Silk fibroin.

[A] Reproduced from Ref. [65] with permission from Nature Publishing Group, Copyright 2017; [B] Reproduced from Ref. [226] with permission from the RSC Publishing, Copyright 2018; [C] Reproduced from Ref. [224] with permission from Wiley-Blackwell, Copyright 2017; [D] Reproduced from Ref. [133] with permission from Springer, Copyright 2016; [E] Reproduced from Ref. [118] with permission from ACS Publications, Copyright 2016; [F] Reproduced from Ref. [276] with permission from ACS

Publications, Copyright 2018; [G] Reproduced from Ref. [264] with permission from Elsevier, Copyright 2018; [H] Reproduced from Ref. [392] with permission from Elsevier, Copyright 2018; [I] Reproduced from Ref. [381] with permission from Elsevier, Copyright 2019; [J] Reproduced from Ref. [198] with permission from Elsevier, Copyright 2002.

Table 11 3D printing of biopolymers for other applications.

Formulation (bioink)	Printing method	Properties	Application	Morphology	Ref.
6% (w/v) chitosan and 1% (w/v) TiO_2 mixed in water	UV Stereolithography	*E*: 0.49 MPa; Amoxicillin degradation: 80%	Wastewater treatment	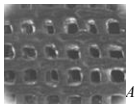 A	[20]
0.5% (w/v) gellan gum and 0.875% (w/v) porcine gelatin mixed at 70 °C	Extrusion	Conductivity: 190±20 mS/cm	Electronic circuit	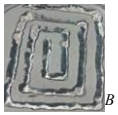 B	[21]
Vegemite or Marmite and white bread substrates	DIW	Conductivity: 20±3 S/cm	Conductive devices	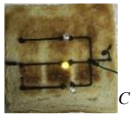 C	[34]
CNCs (10–22.5 wt%) dispersed in DESs (10.17g)/AA solution (30 wt%)	DIW	High sensitivity (gauge factor of 1.5–3.3)	Sensors	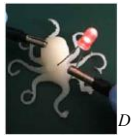 D	[331]
SA (0.08 wt%) mixed with $CaCl_2$ (0.2 M) / PAA (0.2 M) / CNTs (0.1 g) solution	DIW	Gauge factor of 6.29	Wearable strain sensors	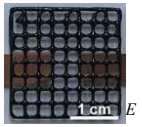 E	[330]
8% (w/v) alginate and 10% (w/v) gelatin dissolved in deionized water	Extrusion	Quantifying UV exposure by decrease in color	Wearable UV sensors	 F	[329]

Abbreviations: AA, Acrylic acid; CNTs, Carbon nanotubes; DES, Deep eutectic solvents; DIW, Direct ink writing; *E*, Young's modulus; PAA, Polyacrylic acid; SA, Sodium alginate.

[A] Reproduced from Ref. [20] with permission from Elsevier, Copyright 2019; [B] Reproduced from Ref. [21] with permission from Cambridge University Press, Copyright

2015; [C] Reproduced from Ref. [34] with permission from Elsevier, Copyright 2018; [D] Reproduced from Ref. [331] with permission from American Chemical Society, Copyright 2020; [E] Reproduced from Ref. [330] with permission from American Chemical Society, Copyright 2021; [F] Reproduced from Ref. [329] with permission from American Chemical Society, Copyright 2020.

Data availability

Data sharing not applicable for this review.

References

[1] A.D. Valino, J.R.C. Dizon, A.H. Espera, Q. Chen, J. Messman, R.C. Advincula, Advances in 3D printing of thermoplastic polymer composites and nanocomposites, Prog. Polym. Sci. 98 (2019) 101162.

[2] I. Donderwinkel, J.C.M. van Hest, N.R. Cameron, Bio-inks for 3D bioprinting: recent advances and future prospects, Polym. Chem. 8(31) (2017) 4451-4471.

[3] W.-J. Long, J.-L. Tao, C. Lin, Y.-c. Gu, L. Mei, H.-B. Duan, F. Xing, Rheology and buildability of sustainable cement-based composites containing micro-crystalline cellulose for 3D-printing, J. Cleaner Prod. 239 (2019) 118054.

[4] Z. Liu, M. Zhang, B. Bhandari, Y. Wang, 3D printing: Printing precision and application in food sector, Trends Food Sci. Technol. 69 (2017) 83-94.

[5] A. Derossi, R. Caporizzi, D. Azzollini, C. Severini, Application of 3D printing for customized food. A case on the development of a fruit-based snack for children, J. Food Eng. 220 (2018) 65-75.

[6] W.E. Katstra, R.D. Palazzolo, C.W. Rowe, B. Giritlioglu, P. Teung, M.J. Cima, Oral dosage forms fabricated by Three Dimensional Printing, J. Controlled Release 66(1) (2000) 1-9.

[7] N. Faramarzi, I.K. Yazdi, M. Nabavinia, A. Gemma, A. Fanelli, A. Caizzone, L.M. Ptaszek, I. Sinha, A. Khademhosseini, J.N. Ruskin, A. Tamayol, Patient-Specific Bioinks for 3D Bioprinting of Tissue Engineering Scaffolds, Adv. Healthcare Mater. 7(11) (2018) 1701347.

[8] G. Palmara, F. Frascella, I. Roppolo, A. Chiappone, A. Chiadò, Functional 3D printing: Approaches and bioapplications, Biosensors and Bioelectronics 175 (2021) 112849.

[9] Z. Liu, M. Zhang, 3D Food Printing Technologies and Factors Affecting Printing Precision, in: F.C. Godoi, B.R. Bhandari, S. Prakash, M. Zhang (Eds.), Fundamentals of 3D Food Printing and Applications, Academic Press2019, pp. 19-40.

[10] P. Liu, H. Shen, Y. Zhi, J. Si, J. Shi, L. Guo, S.G. Shen, 3D bioprinting and in vitro study of bilayered membranous construct with human cells-laden alginate/gelatin composite hydrogels, Colloids Surf., B 181 (2019) 1026-1034.

[11] H. Martínez Ávila, S. Schwarz, N. Rotter, P. Gatenholm, 3D bioprinting of human chondrocyte-laden nanocellulose hydrogels for patient-specific auricular cartilage regeneration, Bioprinting 1-2 (2016) 22-35.

[12] A. Bandyopadhyay, B.B. Mandal, A three-dimensional printed silk-based biomimetic tri-layered meniscus for potential patient-specific implantation, Biofabrication 12(1) (2019) 015003.

[13] V.K. Lee, D.Y. Kim, H. Ngo, Y. Lee, L. Seo, S.-S. Yoo, P.A. Vincent, G. Dai, Creating perfused functional vascular channels using 3D bio-printing technology, Biomaterials 35(28) (2014) 8092-8102.

[14] C. Severini, D. Azzollini, M. Albenzio, A. Derossi, On printability, quality and nutritional properties of 3D printed cereal based snacks enriched with edible insects, Food Res. Int. 106 (2018) 666-676.

[15] M. Lille, A. Nurmela, E. Nordlund, S. Metsä-Kortelainen, N. Sozer, Applicability of protein and fiber-rich food materials in extrusion-based 3D printing, J. Food Eng. 220 (2018) 20-27.

[16] F. Yang, M. Zhang, S. Prakash, Y. Liu, Physical properties of 3D printed baking dough as affected by different compositions, Innovative Food Sci. Emerg. Technol. 49 (2018) 202-210.

[17] Z. Liu, B. Bhandari, S. Prakash, M. Zhang, Creation of internal structure of mashed potato construct by 3D printing and its textural properties, Food Res. Int. 111 (2018) 534-543.

[18] L. Zhao, M. Zhang, B. Chitrakar, B. Adhikari, Recent advances in functional 3D printing of foods: a review of functions of ingredients and internal structures, Crit. Rev. Food Sci. Nutr. n/a(n/a) (2020) 1-15.

[19] A. Kumar, J. Ahlawat, M. Narayan, 3D Bioprinting for Organs, Skin, and Engineered Tissues, in: N. Ahmad, P. Gopinath, R. Dutta (Eds.), 3D Printing Technology in Nanomedicine, Elsevier2019, pp. 115-128.

[20] L. Bergamonti, C. Bergonzi, C. Graiff, P.P. Lottici, R. Bettini, L. Elviri, 3D printed chitosan scaffolds: A new TiO2 support for the photocatalytic degradation of amoxicillin in water, Water Research 163 (2019) 114841.

[21] A. Keller, L. Stevens, G.G. Wallace, M. in het Panhuis, 3D Printed Edible Hydrogel Electrodes, MRS Adv. 1(8) (2015) 527-532.

[22] R.M. Cardoso, D.M.H. Mendonça, W.P. Silva, M.N.T. Silva, E. Nossol, R.A.B. da Silva, E.M. Richter, R.A.A. Muñoz, 3D printing for electroanalysis: From multiuse electrochemical cells to sensors, Anal. Chim. Acta 1033 (2018) 49-57.

[23] G.I. Peterson, M.B. Larsen, M.A. Ganter, D.W. Storti, A.J. Boydston, 3D-Printed Mechanochromic Materials, ACS Appl. Mater. Interfaces 7(1) (2015) 577-583.

[24] C.M. González-Henríquez, M.A. Sarabia-Vallejos, J. Rodriguez-Hernandez, Polymers for

1567 additive manufacturing and 4D-printing: Materials, methodologies, and biomedical applications,
1568 Prog. Polym. Sci. 94 (2019) 57-116.
1569 [25] J. Liu, L. Sun, W. Xu, Q. Wang, S. Yu, J. Sun, Current advances and future perspectives of 3D
1570 printing natural-derived biopolymers, Carbohydr. Polym. 207 (2019) 297-316.
1571 [26] A. Abbasi, M.M. Nasef, W.Z.N. Yahya, Copolymerization of vegetable oils and bio-based
1572 monomers with elemental sulfur: A new promising route for bio-based polymers, Sustainable
1573 Chemistry and Pharmacy 13 (2019) 100158.
1574 [27] L. Dai, T. Cheng, C. Duan, W. Zhao, W. Zhang, X. Zou, J. Aspler, Y. Ni, 3D printing using
1575 plant-derived cellulose and its derivatives: A review, Carbohydr. Polym. 203 (2019) 71-86.
1576 [28] A. Goel, M.K. Meher, K. Gulati, K.M. Poluri, Fabrication of Biopolymer-Based Organs and
1577 Tissues Using 3D Bioprinting, in: N. Ahmad, P. Gopinath, R. Dutta (Eds.), 3D Printing Technology
1578 in Nanomedicine, Elsevier2019, pp. 43-62.
1579 [29] W. Xu, X. Wang, N. Sandler, S. Willför, C. Xu, Three-Dimensional Printing of Wood-Derived
1580 Biopolymers: A Review Focused on Biomedical Applications, ACS Sustainable Chem. Eng. 6(5)
1581 (2018) 5663-5680.
1582 [30] M. Hassan, K. Dave, R. Chandrawati, F. Dehghani, V.G. Gomes, 3D printing of biopolymer
1583 nanocomposites for tissue engineering: Nanomaterials, processing and structure-function relation,
1584 Eur. Polym. J. 121 (2019) 109340.
1585 [31] L. Chaunier, S. Guessasma, S. Belhabib, G. Della Valle, D. Lourdin, E. Leroy, Material
1586 extrusion of plant biopolymers: Opportunities & challenges for 3D printing, Addit. Manuf. 21 (2018)
1587 220-233.

[32] M. Shahbazi, H. Jäger, Current Status in the Utilization of Biobased Polymers for 3D Printing Process: A Systematic Review of the Materials, Processes, and Challenges, ACS Applied Bio Materials 4(1) (2020) 325–369.

[33] Z. Liu, H. Chen, B. Zheng, F. Xie, L. Chen, Understanding the structure and rheological properties of potato starch induced by hot-extrusion 3D printing, Food Hydrocolloids 105 (2020) 105812.

[34] C.A. Hamilton, G. Alici, M. in het Panhuis, 3D printing Vegemite and Marmite: Redefining "breadboards", J. Food Eng. 220 (2018) 83-88.

[35] V. Latza, P.A. Guerette, D. Ding, S. Amini, A. Kumar, I. Schmidt, S. Keating, N. Oxman, J.C. Weaver, P. Fratzl, A. Miserez, A. Masic, Multi-scale thermal stability of a hard thermoplastic protein-based material, Nat. Commun. 6(1) (2015) 8313.

[36] T.M.M. Bernaerts, L. Gheysen, I. Foubert, M.E. Hendrickx, A.M. Van Loey, The potential of microalgae and their biopolymers as structuring ingredients in food: A review, Biotechnol. Adv. 37(8) (2019) 107419.

[37] A. Przekora, The summary of the most important cell-biomaterial interactions that need to be considered during in vitro biocompatibility testing of bone scaffolds for tissue engineering applications, Mater. Sci. Eng., C 97 (2019) 1036-1051.

[38] A. Gilet, C. Quettier, V. Wiatz, H. Bricout, M. Ferreira, C. Rousseau, E. Monflier, S. Tilloy, Unconventional media and technologies for starch etherification and esterification, Green Chem. 20(6) (2018) 1152-1168.

[39] B. Arafat, M. Wojsz, A. Isreb, R.T. Forbes, M. Isreb, W. Ahmed, T. Arafat, M.A. Alhnan, Tablet

fragmentation without a disintegrant: A novel design approach for accelerating disintegration and drug release from 3D printed cellulosic tablets, Eur. J. Pharm. Sci. 118 (2018) 191-199.

[40] J. Chen, F. Xie, X. Li, L. Chen, Ionic liquids for the preparation of biopolymer materials for drug/gene delivery: a review, Green Chem. 20(18) (2018) 4169-4200.

[41] N. Li, M. Niu, B. Zhang, S. Zhao, S. Xiong, F. Xie, Effects of concurrent ball milling and octenyl succinylation on structure and physicochemical properties of starch, Carbohydr. Polym. 155 (2017) 109-116.

[42] Y. Huo, B. Zhang, M. Niu, C. Jia, S. Zhao, Q. Huang, H. Du, An insight into the multi-scale structures and pasting behaviors of starch following citric acid treatment, Int. J. Biol. Macromol. 116 (2018) 793-800.

[43] D. Qiao, B. Zhang, J. Huang, F. Xie, D.K. Wang, F. Jiang, S. Zhao, J. Zhu, Hydration-induced crystalline transformation of starch polymer under ambient conditions, Int. J. Biol. Macromol. 103 (2017) 152-157.

[44] H. Wang, B. Zhang, L. Chen, X. Li, Understanding the structure and digestibility of heat-moisture treated starch, Int. J. Biol. Macromol. 88 (2016) 1-8.

[45] Z. Liu, M. Zhang, C.-h. Yang, Dual extrusion 3D printing of mashed potatoes/strawberry juice gel, LWT - Food Sci. Technol. 96 (2018) 589-596.

[46] F. Xie, P.J. Halley, L. Avérous, Rheology to understand and optimize processibility, structures and properties of starch polymeric materials, Prog. Polym. Sci. 37(4) (2012) 595-623.

[47] S. Wang, C. Li, X. Zhang, L. Copeland, S. Wang, Retrogradation enthalpy does not always reflect the retrogradation behavior of gelatinized starch, Sci. Rep. 6(1) (2016) 20965.

[48] F. Xie, E. Pollet, P.J. Halley, L. Avérous, Starch-based nano-biocomposites, Prog. Polym. Sci. 38(10) (2013) 1590-1628.

[49] S. Wang, C. Chao, F. Xiang, X. Zhang, S. Wang, L. Copeland, New insights into gelatinization mechanisms of cereal endosperm starches, Sci. Rep. 8(1) (2018) 3011.

[50] R. Hoover, T. Hughes, H.J. Chung, Q. Liu, Composition, molecular structure, properties, and modification of pulse starches: A review, Food Res. Int. 43(2) (2010) 399-413.

[51] L.A. Bello Perez, E. Agama-Acevedo, Starch, in: M.A. Villar, S.E. Barbosa, M.A. García, L.A. Castillo, O.V. López (Eds.), Starch-Based Materials in Food Packaging, Academic Press2017, pp. 1-18.

[52] B.C. Maniglia, D.C. Lima, M.D. Matta Junior, P. Le-Bail, A. Le-Bail, P.E.D. Augusto, Preparation of cassava starch hydrogels for application in 3D printing using dry heating treatment (DHT): A prospective study on the effects of DHT and gelatinization conditions, Food Res. Int. 128 (2020) 108803.

[53] H.P.S. Abdul Khalil, A.H. Bhat, A.F. Ireana Yusra, Green composites from sustainable cellulose nanofibrils: A review, Carbohydr. Polym. 87(2) (2012) 963-979.

[54] R. Thakkar, R. Thakkar, A. Pillai, E.A. Ashour, M.A. Repka, Systematic screening of pharmaceutical polymers for hot melt extrusion processing: a comprehensive review, Int. J. Pharm. 576 (2020) 118989.

[55] B. Lindman, G. Karlström, L. Stigsson, On the mechanism of dissolution of cellulose, J. Mol. Liq. 156(1) (2010) 76-81.

[56] S. Sen, J.D. Martin, D.S. Argyropoulos, Review of Cellulose Non-Derivatizing Solvent

Interactions with Emphasis on Activity in Inorganic Molten Salt Hydrates, ACS Sustainable Chem. Eng. 1(8) (2013) 858-870.

[57] B. Zhang, F. Xie, J.L. Shamshina, R.D. Rogers, T. McNally, P.J. Halley, R.W. Truss, L. Chen, S. Zhao, Dissolution of Starch with Aqueous Ionic Liquid under Ambient Conditions, ACS Sustainable Chem. Eng. 5(5) (2017) 3737-3741.

[58] A. Pinkert, K.N. Marsh, S. Pang, M.P. Staiger, Ionic Liquids and Their Interaction with Cellulose, Chem. Rev. 109(12) (2009) 6712-6728.

[59] T. Liebert, Cellulose Solvents – Remarkable History, Bright Future, Cellulose Solvents: For Analysis, Shaping and Chemical Modification, American Chemical Society2010, pp. 3-54.

[60] H. Zhao, J.H. Kwak, Y. Wang, J.A. Franz, J.M. White, J.E. Holladay, Interactions between cellulose and N-methylmorpholine-N-oxide, Carbohydr. Polym. 67(1) (2007) 97-103.

[61] L. Pang, Z. Gao, H. Feng, S. Wang, Q. Wang, Cellulose based materials for controlled release formulations of agrochemicals: A review of modifications and applications, J. Controlled Release 316 (2019) 105-115.

[62] M. Barsbay, O. Güven, Surface modification of cellulose via conventional and controlled radiation-induced grafting, Radiat. Phys. Chem. 160 (2019) 1-8.

[63] K.M.O. Håkansson, I.C. Henriksson, C. de la Peña Vázquez, V. Kuzmenko, K. Markstedt, P. Enoksson, P. Gatenholm, Solidification of 3D Printed Nanofibril Hydrogels into Functional 3D Cellulose Structures, Adv. Mater. Technol. 1(7) (2016) 1600096.

[64] M. Kimura, Y. Shinohara, J. Takizawa, S. Ren, K. Sagisaka, Y. Lin, Y. Hattori, J.P. Hinestroza, Versatile Molding Process for Tough Cellulose Hydrogel Materials, Sci. Rep. 5(1) (2015) 16266.

[65] V.C.-F. Li, C.K. Dunn, Z. Zhang, Y. Deng, H.J. Qi, Direct Ink Write (DIW) 3D Printed Cellulose Nanocrystal Aerogel Structures, Sci. Rep. 7(1) (2017) 8018.

[66] H. Qiao, L. Li, J. Wu, Y. Zhang, Y. Liao, H. Zhou, D. Li, High-strength cellulose films obtained by the combined action of shear force and surface selective dissolution, Carbohydr. Polym. 233 (2020) 115883.

[67] S.P. Alandete Germán, S. Isarria Vidal, M.L. Domingo Montañana, E. De la vía Oraá, J. Vilar Samper, Pacemakers and implantable cardioverter defibrillators, unknown to chest radiography: Review, complications and systematic reading, Eur. J. Radiol. 84(3) (2015) 499-508.

[68] J.L. Sanchez-Salvador, A. Balea, M.C. Monte, C. Negro, M. Miller, J. Olson, A. Blanco, Comparison Of Mechanical And Chemical Nanocellulose As Additives To Reinforce Recycled Cardboard, Sci. Rep. 10(1) (2020) 3778.

[69] Y. Yataka, A. Suzuki, K. Iijima, M. Hashizume, Enhancement of the mechanical properties of polysaccharide composite films utilizing cellulose nanofibers, Polym. J. 52 (2020) 645–653.

[70] K. Varaprasad, T. Jayaramudu, V. Kanikireddy, C. Toro, E.R. Sadiku, Alginate-based composite materials for wound dressing application:A mini review, Carbohydr. Polym. 236 (2020) 116025.

[71] I.P.S. Fernando, W. Lee, E.J. Han, G. Ahn, Alginate-based nanomaterials: Fabrication techniques, properties, and applications, Chem. Eng. J. 391 (2019) 123823.

[72] K.Y. Lee, D.J. Mooney, Alginate: Properties and biomedical applications, Prog. Polym. Sci. 37(1) (2012) 106-126.

[73] L. Li, Q. Lin, M. Tang, A.J.E. Duncan, C. Ke, Advanced Polymer Designs for Direct-Ink-Write 3D Printing, Chemistry – A European Journal 25(46) (2019) 10768-10781.

[74] A. Kirillova, R. Maxson, G. Stoychev, C.T. Gomillion, L. Ionov, 4D Biofabrication Using Shape-Morphing Hydrogels, Adv. Mater. 29(46) (2017) 1703443.

[75] Z.-L. Kang, T.-t. Wang, Y.-p. Li, K. Li, H.-j. Ma, Effect of sodium alginate on physical-chemical, protein conformation and sensory of low-fat frankfurters, Meat Sci. 162 (2020) 108043.

[76] Y. Liu, T. Tang, S. Duan, Z. Qin, C. Li, Z. Zhang, A. Liu, D. Wu, H. Chen, G. Han, B. Lin, J. He, W. Wu, Effects of sodium alginate and rice variety on the physicochemical characteristics and 3D printing feasibility of rice paste, LWT 127 (2020) 109360.

[77] A. Rehman, T. Ahmad, R.M. Aadil, M.J. Spotti, A.M. Bakry, I.M. Khan, L. Zhao, T. Riaz, Q. Tong, Pectin polymers as wall materials for the nano-encapsulation of bioactive compounds, Trends Food Sci. Technol. 90 (2019) 35-46.

[78] G. Mao, D. Wu, C. Wei, W. Tao, X. Ye, R.J. Linhardt, C. Orfila, S. Chen, Reconsidering conventional and innovative methods for pectin extraction from fruit and vegetable waste: Targeting rhamnogalacturonan I, Trends Food Sci. Technol. 94 (2019) 65-78.

[79] V. Vancauwenberghe, L. Katalagarianakis, Z. Wang, M. Meerts, M. Hertog, P. Verboven, P. Moldenaers, M.E. Hendrickx, J. Lammertyn, B. Nicolaï, Pectin based food-ink formulations for 3-D printing of customizable porous food simulants, Innovative Food Sci. Emerg. Technol. 42 (2017) 138-150.

[80] F. van de Velde, Structure and function of hybrid carrageenans, Food Hydrocolloids 22(5) (2008) 727-734.

[81] W. Feng, S. Feng, K. Tang, X. He, A. Jing, G. Liang, A novel composite of collagen-hydroxyapatite/kappa-carrageenan, J. Alloys Compd. 693 (2017) 482-489.

[82] P. Kanmani, J.-W. Rhim, Development and characterization of carrageenan/grapefruit seed extract composite films for active packaging, Int. J. Biol. Macromol. 68 (2014) 258-266.

[83] S. Selvakumaran, I.I. Muhamad, S.I. Abd Razak, Evaluation of kappa carrageenan as potential carrier for floating drug delivery system: Effect of pore forming agents, Carbohydr. Polym. 135 (2016) 207-214.

[84] N.A. Negm, H.H.H. Hefni, A.A.A. Abd-Elaal, E.A. Badr, M.T.H. Abou Kana, Advancement on modification of chitosan biopolymer and its potential applications, Int. J. Biol. Macromol. 152 (2020) 681-702.

[85] M. Dash, F. Chiellini, R.M. Ottenbrite, E. Chiellini, Chitosan—A versatile semi-synthetic polymer in biomedical applications, Prog. Polym. Sci. 36(8) (2011) 981-1014.

[86] P.S. Bakshi, D. Selvakumar, K. Kadirvelu, N.S. Kumar, Chitosan as an environment friendly biomaterial – a review on recent modifications and applications, Int. J. Biol. Macromol. 150 (2019) 1072-1083.

[87] L.C. Yo, Preparation and Characterization of Water-Soluble Chitosan Gel for Skin Hydration, University Sains Malaysia, 2008.

[88] A. Anitha, S. Sowmya, P.T.S. Kumar, S. Deepthi, K.P. Chennazhi, H. Ehrlich, M. Tsurkan, R. Jayakumar, Chitin and chitosan in selected biomedical applications, Prog. Polym. Sci. 39(9) (2014) 1644-1667.

[89] P. Mukhopadhyay, R. Mishra, D. Rana, P.P. Kundu, Strategies for effective oral insulin delivery with modified chitosan nanoparticles: A review, Prog. Polym. Sci. 37(11) (2012) 1457-1475.

[90] F. Hafezi, N. Scoutaris, D. Douroumis, J. Boateng, 3D printed chitosan dressing crosslinked

with genipin for potential healing of chronic wounds, Int. J. Pharm. 560 (2019) 406-415.
[91] M. Rajabi, M. McConnell, J. Cabral, M.A. Ali, Chitosan hydrogels in 3D printing for biomedical applications, Carbohydr. Polym. 260 (2021) 117768.
[92] A.C. Heidenreich, M. Pérez-Recalde, A. González Wusener, É.B. Hermida, Collagen and chitosan blends for 3D bioprinting: A rheological and printability approach, Polym. Test. 82 (2020) 106297.
[93] N.D. Sanandiya, Y. Vijay, M. Dimopoulou, S. Dritsas, J.G. Fernandez, Large-scale additive manufacturing with bioinspired cellulosic materials, Sci. Rep. 8(1) (2018) 8642.
[94] K. Huanbutta, K. Cheewatanakornkool, K. Terada, J. Nunthanid, P. Sriamornsak, Impact of salt form and molecular weight of chitosan on swelling and drug release from chitosan matrix tablets, Carbohydr. Polym. 97(1) (2013) 26-33.
[95] S. Belbekhouche, N. Bousserrhine, V. Alphonse, F. Le Floch, Y. Charif Mechiche, I. Menidjel, B. Carbonnier, Chitosan based self-assembled nanocapsules as antibacterial agent, Colloids Surf., B 181 (2019) 158-165.
[96] P. Zhai, X. Peng, B. Li, Y. Liu, H. Sun, X. Li, The application of hyaluronic acid in bone regeneration, Int. J. Biol. Macromol. 151 (2020) 1224-1239.
[97] E. Ahmadian, A. Eftekhari, S.M. Dizaj, S. Sharifi, M. Mokhtarpour, A.N. Nasibova, R. Khalilov, M. Samiei, The effect of hyaluronic acid hydrogels on dental pulp stem cells behavior, Int. J. Biol. Macromol. 140 (2019) 245-254.
[98] S. Vasvani, P. Kulkarni, D. Rawtani, Hyaluronic acid: A review on its biology, aspects of drug delivery, route of administrations and a special emphasis on its approved marketed products and

recent clinical studies, Int. J. Biol. Macromol. 151 (2019) 1012-1029.

[99] Z. Luo, Y. Dai, H. Gao, Development and application of hyaluronic acid in tumor targeting drug delivery, Acta Pharm. Sin. B 9(6) (2019) 1099-1112.

[100] S.N.A. Bukhari, N.L. Roswandi, M. Waqas, H. Habib, F. Hussain, S. Khan, M. Sohail, N.A. Ramli, H.E. Thu, Z. Hussain, Hyaluronic acid, a promising skin rejuvenating biomedicine: A review of recent updates and pre-clinical and clinical investigations on cosmetic and nutricosmetic effects, Int. J. Biol. Macromol. 120 (2018) 1682-1695.

[101] H. Ying, J. Zhou, M. Wang, D. Su, Q. Ma, G. Lv, J. Chen, In situ formed collagen-hyaluronic acid hydrogel as biomimetic dressing for promoting spontaneous wound healing, Mater. Sci. Eng., C 101 (2019) 487-498.

[102] E.R. Morris, Ordered conformation of xanthan in solutions and “weak gels”: Single helix, double helix – or both?, Food Hydrocolloids 86 (2019) 18-25.

[103] R.A. Hassler, D.H. Doherty, Genetic engineering of polysaccharide structure: production of variants of xanthan gum in Xanthomonas campestris, Biotechnol. Progr. 6(3) (1990) 182-187.

[104] Z. Liu, B. Bhandari, S. Prakash, S. Mantihal, M. Zhang, Linking rheology and printability of a multicomponent gel system of carrageenan-xanthan-starch in extrusion based additive manufacturing, Food Hydrocolloids 87 (2019) 413-424.

[105] A. Kumar, K.M. Rao, S.S. Han, Application of xanthan gum as polysaccharide in tissue engineering: A review, Carbohydr. Polym. 180 (2018) 128-144.

[106] P. García-Segovia, V. García-Alcaraz, S. Balasch-Parisi, J. Martínez-Monzó, 3D printing of gels based on xanthan/konjac gums, Innovative Food Sci. Emerg. Technol. 64 (2020) 102343.

[107] A. Palaniraj, V. Jayaraman, Production, recovery and applications of xanthan gum by Xanthomonas campestris, J. Food Eng. 106(1) (2011) 1-12.

[108] G. Singhvi, N. Hans, N. Shiva, S. Kumar Dubey, Xanthan gum in drug delivery applications, in: M.S. Hasnain, A.K. Nayak (Eds.), Natural Polysaccharides in Drug Delivery and Biomedical Applications, Academic Press2019, pp. 121-144.

[109] I. Chang, J. Im, A.K. Prasidhi, G.-C. Cho, Effects of Xanthan gum biopolymer on soil strengthening, Constr. Build. Mater. 74 (2015) 65-72.

[110] J.Y. Nehete, R.S. Bhambar, M.R. Narkhede, S.R. Gawali, Natural proteins: Sources, isolation, characterization and applications, Pharmacogn. Rev. 7(14) (2013) 107-116.

[111] Y. Liu, D. Liu, G. Wei, Y. Ma, B. Bhandari, P. Zhou, 3D printed milk protein food simulant: Improving the printing performance of milk protein concentration by incorporating whey protein isolate, Innovative Food Sci. Emerg. Technol. 49 (2018) 116-126.

[112] S. Gomes, I.B. Leonor, J.F. Mano, R.L. Reis, D.L. Kaplan, Natural and genetically engineered proteins for tissue engineering, Prog. Polym. Sci. 37(1) (2012) 1-17.

[113] X. Mu, F. Agostinacchio, N. Xiang, Y. Pei, Y. Khan, C. Guo, P. Cebe, A. Motta, D.L. Kaplan, Recent Advances in 3D Printing with Protein-Based Inks, Prog. Polym. Sci. 115 (2021) 101375.

[114] X. Liu, C. Zheng, X. Luo, X. Wang, H. Jiang, Recent advances of collagen-based biomaterials: Multi-hierarchical structure, modification and biomedical applications, Mater. Sci. Eng., C 99 (2019) 1509-1522.

[115] M.C. Gómez-Guillén, B. Giménez, M.E. López-Caballero, M.P. Montero, Functional and bioactive properties of collagen and gelatin from alternative sources: A review, Food Hydrocolloids

25(8) (2011) 1813-1827.

[116] H. Hong, H. Fan, M. Chalamaiah, J. Wu, Preparation of low-molecular-weight, collagen hydrolysates (peptides): Current progress, challenges, and future perspectives, Food Chem. 301 (2019) 125222.

[117] X. Wang, Q. Ao, X. Tian, J. Fan, H. Tong, W. Hou, S. Bai, Gelatin-Based Hydrogels for Organ 3D Bioprinting, Polymers 9(9) (2017).

[118] Y.B. Kim, H. Lee, G.H. Kim, Strategy to Achieve Highly Porous/Biocompatible Macroscale Cell Blocks, Using a Collagen/Genipin-bioink and an Optimal 3D Printing Process, ACS Appl. Mater. Interfaces 8(47) (2016) 32230-32240.

[119] A. Mazzocchi, M. Devarasetty, R. Huntwork, S. Soker, A. Skardal, Optimization of collagen type I-hyaluronan hybrid bioink for 3D bioprinted liver microenvironments, Biofabrication 11(1) (2018) 015003.

[120] S. Cao, H. Li, K. Li, J. Lu, L. Zhang, A dense and strong bonding collagen film for carbon/carbon composites, Appl. Surf. Sci. 347 (2015) 307-314.

[121] M.G. Haugh, M.J. Jaasma, F.J. O'Brien, The effect of dehydrothermal treatment on the mechanical and structural properties of collagen-GAG scaffolds, J. Biomed. Mater. Res. Part A 89A(2) (2009) 363-369.

[122] G.H. Altman, F. Diaz, C. Jakuba, T. Calabro, R.L. Horan, J. Chen, H. Lu, J. Richmond, D.L. Kaplan, Silk-based biomaterials, Biomaterials 24(3) (2003) 401-416.

[123] J. Ming, Z. Liu, S. Bie, F. Zhang, B. Zuo, Novel silk fibroin films prepared by formic acid/hydroxyapatite dissolution method, Mater. Sci. Eng., C 37 (2014) 48-53.

[124] D. Chouhan, B.B. Mandal, Silk biomaterials in wound healing and skin regeneration therapeutics: From bench to bedside, Acta Biomater. 103 (2020) 24-51.

[125] H.-Y. Wang, Z.-G. Wei, Y.-Q. Zhang, Dissolution and regeneration of silk from silkworm Bombyx mori in ionic liquids and its application to medical biomaterials, Int. J. Biol. Macromol. 143 (2020) 594-601.

[126] H.J. Cho, C.S. Ki, H. Oh, K.H. Lee, I.C. Um, Molecular weight distribution and solution properties of silk fibroins with different dissolution conditions, Int. J. Biol. Macromol. 51(3) (2012) 336-341.

[127] L. Lin, J.M. Regenstein, S. Lv, J. Lu, S. Jiang, An overview of gelatin derived from aquatic animals: Properties and modification, Trends Food Sci. Technol. 68 (2017) 102-112.

[128] N. Suderman, M.I.N. Isa, N.M. Sarbon, The effect of plasticizers on the functional properties of biodegradable gelatin-based film: A review, Food Biosci. 24 (2018) 111-119.

[129] M. Mahmoudi Saber, Strategies for surface modification of gelatin-based nanoparticles, Colloids Surf., B 183 (2019) 110407.

[130] J. Du, H. Dai, H. Wang, Y. Yu, H. Zhu, Y. Fu, L. Ma, L. Peng, L. Li, Q. Wang, Y. Zhang, Preparation of high thermal stability gelatin emulsion and its application in 3D printing, Food Hydrocolloids 113 (2021) 106536.

[131] M. Rajabi, A. Ali, M. McConnell, J. Cabral, Keratinous materials: Structures and functions in biomedical applications, Mater. Sci. Eng., C 110 (2020) 110612.

[132] V. Ferraro, M. Anton, V. Santé-Lhoutellier, The “sisters” α-helices of collagen, elastin and keratin recovered from animal by-products: Functionality, bioactivity and trends of application,

Trends Food Sci. Technol. 51 (2016) 65-75.

[133] J.K. Placone, J. Navarro, G.W. Laslo, M.J. Lerman, A.R. Gabard, G.J. Herendeen, E.E. Falco, S. Tomblyn, L. Burnett, J.P. Fisher, Development and Characterization of a 3D Printed, Keratin-Based Hydrogel, Ann. Biomed. Eng. 45 (2017) 237–248.

[134] L. Nunes, G.M. Tavares, Thermal treatments and emerging technologies: Impacts on the structure and techno-functional properties of milk proteins, Trends Food Sci. Technol. 90 (2019) 88-99.

[135] Y. Du, M. Zhang, H. Chen, Effect of whey protein on the 3D printing performance of konjac hybrid gel, LWT 140 (2021) 110716.

[136] M.M. Ross, A.L. Kelly, S.V. Crowley, Potential Applications of Dairy Products, Ingredients and Formulations in 3D Printing, in: F.C. Godoi, B.R. Bhandari, S. Prakash, M. Zhang (Eds.), Fundamentals of 3D Food Printing and Applications, Academic Press2019, pp. 175-206.

[137] J. Sun, F. Ren, Y. Chang, P. Wang, Y. Li, H. Zhang, J. Luo, Formation and structural properties of acid-induced casein–agar double networks: Role of gelation sequence, Food Hydrocolloids 85 (2018) 291-298.

[138] A.V. Dominguez, T. Nicolai, Heat induced gelation of micellar casein with and without whey proteins in the presence of polyphosphate, Int. Dairy J. 104 (2020) 104640.

[139] K. Daffner, L. Ong, E. Hanssen, S. Gras, T. Mills, Journal of Food Hydrocolloids Characterising the influence of milk fat towards an application for extrusion-based 3D-printing of casein−whey protein suspensions via the pH−temperature-route, Food Hydrocolloids n/a (2021) 106642.

[140] S.G. Anema, Y. Li, Association of denatured whey proteins with casein micelles in heated reconstituted skim milk and its effect on casein micelle size, J. Dairy Res. 70(1) (2003) p.73-83.

[141] R.P. Frydenberg, M. Hammershøj, U. Andersen, M.T. Greve, L. Wiking, Protein denaturation of whey protein isolates (WPIs) induced by high intensity ultrasound during heat gelation, Food Chem. 192 (2016) 415-423.

[142] A.R. Jambrak, T.J. Mason, V. Lelas, L. Paniwnyk, Z. Herceg, Effect of ultrasound treatment on particle size and molecular weight of whey proteins, J. Food Eng. 121 (2014) 15-23.

[143] R.R. Koshy, S.K. Mary, S. Thomas, L.A. Pothan, Environment friendly green composites based on soy protein isolate – A review, Food Hydrocolloids 50 (2015) 174-192.

[144] K.B. Chien, E. Makridakis, R.N. Shah, Three-Dimensional Printing of Soy Protein Scaffolds for Tissue Regeneration, Tissue Eng. Part C 19(6) (2012) 417-426.

[145] Ashish, N. Ahmad, P. Gopinath, A. Vinogradov, 3D Printing in Medicine: Current Challenges and Potential Applications, in: N. Ahmad, P. Gopinath, R. Dutta (Eds.), 3D Printing Technology in Nanomedicine, Elsevier2019, pp. 1-22.

[146] Y. Guo, S. Patanwala Huseini, B. Bognet, W.K. Ma Anson, Inkjet and inkjet-based 3D printing: connecting fluid properties and printing performance, Rapid Prototyping J. 23(3) (2017) 562-576.

[147] B. Derby, Inkjet Printing of Functional and Structural Materials: Fluid Property Requirements, Feature Stability, and Resolution, Annu. Rev. Mater. Res. 40(1) (2010) 395-414.

[148] S. Waheed, J.M. Cabot, N.P. Macdonald, T. Lewis, R.M. Guijt, B. Paull, M.C. Breadmore, 3D printed microfluidic devices: enablers and barriers, Lab Chip 16(11) (2016) 1993-2013.

[149] S.F.S. Shirazi, S. Gharehkhani, M. Mehrali, H. Yarmand, H.S.C. Metselaar, N. Adib Kadri,

1882 N.A.A. Osman, A review on powder-based additive manufacturing for tissue engineering: selective
1883 laser sintering and inkjet 3D printing, Sci. Technol. Adv. Mater. 16(3) (2015) 033502.
1884 [150] S.V. Murphy, A. Atala, 3D bioprinting of tissues and organs, Nat. Biotechnol. 32(8) (2014)
1885 773-785.
1886 [151] J. Malda, J. Visser, F.P. Melchels, T. Jüngst, W.E. Hennink, W.J.A. Dhert, J. Groll, D.W.
1887 Hutmacher, 25th Anniversary Article: Engineering Hydrogels for Biofabrication, Adv. Mater. 25(36)
1888 (2013) 5011-5028.
1889 [152] S.S. Crump, Apparatus and Method for Creating Three-dimensional Objects, Stratasys Inc,
1890 1992.
1891 [153] S. Haldar, D. Lahiri, P. Roy, 3D Print Technology for Cell Culturing, in: N. Ahmad, P.
1892 Gopinath, R. Dutta (Eds.), 3D Printing Technology in Nanomedicine, Elsevier2019, pp. 83-114.
1893 [154] J. Sun, W. Zhou, L. Yan, D. Huang, L.-y. Lin, Extrusion-based food printing for digitalized
1894 food design and nutrition control, J. Food Eng. 220 (2018) 1-11.
1895 [155] R. Karyappa, M. Hashimoto, Chocolate-based Ink Three-dimensional Printing (Ci3DP), Sci.
1896 Rep. 9(1) (2019) 14178.
1897 [156] J. Herzberger, J.M. Sirrine, C.B. Williams, T.E. Long, Polymer Design for 3D Printing
1898 Elastomers: Recent Advances in Structure, Properties, and Printing, Prog. Polym. Sci. 97 (2019)
1899 101144.
1900 [157] L.J. Tan, W. Zhu, K. Zhou, Recent Progress on Polymer Materials for Additive Manufacturing,
1901 Adv. Funct. Mater. 30(43) (2020) 2003062.
1902 [158] N.T. Brian, R. Strong, A.G. Scott, A review of melt extrusion additive manufacturing

processes: I. Process design and modeling, Rapid Prototyping J. 20(3) (2014) 192-204.

[159] R. Yadav, M. Naebe, X. Wang, B. Kandasubramanian, Review on 3D Prototyping of Damage Tolerant Interdigitating Brick Arrays of Nacre, Ind. Eng. Chem. Res. 56(38) (2017) 10516-10525.

[160] R.J. Mondschein, A. Kanitkar, C.B. Williams, S.S. Verbridge, T.E. Long, Polymer structure-property requirements for stereolithographic 3D printing of soft tissue engineering scaffolds, Biomaterials 140 (2017) 170-188.

[161] M.W.J. Noort, J.V. Diaz, B.K.J.C. Van, S. Renzetti, J. Henket, M.B. Hoppenbrouwers, Method for the production of an edible object using SLS, Stichting Wageningen Research, 2016.

[162] L.E. Murr, W.L. Johnson, 3D metal droplet printing development and advanced materials additive manufacturing, J. Mater. Res. Technol. 6(1) (2017) 77-89.

[163] E.M. Sachs, J.S. Haggerty, M.J. Cima, P.A. Williams, Three-dimensional printing techniques, Massachusetts Institute of Technology, 1993.

[164] M. Ziaee, N.B. Crane, Binder jetting: A review of process, materials, and methods, Addit. Manuf. 28 (2019) 781-801.

[165] Z. Jiang, B. Diggle, M.L. Tan, J. Viktorova, C.W. Bennett, L.A. Connal, Extrusion 3D Printing of Polymeric Materials with Advanced Properties, Adv. Sci. 7(17) (2020) 2001379.

[166] J.J. Nijdam, D. LeCorre-Bordes, A. Delvart, B.S. Schon, A rheological test to assess the ability of food inks to form dimensionally stable 3D food structures, J. Food Eng. 291 (2021) 110235.

[167] J. Aho, J.P. Boetker, S. Baldursdottir, J. Rantanen, Rheology as a tool for evaluation of melt processability of innovative dosage forms, Int. J. Pharm. 494(2) (2015) 623-642.

[168] A. Gholamipour-Shirazi, I.T. Norton, T. Mills, Designing hydrocolloid based food-ink

formulations for extrusion 3D printing, Food Hydrocolloids 95 (2019) 161-167.

[169] E. Álvarez-Castillo, S. Oliveira, C. Bengoechea, I. Sousa, A. Raymundo, A. Guerrero, A rheological approach to 3D printing of plasma protein based doughs, J. Food Eng. 288 (2021) 110255.

[170] K. Markstedt, A. Mantas, I. Tournier, H. Martinez Avila, D. Hagg, P. Gatenholm, 3D Bioprinting Human Chondrocytes with Nanocellulose-Alginate Bioink for Cartilage Tissue Engineering Applications, Biomacromolecules 16(5) (2015) 1489-1496.

[171] J. Berg, T. Hiller, M.S. Kissner, T.H. Qazi, G.N. Duda, A.C. Hocke, S. Hippenstiel, L. Elomaa, M. Weinhart, C. Fahrenson, J. Kurreck, Optimization of cell-laden bioinks for 3D bioprinting and efficient infection with influenza A virus, Sci. Rep. 8(1) (2018) 13877.

[172] K.D. Roehm, S.V. Madihally, Bioprinted chitosan-gelatin thermosensitive hydrogels using an inexpensive 3D printer, Biofabrication 10(1) (2017) 015002.

[173] C. Guo, M. Zhang, S. Devahastin, 3D extrusion-based printability evaluation of selected cereal grains by computational fluid dynamic simulation, J. Food Eng. 286 (2020) 110113.

[174] N. Paxton, W. Smolan, T. Böck, F. Melchels, J. Groll, T. Jungst, Proposal to assess printability of bioinks for extrusion-based bioprinting and evaluation of rheological properties governing bioprintability, Biofabrication 9(4) (2017) 044107.

[175] T.M. Oyinloye, W.B. Yoon, Stability of 3D printing using a mixture of pea protein and alginate: Precision and application of additive layer manufacturing simulation approach for stress distribution, J. Food Eng. 288 (2021) 110127.

[176] J.M. Townsend, E.C. Beck, S.H. Gehrke, C.J. Berkland, M.S. Detamore, Flow behavior prior

1945 to crosslinking: The need for precursor rheology for placement of hydrogels in medical applications
1946 and for 3D bioprinting, Prog. Polym. Sci. 91 (2019) 126-140.
1947 [177] H. Tian, K. Wang, H. Lan, Y. Wang, Z. Hu, L. Zhao, Effect of hybrid gelator systems of
1948 beeswax-carrageenan-xanthan on rheological properties and printability of litchi inks for 3D food
1949 printing, Food Hydrocolloids 113 (2021) 106482.
1950 [178] M.H. Kim, Y.W. Lee, W.-K. Jung, J. Oh, S.Y. Nam, Enhanced rheological behaviors of alginate
1951 hydrogels with carrageenan for extrusion-based bioprinting, J. Mech. Behav. Biomed. Mater. 98
1952 (2019) 187-194.
1953 [179] Z.H. Stachurski, Deformation mechanisms and yield strength in amorphous polymers, Prog.
1954 Polym. Sci. 22(3) (1997) 407-474.
1955 [180] E.T. Pulatsu, J.-W. Su, J. Lin, M. Lin, Factors affecting 3D printing and post-processing
1956 capacity of cookie dough, Innovative Food Sci. Emerg. Technol. 61 (2020) 102316.
1957 [181] Y. Zhao, Y. Li, S. Mao, W. Sun, R. Yao, The influence of printing parameters on cell survival
1958 rate and printability in microextrusion-based 3D cell printing technology, Biofabrication 7(4) (2015)
1959 045002.
1960 [182] Y. Chen, M. Zhang, P. Phuhongsung, 3D printing of protein-based composite fruit and
1961 vegetable gel system, LWT 141 (2021) 110978.
1962 [183] F. Yang, M. Zhang, B. Bhandari, Y. Liu, Investigation on lemon juice gel as food material for
1963 3D printing and optimization of printing parameters, LWT - Food Sci. Technol. 87 (2018) 67-76.
1964 [184] A. Dick, B. Bhandari, S. Prakash, 3D printing of meat, Meat Sci. 153 (2019) 35-44.
1965 [185] T. Anukiruthika, J.A. Moses, C. Anandharamakrishnan, 3D printing of egg yolk and white with

rice flour blends, J. Food Eng. 265 (2020) 109691.

[186] L. Wang, M. Zhang, B. Bhandari, C. Yang, Investigation on fish surimi gel as promising food material for 3D printing, J. Food Eng. 220 (2018) 101-108.

[187] S.A. Wilson, L.M. Cross, C.W. Peak, A.K. Gaharwar, Shear-Thinning and Thermo-Reversible Nanoengineered Inks for 3D Bioprinting, ACS Appl. Mater. Interfaces 9(50) (2017) 43449-43458.

[188] J. Wang, L.L. Shaw, Rheological and extrusion behavior of dental porcelain slurries for rapid prototyping applications, Mater. Sci. Eng., A 397(1) (2005) 314-321.

[189] J. Göhl, K. Markstedt, A. Mark, K. Håkansson, P. Gatenholm, F. Edelvik, Simulations of 3D bioprinting: predicting bioprintability of nanofibrillar inks, Biofabrication 10(3) (2018) 034105.

[190] C. Guo, M. Zhang, S. Devahastin, Improvement of 3D printability of buckwheat starch-pectin system via synergistic Ca2+-microwave pretreatment, Food Hydrocolloids 113 (2020) 106483.

[191] E. Pulatsu, J.-W. Su, S.M. Kenderes, J. Lin, B. Vardhanabhuti, M. Lin, Effects of ingredients and pre-heating on the printing quality and dimensional stability in 3D printing of cookie dough, J. Food Eng. 294 (2021) 110412.

[192] B.C. Maniglia, G. Pataro, G. Ferrari, P.E.D. Augusto, P. Le-Bail, A. Le-Bail, Pulsed electric fields (PEF) treatment to enhance starch 3D printing application: Effect on structure, properties, and functionality of wheat and cassava starches, Innovative Food Sci. Emerg. Technol. 68 (2021) 102602.

[193] B.C. Maniglia, D.C. Lima, M. da Matta Júnior, A. Oge, P. Le-Bail, P.E.D. Augusto, A. Le-Bail, Dry heating treatment: A potential tool to improve the wheat starch properties for 3D food printing application, Food Res. Int. 137 (2020) 109731.

1987 [194] B. Jiang, Y. Yao, Z. Liang, J. Gao, G. Chen, Q. Xia, R. Mi, M. Jiao, X. Wang, L. Hu, Lignin-
1988 Based Direct Ink Printed Structural Scaffolds, Small 16(31) (2020) 1907212.
1989 [195] H. Fan, M. Zhang, Z. Liu, Y. Ye, Effect of microwave-salt synergetic pre-treatment on the 3D
1990 printing performance of SPI-strawberry ink system, LWT - Food Sci. Technol. 122 (2020) 109004.
1991 [196] L. Xu, L. Gu, Y. Su, C. Chang, J. Wang, S. Dong, Y. Liu, Y. Yang, J. Li, Impact of thermal
1992 treatment on the rheological, microstructural, protein structures and extrusion 3D printing
1993 characteristics of egg yolk, Food Hydrocolloids 100 (2020) 105399.
1994 [197] C. Thibaut, A. Denneulin, S. Rolland du Roscoat, D. Beneventi, L. Orgeas, D. Chaussy, A
1995 fibrous cellulose paste formulation to manufacture structural parts using 3D printing by extrusion,
1996 Carbohydr. Polym. 212 (2019) 119-128.
1997 [198] C.X.F. Lam, X.M. Mo, S.H. Teoh, D.W. Hutmacher, Scaffold development using 3D printing
1998 with a starch-based polymer, Mater. Sci. Eng., C 20(1) (2002) 49-56.
1999 [199] J. Sun, Z. Peng, W. Zhou, J.Y.H. Fuh, G.S. Hong, A. Chiu, A Review on 3D Printing for
2000 Customized Food Fabrication, Procedia Manuf. 1 (2015) 308-319.
2001 [200] Y.P. Singh, A. Bandyopadhyay, B.B. Mandal, 3D Bioprinting Using Cross-Linker-Free Silk–
2002 Gelatin Bioink for Cartilage Tissue Engineering, ACS Appl. Mater. Interfaces 11(37) (2019) 33684-
2003 33696.
2004 [201] J. Lee, M. Yeo, W. Kim, Y. Koo, G.H. Kim, Development of a tannic acid cross-linking process
2005 for obtaining 3D porous cell-laden collagen structure, Int. J. Biol. Macromol. 110 (2018) 497-503.
2006 [202] A.M. Compaan, K. Song, Y. Huang, Gellan Fluid Gel as a Versatile Support Bath Material for
2007 Fluid Extrusion Bioprinting, ACS Appl. Mater. Interfaces 11(6) (2019) 5714-5726.

2008 [203] D.M. Kirchmajer, R. Gorkin Iii, M. in het Panhuis, An overview of the suitability of hydrogel-
2009 forming polymers for extrusion-based 3D-printing, J. Mater. Chem. B 3(20) (2015) 4105-4117.
2010 [204] V. Vancauwenberghe, P. Verboven, J. Lammertyn, B. Nicolaï, Development of a coaxial
2011 extrusion deposition for 3D printing of customizable pectin-based food simulant, J. Food Eng. 225
2012 (2018) 42-52.
2013 [205] S. Isaschar-Ovdat, A. Fishman, Crosslinking of food proteins mediated by oxidative enzymes –
2014 A review, Trends Food Sci. Technol. 72 (2018) 134-143.
2015 [206] H.M.C. Azeredo, K.W. Waldron, Crosslinking in polysaccharide and protein films and coatings
2016 for food contact – A review, Trends Food Sci. Technol. 52 (2016) 109-122.
2017 [207] S. Chameettachal, S. Midha, S. Ghosh, Regulation of Chondrogenesis and Hypertrophy in Silk
2018 Fibroin-Gelatin-Based 3D Bioprinted Constructs, ACS Biomater. Sci. Eng. 2(9) (2016) 1450-1463.
2019 [208] O. Hasturk, K.E. Jordan, J. Choi, D.L. Kaplan, Enzymatically crosslinked silk and silk-gelatin
2020 hydrogels with tunable gelation kinetics, mechanical properties and bioactivity for cell culture and
2021 encapsulation, Biomaterials 232 (2020) 119720.
2022 [209] Z. Zhao, Q. Wang, B. Yan, W. Gao, X. Jiao, J. Huang, J. Zhao, H. Zhang, W. Chen, D. Fan,
2023 Synergistic effect of microwave 3D print and transglutaminase on the self-gelation of surimi during
2024 printing, Innovative Food Sci. Emerg. Technol. 67 (2020) 102546.
2025 [210] Y.R. Choi, E.H. Kim, S. Lim, Y.S. Choi, Efficient preparation of a permanent chitosan/gelatin
2026 hydrogel using an acid-tolerant tyrosinase, Biochem. Eng. J. 129 (2018) 50-56.
2027 [211] N.R. Raia, B.P. Partlow, M. McGill, E.P. Kimmerling, C.E. Ghezzi, D.L. Kaplan,
2028 Enzymatically crosslinked silk-hyaluronic acid hydrogels, Biomaterials 131 (2017) 58-67.

2029 [212] E.A. Kamoun, A. El-Betany, H. Menzel, X. Chen, Influence of photoinitiator concentration and
2030 irradiation time on the crosslinking performance of visible-light activated pullulan-HEMA hydrogels,
2031 Int. J. Biol. Macromol. 120 (2018) 1884-1892.
2032 [213] L. Ruiz-Cantu, A. Gleadall, C. Faris, J. Segal, K. Shakesheff, J. Yang, Multi-material 3D
2033 bioprinting of porous constructs for cartilage regeneration, Mater. Sci. Eng., C 109 (2020) 110578.
2034 [214] J. Deng, L. Wang, L. Liu, W. Yang, Developments and new applications of UV-induced surface
2035 graft polymerizations, Prog. Polym. Sci. 34(2) (2009) 156-193.
2036 [215] C. Decker, Photoinitiated crosslinking polymerisation, Prog. Polym. Sci. 21(4) (1996) 593-
2037 650.
2038 [216] E.R. Ruskowitz, C.A. DeForest, Photoresponsive biomaterials for targeted drug delivery and
2039 4D cell culture, Nat. Rev. Mater. 3(2) (2018) 17087.
2040 [217] T. Mitra, G. Sailakshmi, A. Gnanamani, S.T.K. Raja, T. Thiruselvi, V.M. Gowri, N.V. Selvaraj,
2041 G. Ramesh, A.B. Mandal, Preparation and characterization of a thermostable and biodegradable
2042 biopolymers using natural cross-linker, Int. J. Biol. Macromol. 48(2) (2011) 276-285.
2043 [218] K. Markstedt, A. Escalante, G. Toriz, P. Gatenholm, Biomimetic Inks Based on Cellulose
2044 Nanofibrils and Cross-Linkable Xylans for 3D Printing, ACS Appl. Mater. Interfaces 9(46) (2017)
2045 40878-40886.
2046 [219] M. Stevenson, J. Long, P. Guerrero, K.d.l. Caba, A. Seyfoddin, A. Etxabide, Development and
2047 characterization of ribose-crosslinked gelatin products prepared by indirect 3D printing, Food
2048 Hydrocolloids 96 (2019) 65-71.
2049 [220] A. Derossi, R. Caporizzi, M.O. Oral, C. Severini, Analyzing the effects of 3D printing process

per se on the microstructure and mechanical properties of cereal food products, Innovative Food Sci. Emerg. Technol. 66 (2020) 102531.

[221] V. Vancauwenberghe, M.A. Delele, J. Vanbiervliet, W. Aregawi, P. Verboven, J. Lammertyn, B. Nicolaï, Model-based design and validation of food texture of 3D printed pectin-based food simulants, J. Food Eng. 231 (2018) 72-82.

[222] G.L. Koons, M. Diba, A.G. Mikos, Materials design for bone-tissue engineering, Nat. Rev. Mater. 5 (2020) 584–603.

[223] O. Bretcanu, C. Samaille, A.R. Boccaccini, Simple methods to fabricate Bioglass®-derived glass–ceramic scaffolds exhibiting porosity gradient, J. Mater. Sci. 43(12) (2008) 4127-4134.

[224] W. Shi, M. Sun, X. Hu, B. Ren, J. Cheng, C. Li, X. Duan, X. Fu, J. Zhang, H. Chen, Y. Ao, Structurally and Functionally Optimized Silk-Fibroin–Gelatin Scaffold Using 3D Printing to Repair Cartilage Injury In Vitro and In Vivo, Adv. Mater. 29(29) (2017) 1701089.

[225] P. Joly, G.N. Duda, M. Schöne, P.B. Welzel, U. Freudenberg, C. Werner, A. Petersen, Geometry-Driven Cell Organization Determines Tissue Growths in Scaffold Pores: Consequences for Fibronectin Organization, PLoS One 8(9) (2013) e73545.

[226] S. Sultan, A.P. Mathew, 3D printed scaffolds with gradient porosity based on a cellulose nanocrystal hydrogel, Nanoscale 10(9) (2018) 4421-4431.

[227] H. Han, J. Hou, N. Yang, Y. Zhang, H. Chen, Z. Zhang, Y. Shen, S. Huang, S. Guo, Insight on the changes of cassava and potato starch granules during gelatinization, Int. J. Biol. Macromol. 126 (2019) 37-43.

[228] H. Chen, F. Xie, L. Chen, B. Zheng, Effect of rheological properties of potato, rice and corn

starches on their hot-extrusion 3D printing behaviors, J. Food Eng. 244 (2019) 150-158.
[229] C. He, M. Zhang, C. Guo, 4D printing of mashed potato/purple sweet potato puree with spontaneous color change, Innovative Food Sci. Emerg. Technol. 59 (2020) 102250.
[230] Y. Liu, Y. Yu, C. Liu, J.M. Regenstein, X. Liu, P. Zhou, Rheological and mechanical behavior of milk protein composite gel for extrusion-based 3D food printing, LWT - Food Sci. Technol. 102 (2019) 338-346.
[231] R. Uribe-Alvarez, N. O'Shea, C.P. Murphy, C. Coleman-Vaughan, T.P. Guinee, Evaluation of rennet-induced gelation under different conditions as a potential method for 3D food printing of dairy-based high-protein formulations, Food Hydrocolloids 114 (2021) 106542.
[232] S. Wang, Y. Zhang, L. Chen, X. Xu, G. Zhou, Z. Li, X. Feng, Dose-dependent effects of rosmarinic acid on formation of oxidatively stressed myofibrillar protein emulsion gel at different NaCl concentrations, Food Chem. 243 (2018) 50-57.
[233] G. Ge, Y. Han, J. Zheng, M. Zhao, W. Sun, Physicochemical characteristics and gel-forming properties of myofibrillar protein in an oxidative system affected by partial substitution of NaCl with KCl, MgCl2 or CaCl2, Food Chem. 309 (2020) 125614.
[234] L. Khedmat, A. Izadi, V. Mofid, S.Y. Mojtahedi, Recent advances in extracting pectin by single and combined ultrasound techniques: A review of techno-functional and bioactive health-promoting aspects, Carbohydr. Polym. 229 (2020) 115474.
[235] P.J.P. Espitia, W.-X. Du, R.d.J. Avena-Bustillos, N.d.F.F. Soares, T.H. McHugh, Edible films from pectin: Physical-mechanical and antimicrobial properties - A review, Food Hydrocolloids 35 (2014) 287-296.

2092 [236] V. Vancauwenberghe, V. Baiye Mfortaw Mbong, E. Vanstreels, P. Verboven, J. Lammertyn, B.
2093 Nicolai, 3D printing of plant tissue for innovative food manufacturing: Encapsulation of alive plant
2094 cells into pectin based bio-ink, J. Food Eng. 263 (2019) 454-464.
2095 [237] E. Nordlund, M. Lille, P. Silventoinen, H. Nygren, T. Seppänen-Laakso, A. Mikkelson, A.-M.
2096 Aura, R.-L. Heiniö, L. Nohynek, R. Puupponen-Pimiä, H. Rischer, Plant cells as food – A concept
2097 taking shape, Food Res. Int. 107 (2018) 297-305.
2098 [238] S.M. Park, H.W. Kim, H.J. Park, Callus-based 3D printing for food exemplified with carrot
2099 tissues and its potential for innovative food production, J. Food Eng. 271 (2020) 109781.
2100 [239] J.H. Lee, D.J. Won, H.W. Kim, H.J. Park, Effect of particle size on 3D printing performance of
2101 the food-ink system with cellular food materials, J. Food Eng. 256 (2019) 1-8.
2102 [240] S.M.R. Azam, M. Zhang, A.S. Mujumdar, C. Yang, Study on 3D printing of orange concentrate
2103 and material characteristics, J. Food Process Eng 41(5) (2018) e12689.
2104 [241] J. Montoya, J. Medina, A. Molina, J. Gutiérrez, B. Rodríguez, R. Marín, Impact of viscoelastic
2105 and structural properties from Starch-Mango and Starch-Arabinoxylans hydrocolloids in 3D Food
2106 Printing, Addit. Manuf. 39 (2021) 101891.
2107 [242] M.L. Chinta, A. Velidandi, N.P.P. Pabbathi, S. Dahariya, S.R. Parcha, Assessment of properties,
2108 applications and limitations of scaffolds based on cellulose and its derivatives for cartilage tissue
2109 engineering: A review, Int. J. Biol. Macromol. 175 (2021) 495-515.
2110 [243] D. Rolski, J. Kostrzewa-Janicka, P. Zawadzki, K. Życińska, E. Mierzwińska-Nastalska, The
2111 Management of Patients after Surgical Treatment of Maxillofacial Tumors, BioMed Research
2112 International 2016 (2016) 4045329.

[244] S. Bose, D. Ke, H. Sahasrabudhe, A. Bandyopadhyay, Additive manufacturing of biomaterials, Progress in Materials Science 93 (2018) 45-111.

[245] T. Tu, Y. Shen, X. Wang, W. Zhang, G. Zhou, Y. Zhang, W. Wang, W. Liu, Tendon ECM modified bioactive electrospun fibers promote MSC tenogenic differentiation and tendon regeneration, Appl. Mater. Today 18 (2020) 100495.

[246] S. Yuan, F. Shen, C.K. Chua, K. Zhou, Polymeric composites for powder-based additive manufacturing: Materials and applications, Prog. Polym. Sci. 91 (2019) 141-168.

[247] D.A. Bichara, N.-A. O'Sullivan, I. Pomerantseva, X. Zhao, C.A. Sundback, J.P. Vacanti, M.A. Randolph, The Tissue-Engineered Auricle: Past, Present, and Future, Tissue Engineering Part B: Reviews 18(1) (2012) 51-61.

[248] C. Vyas, J. Zhang, Ø. Øvrebø, B. Huang, I. Roberts, M. Setty, B. Allardyce, H. Haugen, R. Rajkhowa, P. Bartolo, 3D printing of silk microparticle reinforced polycaprolactone scaffolds for tissue engineering applications, Materials Science and Engineering: C 118 (2021) 111433.

[249] S. Critchley, E.J. Sheehy, G. Cunniffe, P. Diaz-Payno, S.F. Carroll, O. Jeon, E. Alsberg, P.A.J. Brama, D.J. Kelly, 3D printing of fibre-reinforced cartilaginous templates for the regeneration of osteochondral defects, Acta Biomater. 113 (2020) 130-143.

[250] V. Martin, I.A. Ribeiro, M.M. Alves, L. Gonçalves, R.A. Claudio, L. Grenho, M.H. Fernandes, P. Gomes, C.F. Santos, A.F. Bettencourt, Engineering a multifunctional 3D-printed PLA-collagen-minocycline-nanoHydroxyapatite scaffold with combined antimicrobial and osteogenic effects for bone regeneration, Mater. Sci. Eng., C 101 (2019) 15-26.

[251] C.H. Jang, Y. Koo, G. Kim, ASC/chondrocyte-laden alginate hydrogel/PCL hybrid scaffold

2134 fabricated using 3D printing for auricle regeneration, Carbohydr. Polym. 248 (2020) 116776.
2135 [252] A. Kosik-Kozioł, M. Costantini, T. Bolek, K. Szöke, A. Barbetta, J. Brinchmann, W.
2136 Święszkowski, PLA short sub-micron fiber reinforcement of 3D bioprinted alginate constructs for
2137 cartilage regeneration, Biofabrication 9(4) (2017) 044105.
2138 [253] J. Kundu, J.H. Shim, J. Jang, S.W. Kim, D.W. Cho, An additive manufacturing-based PCL-
2139 alginate-chondrocyte bioprinted scaffold for cartilage tissue engineering, J. Tissue Eng. Regener.
2140 Med. 9(11) (2015) 1286-1297.
2141 [254] Y.B. Kim, H. Lee, G.-H. Yang, C.H. Choi, D. Lee, H. Hwang, W.-K. Jung, H. Yoon, G.H. Kim,
2142 Mechanically reinforced cell-laden scaffolds formed using alginate-based bioink printed onto the
2143 surface of a PCL/alginate mesh structure for regeneration of hard tissue, J. Colloid Interface Sci. 461
2144 (2016) 359-368.
2145 [255] L.K. Narayanan, P. Huebner, M.B. Fisher, J.T. Spang, B. Starly, R.A. Shirwaiker, 3D-
2146 Bioprinting of Polylactic Acid (PLA) Nanofiber–Alginate Hydrogel Bioink Containing Human
2147 Adipose-Derived Stem Cells, ACS Biomater. Sci. Eng. 2(10) (2016) 1732-1742.
2148 [256] T. Xu, K.W. Binder, M.Z. Albanna, D. Dice, W. Zhao, J.J. Yoo, A. Atala, Hybrid printing of
2149 mechanically and biologically improved constructs for cartilage tissue engineering applications,
2150 Biofabrication 5(1) (2012) 015001.
2151 [257] S.H. Kim, Y.K. Yeon, J.M. Lee, J.R. Chao, Y.J. Lee, Y.B. Seo, M.T. Sultan, O.J. Lee, J.S. Lee,
2152 S.-i. Yoon, I.-S. Hong, G. Khang, S.J. Lee, J.J. Yoo, C.H. Park, Precisely printable and biocompatible
2153 silk fibroin bioink for digital light processing 3D printing, Nat. Commun. 9(1) (2018) 1620.
2154 [258] V.P. Ribeiro, J. Silva-Correia, A.I. Nascimento, A. da Silva Morais, A.P. Marques, A.S. Ribeiro,

2155 C.J. Silva, G. Bonifácio, R.A. Sousa, J.M. Oliveira, A.L. Oliveira, R.L. Reis, Silk-based anisotropical
2156 3D biotextiles for bone regeneration, Biomaterials 123 (2017) 92-106.
2157 [259] C. Xie, W. Li, Q. Liang, S. Yu, L. Li, Fabrication of robust silk fibroin film by controlling the
2158 content of β-sheet via the synergism of Uv-light and ionic liquids, Appl. Surf. Sci. 492 (2019) 55-65.
2159 [260] K. Luo, Y. Yang, Z. Shao, Physically Crosslinked Biocompatible Silk-Fibroin-Based
2160 Hydrogels with High Mechanical Performance, Adv. Funct. Mater. 26(6) (2016) 872-880.
2161 [261] F.A. Sheikh, H.W. Ju, J.M. Lee, B.M. Moon, H.J. Park, O.J. Lee, J.-H. Kim, D.-K. Kim, C.H.
2162 Park, 3D electrospun silk fibroin nanofibers for fabrication of artificial skin, Nanomed. Nanotechnol.
2163 Biol. Med. 11(3) (2015) 681-691.
2164 [262] Y.R. Park, H.W. Ju, J.M. Lee, D.-K. Kim, O.J. Lee, B.M. Moon, H.J. Park, J.Y. Jeong, Y.K.
2165 Yeon, C.H. Park, Three-dimensional electrospun silk-fibroin nanofiber for skin tissue engineering,
2166 Int. J. Biol. Macromol. 93 (2016) 1567-1574.
2167 [263] J. Melke, S. Midha, S. Ghosh, K. Ito, S. Hofmann, Silk fibroin as biomaterial for bone tissue
2168 engineering, Acta Biomater. 31 (2016) 1-16.
2169 [264] H. Lee, G.H. Yang, M. Kim, J. Lee, J. Huh, G. Kim, Fabrication of micro/nanoporous
2170 collagen/dECM/silk-fibroin biocomposite scaffolds using a low temperature 3D printing process for
2171 bone tissue regeneration, Mater. Sci. Eng., C 84 (2018) 140-147.
2172 [265] M.J. Rodriguez, J. Brown, J. Giordano, S.J. Lin, F.G. Omenetto, D.L. Kaplan, Silk based
2173 bioinks for soft tissue reconstruction using 3-dimensional (3D) printing with in vitro and in vivo
2174 assessments, Biomaterials 117 (2017) 105-115.
2175 [266] H. Maleki, S. Montes, N. Hayati-Roodbari, F. Putz, N. Huesing, Compressible, Thermally

Insulating, and Fire Retardant Aerogels through Self-Assembling Silk Fibroin Biopolymers Inside a Silica Structure-An Approach towards 3D Printing of Aerogels, ACS Appl. Mater. Interfaces 10(26) (2018) 22718-22730.

[267] E. Desimone, K. Schacht, T. Jungst, J. Groll, T. Scheibel, Biofabrication of 3D constructs: fabrication technologies and spider silk proteins as bioinks, Pure Appl. Chem. 87(8) (2015).

[268] H. Lee, D. Shin, S. Shin, J. Hyun, Effect of gelatin on dimensional stability of silk fibroin hydrogel structures fabricated by digital light processing 3D printing, J. Ind. Eng. Chem. 89 (2020) 119-127.

[269] D. Chawla, T. Kaur, A. Joshi, N. Singh, 3D bioprinted alginate-gelatin based scaffolds for soft tissue engineering, Int. J. Biol. Macromol. 144 (2020) 560-567.

[270] S. Schwarz, S. Kuth, T. Distler, C. Gögele, K. Stölzel, R. Detsch, A.R. Boccaccini, G. Schulze-Tanzil, 3D printing and characterization of human nasoseptal chondrocytes laden dual crosslinked oxidized alginate-gelatin hydrogels for cartilage repair approaches, Materials Science and Engineering: C 116 (2020) 111189.

[271] F. Pati, J. Jang, D.-H. Ha, S. Won Kim, J.-W. Rhie, J.-H. Shim, D.-H. Kim, D.-W. Cho, Printing three-dimensional tissue analogues with decellularized extracellular matrix bioink, Nat. Commun. 5(1) (2014) 3935.

[272] X. Zhang, Y. Liu, C. Luo, C. Zhai, Z. Li, Y. Zhang, T. Yuan, S. Dong, J. Zhang, W. Fan, Crosslinker-free silk/decellularized extracellular matrix porous bioink for 3D bioprinting-based cartilage tissue engineering, Materials Science and Engineering: C 118 (2021) 111388.

[273] J. Glowacki, S. Mizuno, Collagen scaffolds for tissue engineering, Biopolymers 89(5) (2008)

338-344.

[274] A.M. Ferreira, P. Gentile, V. Chiono, G. Ciardelli, Collagen for bone tissue regeneration, Acta Biomater. 8(9) (2012) 3191-3200.

[275] X. Yang, Z. Lu, H. Wu, W. Li, L. Zheng, J. Zhao, Collagen-alginate as bioink for three-dimensional (3D) cell printing based cartilage tissue engineering, Mater. Sci. Eng., C 83 (2018) 195-201.

[276] J. Lee, G. Kim, Three-Dimensional Hierarchical Nanofibrous Collagen Scaffold Fabricated Using Fibrillated Collagen and Pluronic F-127 for Regenerating Bone Tissue, ACS Appl. Mater. Interfaces 10(42) (2018) 35801-35811.

[277] C. Chen, M.-L. Zhao, R.-K. Zhang, G. Lu, C.-Y. Zhao, F. Fu, H.-T. Sun, S. Zhang, Y. Tu, X.-H. Li, Collagen/heparin sulfate scaffolds fabricated by a 3D bioprinter improved mechanical properties and neurological function after spinal cord injury in rats, J. Biomed. Mater. Res. Part A 105(5) (2017) 1324-1332.

[278] T. Ma, L. Lv, C. Ouyang, X. Hu, X. Liao, Y. Song, X. Hu, Rheological behavior and particle alignment of cellulose nanocrystal and its composite hydrogels during 3D printing, Carbohydr. Polym. 253 (2021) 117217.

[279] P. Fisch, N. Broguiere, S. Finkielsztein, T. Linder, M. Zenobi-Wong, Bioprinting of Cartilaginous Auricular Constructs Utilizing an Enzymatically Crosslinkable Bioink, Adv. Funct. Mater. n/a(n/a) (2021) 2008261.

[280] J. Leppiniemi, P. Lahtinen, A. Paajanen, R. Mahlberg, S. Metsa-Kortelainen, T. Pinomaa, H. Pajari, I. Vikholm-Lundin, P. Pursula, V.P. Hytonen, 3D-Printable Bioactivated Nanocellulose-

2218 Alginate Hydrogels, ACS Appl. Mater. Interfaces 9(26) (2017) 21959-21970.
2219 [281] K.J. De France, T. Hoare, E.D. Cranston, Review of Hydrogels and Aerogels Containing
2220 Nanocellulose, Chem. Mater. 29(11) (2017) 4609-4631.
2221 [282] C. Ruiz-Palomero, M.L. Soriano, M. Valcárcel, Nanocellulose as analyte and analytical tool:
2222 Opportunities and challenges, TrAC, Trends Anal. Chem. 87 (2017) 1-18.
2223 [283] S.D. Dutta, J. Hexiu, D.K. Patel, K. Ganguly, K.-T. Lim, 3D-printed bioactive and
2224 biodegradable hydrogel scaffolds of alginate/gelatin/cellulose nanocrystals for tissue engineering,
2225 Int. J. Biol. Macromol. 167 (2021) 644-658.
2226 [284] D. Nguyen, D.A. Hägg, A. Forsman, J. Ekholm, P. Nimkingratana, C. Brantsing, T.
2227 Kalogeropoulos, S. Zaunz, S. Concaro, M. Brittberg, A. Lindahl, P. Gatenholm, A. Enejder, S.
2228 Simonsson, Cartilage Tissue Engineering by the 3D Bioprinting of iPS Cells in a
2229 Nanocellulose/Alginate Bioink, Sci. Rep. 7(1) (2017) 658.
2230 [285] M. Müller, E. Öztürk, Ø. Arlov, P. Gatenholm, M. Zenobi-Wong, Alginate Sulfate–
2231 Nanocellulose Bioinks for Cartilage Bioprinting Applications, Ann. Biomed. Eng. 45(1) (2016) 210-
2232 223.
2233 [286] R.E. Abouzeid, R. Khiari, A. Salama, M. Diab, D. Beneventi, A. Dufresne, In situ
2234 mineralization of nano-hydroxyapatite on bifunctional cellulose nanofiber/polyvinyl alcohol/sodium
2235 alginate hydrogel using 3D printing, Int. J. Biol. Macromol. 160 (2020) 538-547.
2236 [287] H. Maleki, L. Durães, C.A. García-González, P. del Gaudio, A. Portugal, M. Mahmoudi,
2237 Synthesis and biomedical applications of aerogels: Possibilities and challenges, Adv. Colloid
2238 Interface Sci. 236 (2016) 1-27.

2239 [288] J. Lee, Y. Deng, The morphology and mechanical properties of layer structured cellulose
2240 microfibril foams from ice-templating methods, Soft Matter 7(13) (2011) 6034-6040.
2241 [289] W. Zhang, Y. Zhang, C. Lu, Y. Deng, Aerogels from crosslinked cellulose nano/micro-fibrils
2242 and their fast shape recovery property in water, J. Mater. Chem. 22(23) (2012) 11642-11650.
2243 [290] X. Yang, E.D. Cranston, Chemically Cross-Linked Cellulose Nanocrystal Aerogels with Shape
2244 Recovery and Superabsorbent Properties, Chem. Mater. 26(20) (2014) 6016-6025.
2245 [291] H. Sehaqui, Q. Zhou, L.A. Berglund, High-porosity aerogels of high specific surface area
2246 prepared from nanofibrillated cellulose (NFC), Compos. Sci. Technol. 71(13) (2011) 1593-1599.
2247 [292] A. Mulyadi, Z. Zhang, Y. Deng, Fluorine-Free Oil Absorbents Made from Cellulose Nanofibril
2248 Aerogels, ACS Appl. Mater. Interfaces 8(4) (2016) 2732-2740.
2249 [293] H. Sehaqui, Q. Zhou, O. Ikkala, L.A. Berglund, Strong and Tough Cellulose Nanopaper with
2250 High Specific Surface Area and Porosity, Biomacromolecules 12(10) (2011) 3638-3644.
2251 [294] R.T. Olsson, M.A.S. Azizi Samir, G. Salazar-Alvarez, L. Belova, V. Ström, L.A. Berglund, O.
2252 Ikkala, J. Nogués, U.W. Gedde, Making flexible magnetic aerogels and stiff magnetic nanopaper
2253 using cellulose nanofibrils as templates, Nat. Nanotechnol. 5(8) (2010) 584-588.
2254 [295] S. Chattopadhyay, R.T. Raines, Collagen-based biomaterials for wound healing, Biopolymers
2255 101(8) (2014) 821-833.
2256 [296] C. Intini, L. Elviri, J. Cabral, S. Mros, C. Bergonzi, A. Bianchera, L. Flammini, P. Govoni, E.
2257 Barocelli, R. Bettini, M. McConnell, 3D-printed chitosan-based scaffolds: An in vitro study of
2258 human skin cell growth and an in-vivo wound healing evaluation in experimental diabetes in rats,
2259 Carbohydr. Polym. 199 (2018) 593-602.

[297] P.R. Turner, E. Murray, C.J. McAdam, M.A. McConnell, J.D. Cabral, Peptide Chitosan/Dextran Core/Shell Vascularized 3D Constructs for Wound Healing, ACS Appl. Mater. Interfaces 12(29) (2020) 32328-32339.

[298] J. Long, A.E. Etxeberria, A.V. Nand, C.R. Bunt, S. Ray, A. Seyfoddin, A 3D printed chitosan-pectin hydrogel wound dressing for lidocaine hydrochloride delivery, Mater. Sci. Eng., C 104 (2019) 109873.

[299] S. Xiong, X. Zhang, P. Lu, Y. Wu, Q. Wang, H. Sun, B.C. Heng, V. Bunpetch, S. Zhang, H. Ouyang, A Gelatin-sulfonated Silk Composite Scaffold based on 3D Printing Technology Enhances Skin Regeneration by Stimulating Epidermal Growth and Dermal Neovascularization, Sci. Rep. 7(1) (2017) 4288.

[300] H. Hamedi, S. Moradi, S.M. Hudson, A.E. Tonelli, Chitosan based hydrogels and their applications for drug delivery in wound dressings: A review, Carbohydr. Polym. 199 (2018) 445-460.

[301] M. Naseri-Nosar, Z.M. Ziora, Wound dressings from naturally-occurring polymers: A review on homopolysaccharide-based composites, Carbohydr. Polym. 189 (2018) 379-398.

[302] E. Ilhan, S. Cesur, E. Guler, F. Topal, D. Albayrak, M.M. Guncu, M.E. Cam, T. Taskin, H.T. Sasmazel, B. Aksu, F.N. Oktar, O. Gunduz, Development of Satureja cuneifolia-loaded sodium alginate/polyethylene glycol scaffolds produced by 3D-printing technology as a diabetic wound dressing material, Int. J. Biol. Macromol. 161 (2020) 1040-1054.

[303] C. Karavasili, K. Tsongas, I.I. Andreadis, E.G. Andriotis, E.T. Papachristou, R.M. Papi, D. Tzetzis, D.G. Fatouros, Physico-mechanical and finite element analysis evaluation of 3D printable alginate-methylcellulose inks for wound healing applications, Carbohydr. Polym. 247 (2020)

116666.

[304] J. Leppiniemi, P. Lahtinen, A. Paajanen, R. Mahlberg, S. Metsä-Kortelainen, T. Pinomaa, H. Pajari, I. Vikholm-Lundin, P. Pursula, V.P. Hytönen, 3D-Printable Bioactivated Nanocellulose–Alginate Hydrogels, ACS Appl. Mater. Interfaces 9(26) (2017) 21959-21970.

[305] B. Chu, J.-m. He, Z. Wang, L.-l. Liu, X.-l. Li, C.-X. Wu, C.-s. Chen, M. Tu, Proangiogenic peptide nanofiber hydrogel/3D printed scaffold for dermal regeneration, Chem. Eng. J. n/a (2020) 128146.

[306] A. Lee, A.R. Hudson, D.J. Shiwarski, J.W. Tashman, T.J. Hinton, S. Yerneni, J.M. Bliley, P.G. Campbell, A.W. Feinberg, 3D bioprinting of collagen to rebuild components of the human heart, Science 365(6452) (2019) 482.

[307] Q. Gao, Z. Liu, Z. Lin, J. Qiu, Y. Liu, A. Liu, Y. Wang, M. Xiang, B. Chen, J. Fu, Y. He, 3D Bioprinting of Vessel-like Structures with Multilevel Fluidic Channels, ACS Biomater. Sci. Eng. 3(3) (2017) 399-408.

[308] S. Liu, H. Zhang, Q. Hu, Z. Shen, D. Rana, M. Ramalingam, Designing vascular supportive albumen-rich composite bioink for organ 3D printing, J. Mech. Behav. Biomed. Mater. 104 (2020) 103642.

[309] V.K. Lee, A.M. Lanzi, N. Haygan, S.S. Yoo, P.A. Vincent, G. Dai, Generation of Multi-Scale Vascular Network System within 3D Hydrogel using 3D Bio-Printing Technology, Cell. Mol. Bioeng. 7(3) (2014) 460-472.

[310] K. Christensen, C. Xu, W. Chai, Z. Zhang, Y. Huang, Freeform Inkjet Printing of Cellular Structures with Bifurcations, Biotechnol. Bioeng. 112(5) (2015).

[311] H. Stratesteffen, M. Köpf, F. Kreimendahl, A. Blaeser, S. Jockenhoevel, H. Fischer, GelMA-collagen blends enable drop-on-demand 3D printablility and promote angiogenesis, Biofabrication 9(4) (2017) 045002.

[312] C. Xu, W. Chai, Y. Huang, R.R. Markwald, Scaffold-free inkjet printing of three-dimensional zigzag cellular tubes, Biotechnol. Bioeng. 109(12) (2012) 3152-60.

[313] Q. Gao, Y. He, J.-z. Fu, A. Liu, L. Ma, Coaxial nozzle-assisted 3D bioprinting with built-in microchannels for nutrients delivery, Biomaterials 61 (2015) 203-215.

[314] M. Carrabba, P. Madeddu, Current Strategies for the Manufacture of Small Size Tissue Engineering Vascular Grafts, Frontiers in Bioengineering and Biotechnology 6(41) (2018).

[315] L. Li, S. Qin, J. Peng, A. Chen, Y. Nie, T. Liu, K. Song, Engineering gelatin-based alginate/carbon nanotubes blend bioink for direct 3D printing of vessel constructs, Int. J. Biol. Macromol. 145 (2020) 262-271.

[316] X. Zhou, M. Nowicki, H. Sun, S.Y. Hann, H. Cui, T. Esworthy, J.D. Lee, M. Plesniak, L.G. Zhang, 3D Bioprinting-Tunable Small-Diameter Blood Vessels with Biomimetic Biphasic Cell Layers, ACS Appl. Mater. Interfaces 12(41) (2020) 45904-45915.

[317] H.M. Howarth, E. Orozco, R.M. Lovering, S.B. Shah, A comparative assessment of lengthening followed by end-to-end repair and isograft repair of chronically injured peripheral nerves, Exp. Neurol. 331 (2020) 113328.

[318] R. Deumens, A. Bozkurt, M.F. Meek, M.A.E. Marcus, E.A.J. Joosten, J. Weis, G.A. Brook, Repairing injured peripheral nerves: Bridging the gap, Progress in Neurobiology 92(3) (2010) 245-276.

[319] C. Bikis, L. Degrugillier, P. Thalmann, G. Schulz, B. Müller, S.E. Hieber, D.F. Kalbermatten, S. Madduri, Three-dimensional imaging and analysis of entire peripheral nerves after repair and reconstruction, Journal of Neuroscience Methods 295 (2018) 37-44.

[320] W. Ye, H. Li, K. Yu, C. Xie, P. Wang, Y. Zheng, P. Zhang, J. Xiu, Y. Yang, F. Zhang, Y. He, Q. Gao, 3D printing of gelatin methacrylate-based nerve guidance conduits with multiple channels, Materials & Design 192 (2020) 108757.

[321] Z. Wu, Q. Li, S. Xie, X. Shan, Z. Cai, In vitro and in vivo biocompatibility evaluation of a 3D bioprinted gelatin-sodium alginate/rat Schwann-cell scaffold, Materials Science and Engineering: C 109 (2020) 110530.

[322] V. Kuzmenko, E. Karabulut, E. Pernevik, P. Enoksson, P. Gatenholm, Tailor-made conductive inks from cellulose nanofibrils for 3D printing of neural guidelines, Carbohydr. Polym. 189 (2018) 22-30.

[323] J. Jiang, X. Liu, H. Chen, C. Dai, X. Niu, L. Dai, X. Chen, S. Zhang, 3D printing collagen/heparin sulfate scaffolds boost neural network reconstruction and motor function recovery after traumatic brain injury in canine, Biomater. Sci. 8(22) (2020) 6362-6374.

[324] I. Henriksson, P. Gatenholm, D.A. Hägg, Increased lipid accumulation and adipogenic gene expression of adipocytes in 3D bioprinted nanocellulose scaffolds, Biofabrication 9(1) (2017) 015022.

[325] M.M. Sk, P. Das, A. Panwar, L.P. Tan, Synthesis and characterization of site selective photo-crosslinkable glycidyl methacrylate functionalized gelatin-based 3D hydrogel scaffold for liver tissue engineering, Materials Science and Engineering: C 123 (2021) 111694.

[326] L. Elviri, M. Asadzadeh, R. Cucinelli, A. Bianchera, R. Bettini, Macroporous chitosan hydrogels: Effects of sulfur on the loading and release behaviour of amino acid-based compounds, Carbohydr. Polym. 132 (2015) 50-58.

[327] D. Li, Q. Zhu, C. Han, Y. Yang, W. Jiang, Z. Zhang, Photocatalytic degradation of recalcitrant organic pollutants in water using a novel cylindrical multi-column photoreactor packed with TiO2-coated silica gel beads, J. Hazard. Mater. 285 (2015) 398-408.

[328] M. Shahbazi, H. Jäger, S.J. Ahmadi, M. Lacroix, Electron beam crosslinking of alginate/nanoclay ink to improve functional properties of 3D printed hydrogel for removing heavy metal ions, Carbohydr. Polym. 240 (2020) 116211.

[329] A.S. Finny, C. Jiang, S. Andreescu, 3D Printed Hydrogel-Based Sensors for Quantifying UV Exposure, ACS Appl. Mater. Interfaces 12(39) (2020) 43911-43920.

[330] J. Wei, J. Xie, P. Zhang, Z. Zou, H. Ping, W. Wang, H. Xie, J.Z. Shen, L. Lei, Z. Fu, Bioinspired 3D Printable, Self-Healable, and Stretchable Hydrogels with Multiple Conductivities for Skin-like Wearable Strain Sensors, ACS Appl. Mater. Interfaces 13(2) (2021) 2952-2960.

[331] C.-W. Lai, S.-S. Yu, 3D Printable Strain Sensors from Deep Eutectic Solvents and Cellulose Nanocrystals, ACS Appl. Mater. Interfaces 12(30) (2020) 34235-34244.

[332] Y. Zhang, F. Zhang, Z. Yan, Q. Ma, X. Li, Y. Huang, J.A. Rogers, Printing, folding and assembly methods for forming 3D mesostructures in advanced materials, Nat. Rev. Mater. 2(4) (2017) 17019.

[333] I. Dankar, A. Haddarah, F.E.L. Omar, F. Sepulcre, M. Pujolà, 3D printing technology: The new era for food customization and elaboration, Trends Food Sci. Technol. 75 (2018) 231-242.

[334] Z. Liu, M. Zhang, B. Bhandari, C. Yang, Impact of rheological properties of mashed potatoes on 3D printing, J. Food Eng. 220 (2018) 76-82.

[335] B.C. Maniglia, D.C. Lima, M.D. Matta Junior, P. Le-Bail, A. Le-Bail, P.E.D. Augusto, Hydrogels based on ozonated cassava starch: Effect of ozone processing and gelatinization conditions on enhancing 3D-printing applications, Int. J. Biol. Macromol. 138 (2019) 1087-1097.

[336] K. Konca, P.Z. Çulfaz-Emecen, Effect of carboxylic acid crosslinking of cellulose membranes on nanofiltration performance in ethanol and dimethylsulfoxide, J. Membr. Sci. 587 (2019) 117175.

[337] B.M. Simões, C. Cagnin, F. Yamashita, J.B. Olivato, P.S. Garcia, S.M. de Oliveira, M.V. Eiras Grossmann, Citric acid as crosslinking agent in starch/xanthan gum hydrogels produced by extrusion and thermopressing, LWT - Food Sci. Technol. 125 (2020) 108950.

[338] G.N. Fazolin, G.H.C. Varca, L.F. de Freitas, B. Rokita, S. Kadlubowski, A.B. Lugão, Simultaneous intramolecular crosslinking and sterilization of papain nanoparticles by gamma radiation, Radiat. Phys. Chem. 171 (2020) 108697.

[339] A. Fathy Ghazal, M. Zhang, B. Bhandari, H. Chen, Investigation on spontaneous 4D changes in color and flavor of healthy 3D printed food materials over time in response to external or internal pH stimulus, Food Res. Int. 142 (2021) 110215.

[340] X. Teng, M. Zhang, A.S. Mujumdar, 4D printing: Recent advances and proposals in the food sector, Trends Food Sci. Technol. 110 (2021) 349-363.

[341] A. Haleem, M. Javaid, Future applications of five-dimensional printing in dentistry, Curr. Med. Res. Pract. 9(2) (2019) 85-86.

[342] W.S. Yerazunis, J.C. Barnwell III, J. Katz, D. Brinkman, Method and Apparatus for Printing

3D Objects Using Additive Manufacturing and Material Extruder with Translational and Rotational Axes, Mitsubishi Electric Research Laboratories, Inc, 2015.

[343] A. Haleem, M. Javaid, Expected applications of five-dimensional (5D) printing in the medical field, Curr. Med. Res. Pract. 9(5) (2019) 208-209.

[344] P. Liu, Y. Li, X. Shang, F. Xie, Starch–zinc complex and its reinforcement effect on starch-based materials, Carbohydr. Polym. 206 (2019) 528-538.

[345] C.A. Murphy, M.N. Collins, Microcrystalline cellulose reinforced polylactic acid biocomposite filaments for 3D printing, Polym. Compos. 39(4) (2018) 1311-1320.

[346] V.C.-F. Li, X. Kuang, C.M. Hamel, D. Roach, Y. Deng, H.J. Qi, Cellulose nanocrystals support material for 3D printing complexly shaped structures via multi-materials-multi-methods printing, Addit. Manuf. 28 (2019) 14-22.

[347] J. Liu, S. Willför, C. Xu, A review of bioactive plant polysaccharides: Biological activities, functionalization, and biomedical applications, Bioact. Carbohydr. Dietary Fibre 5(1) (2015) 31-61.

[348] M. Sun, C. Sun, H. Xie, S. Yan, H. Yin, A simple method to calculate the degree of polymerization of alginate oligosaccharides and low molecular weight alginates, Carbohydr. Res. 486 (2019) 107856.

[349] A.I. Cernencu, A. Lungu, I.C. Stancu, A. Serafim, E. Heggset, K. Syverud, H. Iovu, Bioinspired 3D printable pectin-nanocellulose ink formulations, Carbohydr. Polym. 220 (2019) 12-21.

[350] Sucheta, S.K. Rai, K. Chaturvedi, S.K. Yadav, Evaluation of structural integrity and functionality of commercial pectin based edible films incorporated with corn flour, beetroot, orange

2407 peel, muesli and rice flour, Food Hydrocolloids 91 (2019) 127-135.
2408 [351] P. Jiang, C. Yan, Y. Guo, X. Zhang, M. Cai, X. Jia, X. Wang, F. Zhou, Direct ink writing with
2409 high-strength and swelling-resistant biocompatible physically crosslinked hydrogels, Biomater. Sci.
2410 7(5) (2019) 1805-1814.
2411 [352] I. Diañez, C. Gallegos, E. Brito-de la Fuente, I. Martínez, C. Valencia, M.C. Sánchez, M.J.
2412 Diaz, J.M. Franco, 3D printing in situ gelification of κ-carrageenan solutions: Effect of printing
2413 variables on the rheological response, Food Hydrocolloids 87 (2019) 321-330.
2414 [353] S. Liu, L. Li, Ultrastretchable and Self-Healing Double-Network Hydrogel for 3D Printing and
2415 Strain Sensor, ACS Appl. Mater. Interfaces 9(31) (2017) 26429-26437.
2416 [354] V.L. Campo, D.F. Kawano, D.B.d. Silva, I. Carvalho, Carrageenans: Biological properties,
2417 chemical modifications and structural analysis – A review, Carbohydr. Polym. 77(2) (2009) 167-180.
2418 [355] V.B. Morris, S. Nimbalkar, M. Younesi, P. McClellan, O. Akkus, Mechanical Properties,
2419 Cytocompatibility and Manufacturability of Chitosan:PEGDA Hybrid-Gel Scaffolds by
2420 Stereolithography, Ann. Biomed. Eng. 45(1) (2017) 286-296.
2421 [356] S. Akbari-Alavijeh, R. Shaddel, S.M. Jafari, Encapsulation of food bioactives and
2422 nutraceuticals by various chitosan-based nanocarriers, Food Hydrocolloids 105 (2020) 105774.
2423 [357] S. Holland, T. Foster, W. MacNaughtan, C. Tuck, Design and characterisation of food grade
2424 powders and inks for microstructure control using 3D printing, J. Food Eng. 220 (2018) 12-19.
2425 [358] S. Shin, H. Kwak, J. Hyun, Melanin Nanoparticle-Incorporated Silk Fibroin Hydrogels for the
2426 Enhancement of Printing Resolution in 3D-Projection Stereolithography of Poly(ethylene glycol)-
2427 Tetraacrylate Bio-ink, ACS Appl. Mater. Interfaces 10(28) (2018) 23573-23582.

[359] S. Shang, L. Zhu, J. Fan, Intermolecular interactions between natural polysaccharides and silk fibroin protein, Carbohydr. Polym. 93(2) (2013) 561-573.

[360] J.A. Inzana, D. Olvera, S.M. Fuller, J.P. Kelly, O.A. Graeve, E.M. Schwarz, S.L. Kates, H.A. Awad, 3D printing of composite calcium phosphate and collagen scaffolds for bone regeneration, Biomaterials 35(13) (2014) 4026-4034.

[361] Z. Wang, H. Kumar, Z. Tian, X. Jin, J.F. Holzman, F. Menard, K. Kim, Visible Light Photoinitiation of Cell-Adhesive Gelatin Methacryloyl Hydrogels for Stereolithography 3D Bioprinting, ACS Appl. Mater. Interfaces 10(32) (2018) 26859-26869.

[362] A. Alemán Pérez, O. Martinez Alvarez, Marine Collagen as a Source of Bioactive Molecules: A Review, Nat. Prod. J. 3 (2013) 105-114.

[363] L. Wang, C. Hu, K. Yan, A one-step inkjet printing technology with reactive dye ink and cationic compound ink for cotton fabrics, Carbohydr. Polym. 197 (2018) 490-496.

[364] Wusigale, L. Liang, Y. Luo, Casein and pectin: Structures, interactions, and applications, Trends Food Sci. Technol. 97 (2020) 391-403.

[365] H.-H. Lin, F.-Y. Hsieh, C.-S. Tseng, S.-h. Hsu, Preparation and characterization of a biodegradable polyurethane hydrogel and the hybrid gel with soy protein for 3D cell-laden bioprinting, J. Mater. Chem. B 4(41) (2016) 6694-6705.

[366] C. López-Iglesias, A.M. Casielles, A. Altay, R. Bettini, C. Alvarez-Lorenzo, C.A. García-González, From the printer to the lungs: Inkjet-printed aerogel particles for pulmonary delivery, Chem. Eng. J. 357 (2019) 559-566.

[367] L. Chaunier, E. Leroy, G.D. Valle, M. Dalgalarrondo, B. Bakan, D. Marion, B. Madec, D.

2449 Lourdin, 3D Printing of Maize Protein By Fused Deposition Modeling, AIP Conference Proceedings,
2450 2017, p. 190003.
2451 [368] R. Xiong, Z. Zhang, W. Chai, Y. Huang, D.B. Chrisey, Freeform drop-on-demand laser printing
2452 of 3D alginate and cellular constructs, Biofabrication 7(4) (2015) 045011.
2453 [369] S. Kumar, M. Hofmann, B. Steinmann, E.J. Foster, C. Weder, Reinforcement of
2454 stereolithographic resins for rapid prototyping with cellulose nanocrystals, ACS Appl. Mater.
2455 Interfaces 4(10) (2012) 5399-53407.
2456 [370] N.B. Palaganas, J.D. Mangadlao, A.C.C. de Leon, J.O. Palaganas, K.D. Pangilinan, Y.J. Lee,
2457 R.C. Advincula, 3D Printing of Photocurable Cellulose Nanocrystal Composite for Fabrication of
2458 Complex Architectures via Stereolithography, ACS Appl. Mater. Interfaces 9(39) (2017) 34314-
2459 34324.
2460 [371] D.J. Villarama, v.B.K.J. Cornelis, N.M. Willem-Jan, H. Jolanda, P. Brier, Method for the
2461 production of edible objects using SLS and food products, TNO, US, 2016.
2462 [372] S. Singamneni, R. Velu, M.P. Behera, S. Scott, P. Brorens, D. Harland, J. Gerrard, Selective
2463 laser sintering responses of keratin-based bio-polymer composites, Mater. Des. 183 (2019) 108087.
2464 [373] S. Holland, C. Tuck, T. Foster, Selective recrystallization of cellulose composite powders and
2465 microstructure creation through 3D binder jetting, Carbohydr. Polym. 200 (2018) 229-238.
2466 [374] S. Zhu, M.A. Stieger, A.J. van der Goot, M.A.I. Schutyser, Extrusion-based 3D printing of
2467 food pastes: Correlating rheological properties with printing behaviour, Innovative Food Sci. Emerg.
2468 Technol. 58 (2019) 102214.
2469 [375] P. Phuhongsung, M. Zhang, S. Devahastin, Investigation on 3D printing ability of soybean

protein isolate gels and correlations with their rheological and textural properties via LF-NMR spectroscopic characteristics, LWT - Food Sci. Technol. 122 (2020) 109019.

[376] W. Xu, B.Z. Molino, F. Cheng, P.J. Molino, Z. Yue, D. Su, X. Wang, S. Willfor, C. Xu, G.G. Wallace, On Low-Concentration Inks Formulated by Nanocellulose Assisted with Gelatin Methacrylate (GelMA) for 3D Printing toward Wound Healing Application, ACS Appl. Mater. Interfaces 11(9) (2019) 8838-8848.

[377] M. Ojansivu, A. Rashad, A. Ahlinder, J. Massera, A. Mishra, K. Syverud, A. Finne-Wistrand, S. Miettinen, K. Mustafa, Wood-based nanocellulose and bioactive glass modified gelatin–alginate bioinks for 3D bioprinting of bone cells, Biofabrication 11(3) (2019) 035010.

[378] Z. Zheng, J. Wu, M. Liu, H. Wang, C. Li, M.J. Rodriguez, G. Li, X. Wang, D.L. Kaplan, 3D Bioprinting of Self-Standing Silk-Based Bioink, Adv. Healthcare Mater. 7(6) (2018) 1701026.

[379] L. Huang, X. Du, S. Fan, G. Yang, H. Shao, D. Li, C. Cao, Y. Zhu, M. Zhu, Y. Zhang, Bacterial cellulose nanofibers promote stress and fidelity of 3D-printed silk based hydrogel scaffold with hierarchical pores, Carbohydr. Polym. 221 (2019) 146-156.

[380] Y. Jin, A. Compaan, T. Bhattacharjee, Y. Huang, Granular gel support-enabled extrusion of three-dimensional alginate and cellular structures, Biofabrication 8(2) (2016) 025016.

[381] L. Cheng, B. Yao, T. Hu, X. Cui, X. Shu, S. Tang, R. Wang, Y. Wang, Y. Liu, W. Song, X. Fu, H. Li, S. Huang, Properties of an alginate-gelatin-based bioink and its potential impact on cell migration, proliferation, and differentiation, Int. J. Biol. Macromol. 135 (2019) 1107-1113.

[382] R. Urruela-Barrios, E. Ramírez-Cedillo, A. Díaz De León, A. Alvarez, W. Ortega-Lara, Alginate/Gelatin Hydrogels Reinforced with TiO2 and β-TCP Fabricated by Microextrusion-based

Printing for Tissue Regeneration, Polymers 11(3) (2019) 457.

[383] J. Park, S.J. Lee, H. Lee, S.A. Park, J.Y. Lee, Three dimensional cell printing with sulfated alginate for improved bone morphogenetic protein-2 delivery and osteogenesis in bone tissue engineering, Carbohydr. Polym. 196 (2018) 217-224.

[384] L. Pescosolido, W. Schuurman, J. Malda, P. Matricardi, F. Alhaique, T. Coviello, P.R. van Weeren, W.J.A. Dhert, W.E. Hennink, T. Vermonden, Hyaluronic Acid and Dextran-Based Semi-IPN Hydrogels as Biomaterials for Bioprinting, Biomacromolecules 12(5) (2011) 1831-1838.

[385] T.T. Demirtaş, G. Irmak, M. Gümüşderelioğlu, A bioprintable form of chitosan hydrogel for bone tissue engineering, Biofabrication 9(3) (2017) 035003.

[386] B. Duan, L.A. Hockaday, K.H. Kang, J.T. Butcher, 3D Bioprinting of heterogeneous aortic valve conduits with alginate/gelatin hydrogels, J. Biomed. Mater. Res. Part A 101A(5) (2013) 1255-1264.

[387] S. Sakai, H. Ohi, T. Hotta, H. Kamei, M. Taya, Differentiation potential of human adipose stem cells bioprinted with hyaluronic acid/gelatin-based bioink through microextrusion and visible light-initiated crosslinking, Biopolymers 109(2) (2018) 1-8.

[388] X. Zhang, J.G. Kim, G.M. Kang, K.J. Lee, W.J. Seo, T.J. Do, K. Hong, M.J. Cha, R.S. Shin, H. Bae, Marine Biomaterial-Based Bioinks for Generating 3D Printed Tissue Constructs, Mar. Drugs 16(12) (2018).

[389] H. Suo, D. Zhang, J. Yin, J. Qian, Z.L. Wu, J. Fu, Interpenetrating polymer network hydrogels composed of chitosan and photocrosslinkable gelatin with enhanced mechanical properties for tissue engineering, Mater. Sci. Eng., C 92 (2018) 612-620.

[390] M.D. Giuseppe, N. Law, B. Webb, A.M. R, L.J. Liew, T.B. Sercombe, R.J. Dilley, B.J. Doyle, Mechanical behaviour of alginate-gelatin hydrogels for 3D bioprinting, J. Mech. Behav. Biomed. Mater. 79 (2018) 150-157.

[391] H. Li, Y.J. Tan, L. Li, A strategy for strong interface bonding by 3D bioprinting of oppositely charged κ-carrageenan and gelatin hydrogels, Carbohydr. Polym. 198 (2018) 261-269.

[392] S. Dehghani, M. Rasoulianboroujeni, H. Ghasemi, S.H. Keshel, Z. Nozarian, M.N. Hashemian, M. Zarei-Ghanavati, G. Latifi, R. Ghaffari, Z. Cui, H. Ye, L. Tayebi, 3D-Printed membrane as an alternative to amniotic membrane for ocular surface/conjunctival defect reconstruction: An in vitro & in vivo study, Biomaterials 174 (2018) 95-112.